



Title	Study on Catalysis of Copper Nitride Nanoparticles for Environmentally-benign Organic Synthesis
Author(s)	徐, 航
Citation	大阪大学, 2023, 博士論文
Version Type	VoR
URL	https://doi.org/10.18910/92199
rights	
Note	

Osaka University Knowledge Archive : OUKA

<https://ir.library.osaka-u.ac.jp/>

Osaka University

*Study on Catalysis of Copper Nitride Nanoparticles for
Environmentally-benign Organic Synthesis*

HANG XU

MARCH 2023

***Study on Catalysis of Copper Nitride Nanoparticles for
Environmentally-benign Organic Synthesis***

A dissertation submitted to

THE GRADUATE SCHOOL OF ENGINEERING SCIENCE

OSAKA UNIVERSITY

in partial fulfillment of the requirements for the degree of

DOCTOR OF PHILOSOPHY IN ENGINEERING

BY

HANG XU

MARCH 2023

Abstract

This thesis deals with the development of nanosized copper nitride (Cu_3N) catalysts for environmentally benign organic reactions. The present thesis consists of five chapters.

In Chapter I, the author encapsulated the fundamental background of metal nitrides and focused on the application of Cu_3N as potential catalysts to various fields, such as electrocatalysis, photocatalysis, and organic synthesis. Moreover, the characteristics and preparation methods of Cu_3N materials were systematically summarized. Finally, recent reports on the catalysis of Cu_3N were specifically reviewed.

In Chapter II, the author described that nanocubic Cu_3N (nano- Cu_3N) was prepared and used as an efficient heterogeneous catalyst for the hydroxylation of aryl halides. The nano- Cu_3N catalyst exhibited high catalytic activity, comparable to that of homogeneous Cu salts/N ligands catalytic systems, suggesting that the N atoms in Cu_3N act as functional ligands to promote the catalytic hydroxylation reaction. Furthermore, this method showed good functional group tolerance to provide various substituted phenols in excellent yields. After the catalytic reaction, the nano- Cu_3N could also be separated and reused without significant loss of the original activity. This is the first example of the heterogeneous Cu-catalyzed hydroxylation of aryl chlorides without additives.

Chapter III demonstrates that the Cu_3N nanocube (Cu_3N NC) is an efficient heterogeneous catalyst for green oxidative functionalization of indoles in an aqueous solvent with O_2 as a sole oxidant under additive-free conditions. The catalytic activity of Cu_3N NC outperformed other conventional Cu compounds in the oxidative trimerization and Witkop oxidation of indoles. A wide range of indoles could be converted to the corresponding products in moderate to good yields. This is the first application of the Cu_3N in oxidative organic reactions. The high catalytic activity of Cu_3N NC may be attributed to the essential regularly arranged N-Cu-N structure on Cu_3N NC, which promotes the

conversion of O₂ to active superoxide species.

In Chapter IV, the efficient synthesis of vinyl boronate esters through the hydroboration of alkynes was achieved over Cu₃N NC catalyst. Good functional group tolerance was observed to produce a wide range of vinyl boronate esters in excellent yields. Furthermore, the Cu₃N NC could be recovered and reused for several times without loss in its catalytic activity. This is the first time that the hydroboration of alkynes is achieved under mild and additive-free conditions with a heterogeneous Cu catalyst. The several control experiments and spectroscopic analyses revealed that the Lewis acid-base sites on Cu₃N NC surface play an essential role in ensuring the distinguished catalytic activity of Cu₃N NC.

Chapter V describes an efficient method for synthesizing silanes via Cu₃N NC catalyzed-hydrosilylation of unsaturated compounds under base- and solvent-free, and mild reaction conditions. In this reaction, various substrates including alkynes, alkenes, allenes, and imines, were converted to desired products in good yields. Moreover, the dihydrosilylation of alkynes was achieved over Cu₃N NC catalyst, providing a novel method for *gem*-(bis)silanes synthesis. This is the first example that the hydrosilylation of various unsaturated compounds was achieved over a heterogeneous Cu catalyst.

Preface

This dissertation is a collection of the author's studies which were carried out from 2020 to 2023 under the supervision of Professor Tomoo Mizugaki at the Division of Chemical Engineering Department of Materials Engineering Science, Graduate School of Engineering Science, Osaka University.

The development of efficient catalysts based on non-precious metals for environmentally benign organic reactions has attracted high interest. Traditionally, homogeneous metal complexes have been widely used in organic synthesis. However, they required the additive ligands to tune the electronic and steric properties of metal species and suffered from the instability and low recyclability. Keeping the "green and sustainable chemistry" in mind, this is an increasing emphasis on the design of efficient heterogeneous catalysts for green chemical processes. Therefore, in this thesis, the author demonstrates that the nanosized Cu_3N catalysts exhibited excellent catalytic activity in the various environmentally benign organic reactions, making them a leading candidate to substitute the conventional metal catalysts.

The author firmly believes that this study will be a landmark attempt to develop novel and efficient metal nitride catalysts for organic synthesis and provides future researchers with a worthwhile background to realize efficient, sustainable, and environmentally-benign reaction processes for valuable chemical productions.

Contents

<i>Chapter I. General Introduction</i>	1
1. Preliminary	2
2. Background	4
3. Catalytic activity of Cu ₃ N	10
4. Purpose of this thesis	16
5. Outline of this thesis	18
<i>Chapter II. Highly Active Copper Nitride Catalyst for Hydroxylation of Aryl Halides</i>	25
1. Introduction	26
2. Experimental section	28
3. Results and discussion	33
4. Conclusion	41
<i>Chapter III. Green Oxidation of Indoles by Copper Nitride Catalyst</i>	45
1. Introduction	46
2. Experimental section	48
3. Results and discussion	58
4. Conclusion	70
<i>Chapter IV. Efficient Hydroboration of Alkynes to Vinyl Boronates by Copper Nitride Nanocube</i>	74
1. Introduction	75
2. Experimental section	77
3. Results and discussion	87
4. Conclusion	97
<i>Chapter V. A Green and Efficient Method for Silanes Synthesis via Hydrosilylation of Unsaturated Compounds</i>	101
1. Introduction	102
2. Experimental section	104
3. Results and discussion	115
4. Conclusion	124
General Conclusions	127
List of Publications	130
Acknowledgement	131

Chapter I.

General Introduction

1. Preliminary

Chemistry plays an indispensable and important role in human development. It improves the quality of human life and changes the way of life of human beings. For instance, the discovery of drugs has extended human lifespan, and the development of pesticides has relieved the pressure on food demand from population growth. However, with the industrialization of chemistry, the environmental pollution and resource depletion problems have become the hot issues. Studies have shown that human diseases are mainly caused by environmental pollutions [1], so that people, especially, chemists realize the importance of "green and sustainable chemistry". In 1990s, the concept of "green chemistry" was firstly proposed [2]: "green chemistry" is an area of chemistry or chemical engineering focused on the establishment of chemical principles, technologies and methods to reduce the use of harmful raw materials, catalysts, and solvents, thereby achieving high reaction efficiency and sustainable development without generating by-products. Therefore, while achieving 100% atomic utilization, the consumption of energy originating from petroleum and coal should be avoided in the chemical conversion process.

The development and utilization of novel catalysts is an important mean to achieve "green chemistry", because catalysts can reduce the activation energy required for the reaction, thus increasing the reaction rate. In addition, catalysts play a crucial role in the selectivity of the reaction. According to statistics, more than 80% of the reactions achieved high reaction rates and yields with the assistance of catalysts [3]. Generally, catalysts can be simply divided into homogeneous and heterogeneous catalysts, depending on their solubility in the reaction solvents. Due to high solubility of homogeneous catalysts in reaction mixture, the active metal sites will efficiently interact with reactant molecules, providing its outstanding catalytic activities. Moreover, the activity of homogeneous catalysts will be further enhanced with cooperative ligands, since electron state of metal species can be precisely modified. However, the inevitable and main drawback of homogeneous

catalysis is that the hardly recoverable of catalysts, leading to the high costs and wastes. On the other hand, heterogeneous catalysts can be easily separated by centrifugation or filtration and have been widely used in chemical industries due to its good reusability. Among them, heterogeneous catalysts based on cheap, earth-abundant, and low-toxic metals such as Fe, Co, Ni, and Cu have attracted high attentions [4], whereas conventional non-precious metal-based heterogeneous catalysts exhibited unsatisfactory catalytic performance and stability compared to precious metal catalysts, thus limiting their application to chemical conversions. Therefore, the development of novel non-precious metal-based heterogeneous catalysts with outstanding activity and durability is highly desired.

Metal–non-oxide compounds, such as metal nitrides, metal borides, and metal phosphides, have modified electronic properties of active metal species and high catalytic performance [5, 6]. Recently, Mitsudome et al. have reported that the metal phosphide nanoalloys (Ni_2P , Co_2P , and Ru_2P) exhibited glorious catalytic performance in hydrogenative reactions [7–9]. The excellent activity of metal phosphide nanoalloys in organic conversions is attributed to the modified electronic property of metal sites which is caused by the interaction of metal sites with phosphate atoms. Similarly, metal nitrides contain the metal with nitrogen atoms, which have attracted increased attention as photocatalysts and electrocatalysts for energy conversion [10, 11]. Despite of the high catalytic potential of metal nitrides, the application of metal nitrides in organic synthesis is still rare. Therefore, investigation of the catalytic potential of metal nitrides for organic transformation not only helps us to understand the chemical property of metal nitrides but also improve the development of organic chemistry.

2. Background

Transition metal nitrides (TMNs) consist of the nitrogen atom with one or several metal elements. Generally, TMNs are dominated simultaneously by covalent, ionic, and metallic bonding [12, 13]. Moreover, the metal species in TMNs possess the deficiency in metal d-band and the higher density of states (DOS) near metal Fermi level [14]. Based on these properties, the metal nitrides have been widely used in electron- and photocatalysis for energy conversion [15].

Cu has been considered as one of the most promising non-precious metal catalysts since it is cheap, earth-abundant, and low toxic [16]. Cu nitride (Cu_3N) has an anti-perovskite lattice structure (Pm3m), each N atom in the lattice structure of Cu_3N is shared by eight cells, and each Cu atom is shared by four cells (**Figure 1-1**) [17]. Cu_3N material exhibits several unique chemical and physical properties, which are attributed to the interaction of Cu with N. For example, the defect states generated by metallic and non-metallic vacancies of Cu and N atoms, respectively, lead to the insulated Cu_3N material [18]. Moreover, due to the anti-bonding states, Cu_3N is a p-type semiconductor with a strong hybridization of the Cu 3d and N 2p orbitals close to the valence band, causing good tolerance to defects [19]. Benefits from these properties, Cu_3N as one of the heterogeneous Cu catalysts has obtained high attention in various fields, especially electron- and photochemistry [20].

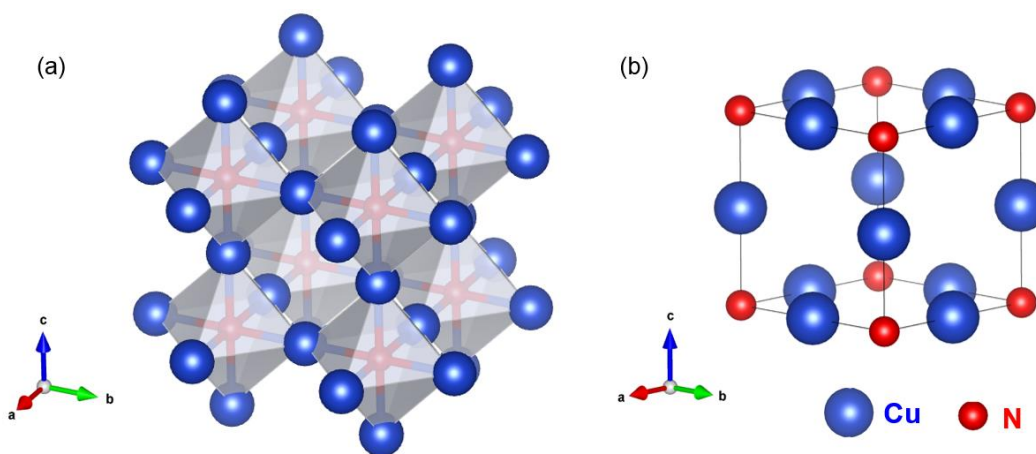


Figure 1-1. Crystal structures of Cu_3N .

2.1. Preparation of Cu₃N

Generally, the activity of metal nanoparticles (NPs) is dependent on their size and morphology. In this regard, the development of novel synthetic methods for synthesizing Cu₃N with various sizes and morphologies has attracted high attention in the field of Cu₃N chemistry [21]. There are two methods for preparing Cu₃N materials, i.e., the chemical and the physical methods. The chemical method can be further divided into the gas-phase and the solution-phase synthetic methods. Alternatively, physical routes for Cu₃N mostly concentrate on thin-film growth.

2.1.1. Gas-phase method

The ammonolysis reaction is the most common and practical approach for TMNs syntheses. In this method, a solid Cu precursor reacts with gaseous ammonia (NH₃), and the reaction can be controlled by changing parameters for example the temperature, time, or NH₃ flow rate. In 2007, the Cu₃N powders were successfully synthesized using anhydrous copper(II) fluoride (CuF₂) and NH₃ gas at the temperature from 250 to 325 °C. The scanning electron microscope (SEM) images reveal that the plate-shaped particles with a side length of 600–800 nm and thickness about 100 nm were formed. It is worth noting that when the reaction temperature is higher than 350 °C, the mixture of Cu₃N and metallic Cu is formed [22]. This result demonstrates that the Cu₃N crystal will decompose under high temperature.

In addition, the supported Cu₃N material can be prepared through gas-phase method. Hu group has successfully prepared the SiO₂ supported Cu₃N (Cu₃N/Fe₃N@SiO₂) catalyst with copper acetate (Cu(OAc)₂) under NH₃ flowing conditions (**Figure 1-2**) [23]. This study demonstrated the possibility for the generation of uniformed Cu₃N material on the functional supports.

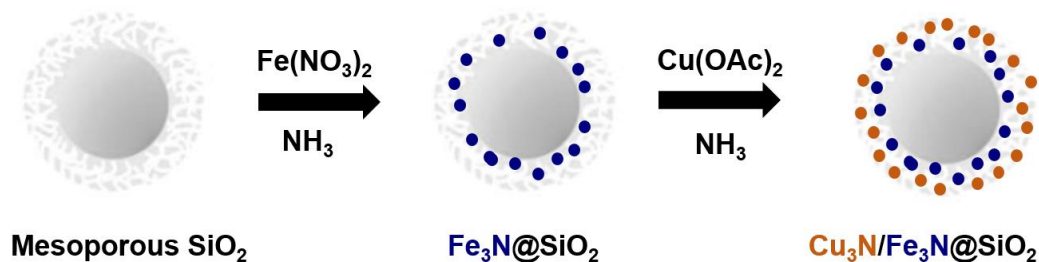


Figure 1-2. Preparation of $\text{Cu}_3\text{N/Fe}_3\text{N@SiO}_2$ catalyst under NH_3 flowing conditions.

Despite the high efficiency of NH_3 gas in preparing Cu_3N , the direct use of NH_3 gas in the laboratory has high safety risks. Thus, urea has been considered as an alternative, which generates NH_3 by thermal decomposition at an elevated temperature [24]. For instance, cubic Cu_3N with a range of 50–200 nm was successfully prepared using urea and Cu(OAc)_2 at 300 °C for 2 h (**Figure 1-3**) [25]. This research provides a safe and convenient method for preparation of Cu_3N .

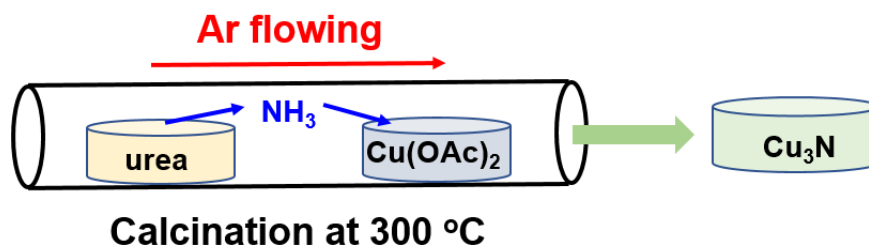


Figure 1-3. Formation of Cu_3N using urea as nitrogen source.

2.1.2. Solution-phase method

Generally, the preferential chemisorption of capping agents on particular facets can lead to shape-controlled synthesis of nanocrystals with tiny size [26, 27]. Therefore, in solution-phase synthesis, organic surfactants, such as primary amines and alcohols, were used to control the size, shape, and phase of Cu_3N . According to the report by Nakamura et al., the Cu_3N NPs (~200 nm in diameter) were synthesized through the reaction of Cu(OAc)_2 in alcohol solvents under NH_3 flowing

at 170 °C [28]. The transmission electron microscopy (TEM) images reveal that utilizing different aliphatic alcohols such as 1-octanol, 1-heptanol, 1-hexanol, and 1-pentanol provides the Cu_3N NPs with diverse sizes and morphologies (**Figure 1-4**).

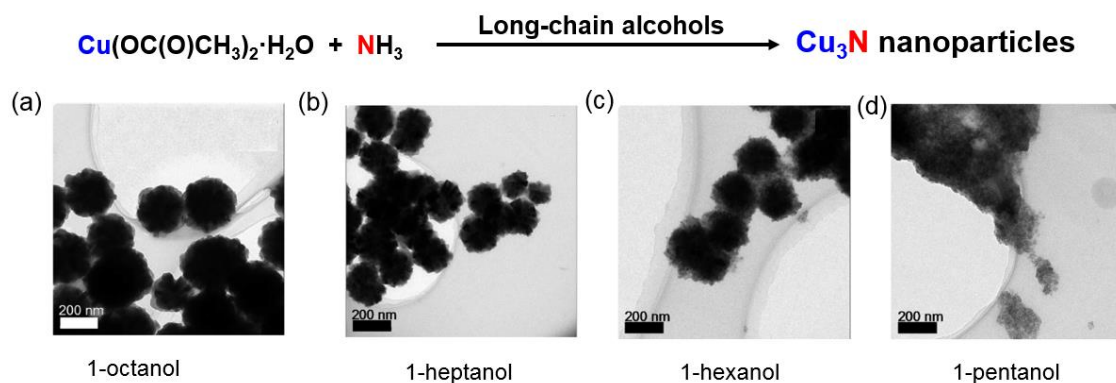


Figure 1-4. TEM images of synthesized Cu_3N in different alcohols.

Similar results were also reported by Chen's group [29]: cubic Cu_3N nanocrystals with tunable size were formed in different primary amines. In particular, the Cu_3N nanocube (NC) with an average 10.8 nm was obtained in oleylamine and octadecene mixture, while a large size of Cu_3N NC (26.0 nm) was formed with hexadecylamine instead of oleylamine as capping agent (**Figure 1-5**).

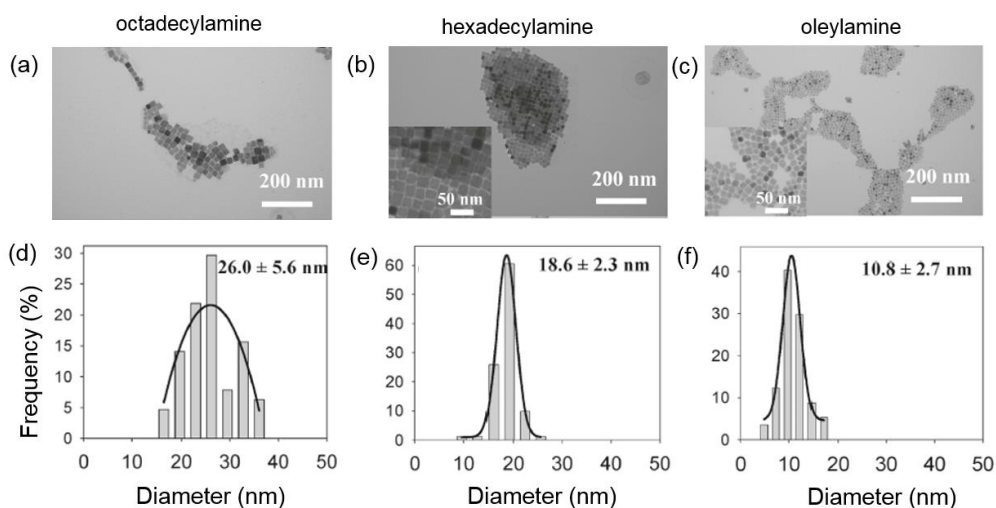
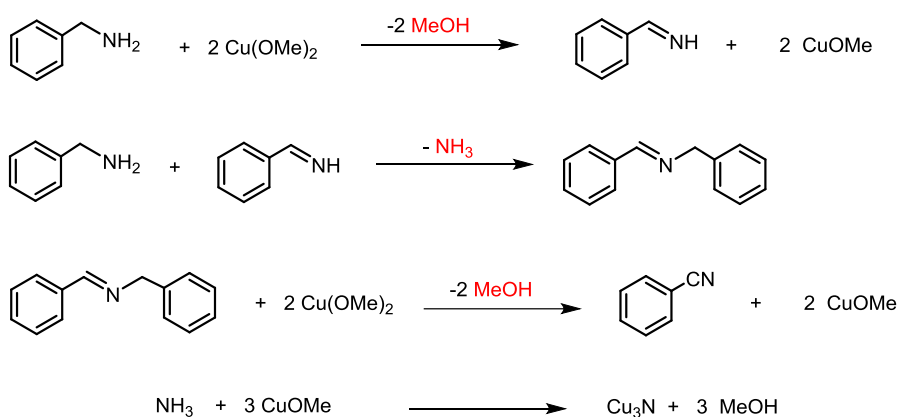


Figure 1-5. TEM images and the corresponding crystal size histograms of Cu_3N nanocrystals formed in various amine surfactants: (a, d) octadecylamine, (b, e) hexadecylamine, and (c, f) oleylamine.

Besides the aliphatic amines, aromatic amine, i.e., benzylamine, is also a suitable surfactant for Cu₃N synthesis. In this case, the uniformed sphere-like Cu₃N NPs with 2.2 ± 0.5 nm diameter were successfully formed with benzylamine and Cu(OMe)₂ at 140 °C [30]. The reaction process is presented in **Scheme 1-1**: the authors speculated that the NH₃ was generated through the condensation of benzylamine and then reacted with Cu(OMe)₂ to afford Cu₃N material.



Scheme 1-1. Proposed pathway for Cu₃N synthesis.

Reaction temperature is another important parameter that affects the nucleation speed of nanocrystal, thus generating different sizes and morphology of catalysts. For instance, Sun et al. found that Cu₃N NC with an average length of 25 nm was synthesized through the reducing Cu(NO₃)₂·3H₂O in octadecylamine and oleylamine mixture at 240 °C, whereas 20 and 10 nm Cu₃N NC were formed at 250 and 260 °C, respectively [31]. When the reaction temperature was 230 °C, the 20 nm sphere-like Cu₃N NPs were obtained instead of cubic Cu₃N. Overall, the solvothermal method provides a practical strategy for preparation of various uniformed Cu₃N nanosized materials which have tunable morphology and size.

2.1.3. Physical synthetic method

The plasma ignition is also an efficient method for synthesizing the Cu_3N . Perng group explored that carbon nanotubes (CNTs) supported Cu_3N was successfully prepared by plasma enhanced atomic layer deposition (ALD) with copper(II) hexafluoroacetylacetonate ($\text{Cu}(\text{hfac})_2$) and NH_3 gas at $250\text{ }^\circ\text{C}$ (**Figure 1-6**) [32].

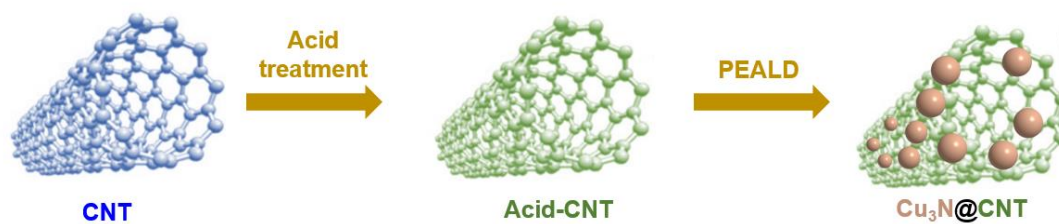


Figure 1-6. Preparation of $\text{Cu}_3\text{N}@$ CNT through ALD method.

3. Catalytic activity of Cu₃N

3.1. Photocatalysis

Photocatalysis is a redox process, which contains three main steps: (i) the generation of electron-hole pairs (e^-/h^+) by photoexcitation, (ii) transportation of the excitons to the semiconductor surface, and (iii) the utilization of charge for surface oxidation–reduction reactions [33]. The total efficiency of redox process is affected by the physical properties of the semiconductor photocatalysts, for example, the electronic structure, surface structure, and band gap [34]. The material that possesses a wide bandgap is considered as ideal photocatalysts, since it is optimal for absorbing in the entire range of the solar spectrum [35]. Generally, the combination of N atoms with metal species will improve the contraction of the d-band of metals in TMNs, thus giving some unique physical properties of TMNs. For instance, Cu₃N is a semiconductor with an indirect band gap energy ~ 1.4 eV and its optical absorption coefficient value of ~ 105 cm⁻¹. Benefiting from this essential property, the Cu₃N has good catalytic potential in photocatalysis.

In 2020, Moloto et al. prepared Cu₃N NC with 41 nm and utilized it as photocatalyst in degradation of methyl orange with 89% efficiency, which is superior to that of Cu₂S NPs [36]. Similar result was also reported by Xiao group. Cu₃N films were prepared by magnetron sputtering method, which possesses an optical band gap (2.0 eV) and energy gap (2.5 eV), exhibiting outstanding photocatalytic activity for degrading methyl orange (degradation ratio of 99.5% in 30 min) [37]. The study demonstrated that the catalytic activity of Cu₃N mainly is attributed to the vacancies in the crystal and Cu self-doping.

In general, the combination of metal NPs with functional supports leads to enhanced catalytic activities in photocatalysts, due to unique metal-support interaction [38]. Subodh Kumar De group prepared the Au-Cu₃N catalysts through the thermal- and light-induced thermal processes (**Figure 1-7**), which exhibited better catalytic activity than that of pure Cu₃N NC in the environmental

purification of organic dyes [39]. This study demonstrated that the high activity of Au-Cu₃N catalysts originates from the electromagnetic coupling between Au metal and Cu₃N semiconductor in nanoheterostructures.

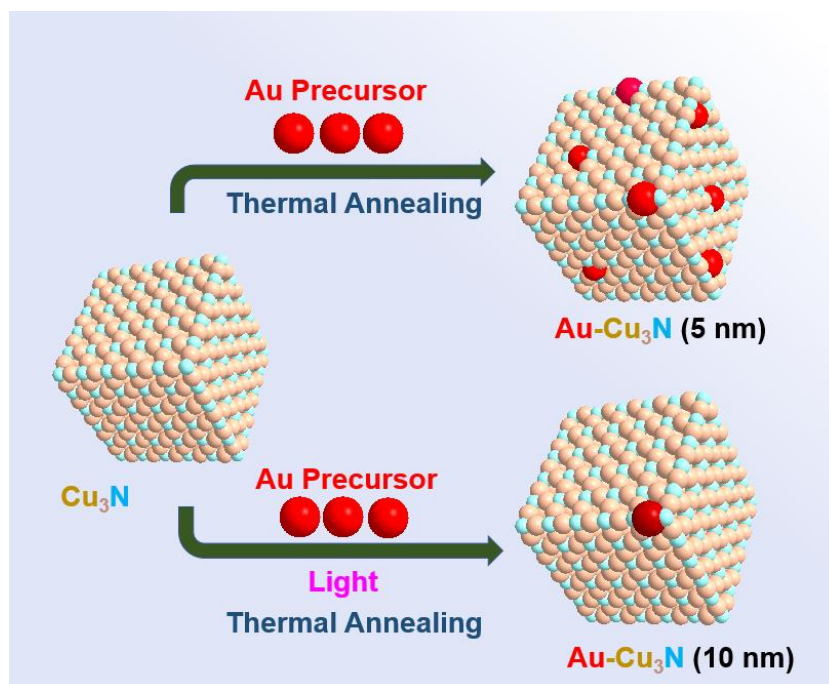


Figure 1-7. Growth process of Au-decorated Cu₃N NCs.

Furthermore, Cu₃N can be applied to sustainable H₂ generation through photocatalytic water splitting. In 2020, Huang et al. utilized Cu₃N nanocrystals (15 nm) as a cocatalyst coupled with CdS for efficient photocatalytic H₂ evolution with a rate of 4512 mmol g⁻¹ h⁻¹ [40]. According to the results of mechanistic studies, the excellent H₂ evolution activity is benefited from the appropriate d-band center of Cu₃N for the adsorption and desorption of H species, as well as the promoted charge separation and interfacial electron transfer in the nanocrystal structure. In summary, these findings demonstrate the outstanding catalytic activity of Cu₃N in photocatalysis.

3.2. Electrocatalysis

In the last decades, TMNs have exhibited inherent merits over other metal materials in the electrocatalysis due to the covalent bond between N and the metal species in metal nitrides, which results in metal-like characteristics [41]. Moreover, the electron transfer between N atoms with metal atoms leads to the electron-donating character of TMNs, thus providing the high electrocatalytic activity of TMNs [42, 43]. In this context, Cu_3N has been widely used in electrocatalytic processes such as H_2 evolution reaction (HER), oxygen evolution reaction (OER), and carbon dioxide reduction reaction (CO_2RR). For example, Chen et al. prepared Cu_3N NC through a facile solution-phase process and applied it as cathode catalyst in alkaline fuel cells [29]. In the ORR, the Cu_3N NC showed outstanding catalytic activity comparable with or even better than that of other non-Pt materials.

Chen group has also reported that the Cu_3N NC with 30 nm size exhibited high catalytic activity in the ORR and nitrobenzene reduction [44]. The prepared Cu_3N NC showed magnetic hysteresis loop and prominent ferromagnetic resonance signals at room temperature. This research demonstrates that Cu_3N is a promising electrochemical sensor due to the relatively low detection limitation.

The catalytic activity of Cu_3N in CO_2RR was investigated by Sun et al. [30]. The study about CO_2RR using Cu_3N NC with different sizes revealed that the Cu_3N with 25 nm size and cubic morphology was the most active one in the selective conversion of CO_2 to C_2H_4 . The DFT calculation results demonstrate that the Cu(I) species in Cu_3N NC stabilized by N atoms plays an essential role in the reaction selectivity.

Cu_3N crystal is an ideal host structure because in its cubic lattice, the Cu atoms are positioned at the middle of the edges and the N atoms are situated at the corners of a cube [45]. As shown in **Figure 1-8** (a), the center of the cubic unit cell is empty so that an additional metal atom

such as Pd, Ag, Ni, and Cu can easily occupy the center to form a novel anti-perovskite structure (Cu_3MN) (**Figure 1-8** (b)). With the insertion of another metal atom into Cu_3N crystal, the formed Cu_3MN has several unique properties [46]. For instance, the Cu–N bond in Cu_3N is covalent bond, but the Cu_3PdN has metallic behavior. Therefore, the Cu_3MN has been considered as a good candidate catalyst for electrocatalysis.

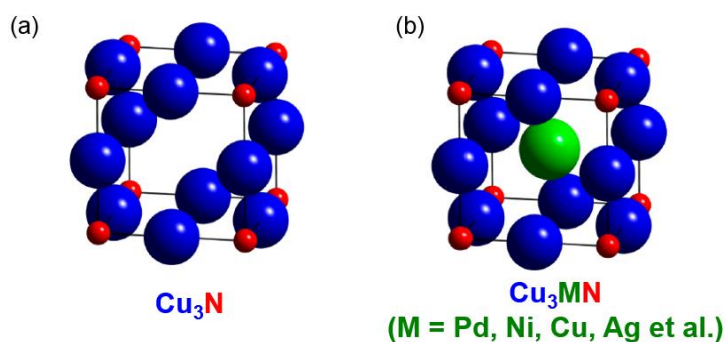


Figure 1-8. Crystal structure of (a) Cu_3N and (b) Cu_3MN .

In 2021, Schaak group developed Cu_3PdN NPs catalyst for the ORR under alkaline conditions [47]. The prepared Cu_3PdN NPs showed superior catalytic activity to Cu_3N and comparable catalytic performance to Pd NPs. Moreover, the stability of Cu_3PdN NPs was outperformed the synthesized Pd nanocrystals during repeated cycling.

The Cu_3PdN NCs were also applied to selective CO_2RR by Jia group [48]. The synthesized Cu_3PdN NCs showed higher electrocatalytic activity for CO_2 reduction to formic acid than as-prepared Cu_3N and Cu_3Pd NCs catalysts. This study made the conclusion that the distinguished catalytic performance of the Cu_3PdN NCs is attributed to the modification with N and Pd atoms.

It is generally accepted that functional supports significantly affect the electrocatalytic performance of catalysts [49]. The ideal functional supports should have a large surface area, good durability in harsh conditions, and high electronic conductivity. In this context, nitrogen-doped reduced graphene oxide supported Cu_3N (N-rGO/ Cu_3N) has significantly higher activity compared to

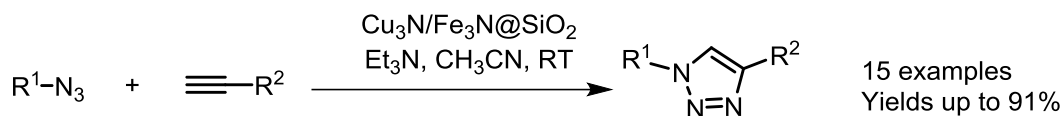
the as-synthesized Cu₃N and reduced graphene oxide supported Cu₃N (rGO/Cu₃N) [50]. The study revealed that the d10 configuration of Cu(I) weakens the strong adsorption of intermediate, and such an electronic effect enhances the overall performance of the composite catalyst.

A 3D NC@CoN/Cu₃N/CF electrocatalyst for highly efficient overall water splitting unique 3D configuration was reported by Liang group, the Cu₃N based-catalyst showed outstanding catalytic activity and stability toward HER and OER in alkaline conditions [51]. In addition, NC@CoN/Cu₃N/CF served as both the anode and cathode and delivered a current density of 10 mA cm⁻² at a quite low cell voltage of 1.62 V. Overall, these results clearly demonstrated that Cu₃N has high catalytic activity in electrocatalysis.

3.3. Organic catalysis

Organic synthesis is an essential basis for industries such as pharmaceuticals, biomedicine, and materials [52]. Cu catalyzed-organic synthesis has been considered as a useful and practical method for producing various important organic compounds, due to the tunable electronic property of Cu species and the resulted high catalytic activity [53, 54]. In this regard, Cu₃N has the Cu (+1) species, which is an active species for organic conversion. In addition, the Cu₃N lattice possesses a regularly arranged N–Cu–N structure on surface, which may serve as the N ligands assisted Cu complexes. These properties predicted that Cu₃N is a potential catalyst for organic reactions.

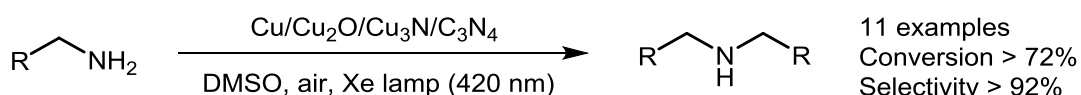
Hur group demonstrated that the click reaction of azides and alkynes was achieved over a mesoporous superparamagnetic silica microsphere supported copper nitride nanoparticles (Cu₃N/Fe₃N@SiO₂) (**Scheme 1-2**). This heterogeneous catalyst exhibited a comparable catalytic activity to Cu^I complexes with good reusability.



Scheme 1-2. Cu₃N/Fe₃N@SiO₂ catalyzed click reaction of azides and alkynes.

Recently, Qiao et al. prepared an atomically dispersed Pd₁/Cu₃N catalyst and applied to the *cis-to-trans* isomerization of alkenes [55]. The experimental results and theoretical calculations revealed that the H₂ dissociates heterolytically on Pd₁/Cu₃N to H^{δ+} and H^{δ-}, yielding excellent selectivity for both hydrogen-mediated isomerization and H-D exchange of alkenes.

Encouraged by the outstanding activity of Cu₃N in photocatalysis, Jiang group designed a novel photocatalyst (Cu/Cu₂O/Cu₃N/C₃N₄) for the oxidative self-coupling of benzylamine with Xe lamp (420 nm) (**Scheme 1-3**) [56]. The ternary Cu/Cu₂O/Cu₃N heterostructures have been successfully synthesized on C₃N₄ tubes through the hydrothermal synthesis and heat treatment. The high efficiency of the catalyst originated from their ability to provide large quantities of free oxygen radicals, for instance, hydroxyl radical (·OH) and superoxide radical (·O²⁻) species under visible-light irradiation.



Scheme 1-3. Oxidative coupling of benzylamines using Cu/Cu₂O/Cu₃N/C₃N₄ photocatalyst.

4. Purpose of this thesis

Over the past decades, the development of the green and sustainable chemical process that can alleviate environmental pollution and excessive resource consumption problems has become one of the important research targets in chemistry. Catalysts play an irreplaceable role in the chemical process since it improves the reaction efficiency and decreases energy consumption. Hitherto, many precious metal catalysts (e.g., Pt and Pd) have been developed and exhibited high performance in chemical conversions. However, the high cost and low reserve limit their application on an industrial scale. Hence, developing novel and efficient non-noble metal catalysts are highly desired for the chemical industry.

It is well known that the homogeneous Cu catalytic systems (e.g., Cu salts/N ligands) have been widely used in the organic reaction, because the electronic state of active Cu atoms are tunable through the combination with different N ligands, thus providing high reaction activity and selectivity. On the other hand, heterogeneous Cu catalysts, for example, Cu NPs have unique chemical and physical properties due to the size effect, and also exhibit outstanding catalytic performance in organic synthesis. Thus, Cu₃N nanocrystal possesses both the ligand effect from N atoms and naturally size effect, which is considered as an ideal heterogeneous catalyst for organic transformations (**Figure 1-**

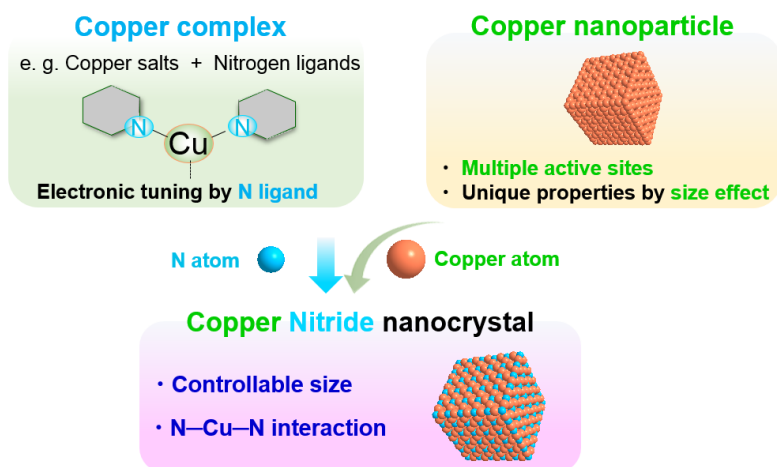


Figure 1-9. Design of high catalytic activity Cu₃N nanocrystal for organic reactions.

9). Even though the catalytic potential and activity of Cu_3N in photo- and electrocatalysis has been intensely studied in the last decades, the application of the Cu_3N to liquid-phase organic synthesis is rarely reported, which is of interest for organic and catalytic chemistry. In this regard, the author gave heed to discovering the unique catalytic potential of Cu_3N in the environmentally-benign organic reactions, which will provide many important contributions to environmental remediation. The main purpose of this thesis is to develop and synthesize efficient Cu_3N catalysts for green organic transformations. This study points out the important function of the interaction of N atoms with Cu atoms on the outstanding catalytic activity, thus providing Cu_3N a promising route for the next generation of applications.

5. Outline of this thesis

The present thesis deals with the study on the Cu_3N catalysis in the organic synthesis under environmental-friendly reaction conditions.

In chapter II, the authors prepared the nanocubic Cu_3N (nano- Cu_3N) and used it for the hydroxylation of various aryl halides under ligand-free conditions (**Figure 1-10**). In this nano- Cu_3N catalytic system, various aryl halides were transformed to phenols in good yields. This is the first example of the heterogeneous Cu-catalyzed hydroxylation of aryl chlorides without additives. Moreover, the nano- Cu_3N exhibited comparable catalytic activity with homogeneous Cu catalytic systems (Cu salts/N ligands), demonstrating that the N atoms in nano- Cu_3N may serve as a functional ligand to accelerate the hydroxylation of aryl halides.

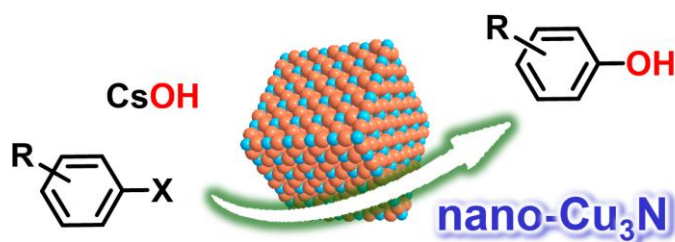


Figure 1-10. Highly efficient hydroxylation of aryl halides to phenols using nano- Cu_3N under ligand-free conditions.

In Chapter III, the author demonstrated the green oxidation of indoles catalyzed by Cu_3N nanocube ($\text{Cu}_3\text{N NC}$) (**Figure 1-11**). With oxygen (O_2) as single oxidant, several indolin-3-ones and 2-ketoanilide derivatives were efficiently obtained over $\text{Cu}_3\text{N NC}$ catalyst. This is the first example of a non-noble-metal heterogeneous catalyst for improving the O_2 -mediated trimerization and Witkop reaction of indoles under additive-free conditions. The high reaction efficiency is attributed to the activation of O_2 to superoxide species achieved over the N-Cu-N sites on $\text{Cu}_3\text{N NC}$.

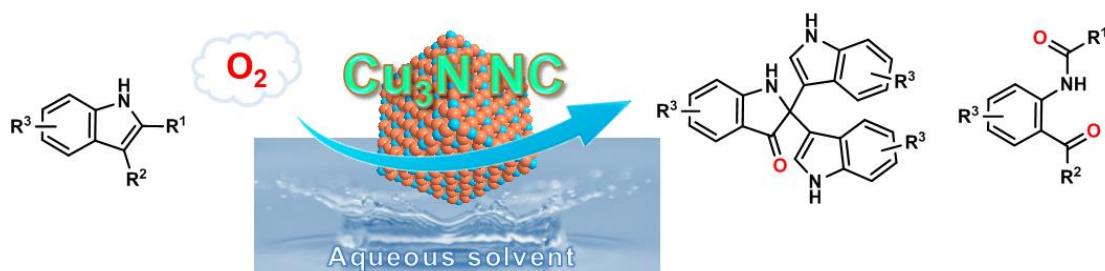


Figure 1-11. Oxidative trimerization and Witkop reactions of indoles catalyzed by Cu₃N NC.

The next chapter describes the hydroboration of alkynes to vinyl boronate esters by Cu₃N NC catalyst (**Figure 1-12**). This method showed broad substrate scope and good functional group tolerance. This is the first time that the hydroboration of alkynes is achieved over a heterogeneous Cu catalyst under mild and additive-free conditions. The spectroscopic analyses and deuterium-labeling study revealed that cooperative effect of Cu (Lewis acid) and nitrogen atoms (Lewis base) on the Cu₃N NC surface enables the activation of alcohol, diboron reagents, and alkynes, thus promoting the hydroboration of alkynes.

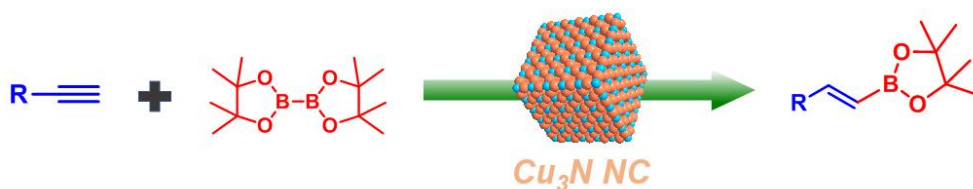


Figure 1-12. Selective hydroboration of alkynes over Cu₃N NC catalyst.

The final chapter represents a general method for synthesizing diverse silanes through the hydrosilylation of unsaturated organic compounds catalyzed by Cu₃N NC catalyst (**Figure 1-13**). Under the base and solvent-free conditions, a wide variety of substrates, including alkynes, alkenes, and imines, was converted to the corresponding silanes in good yields, which provides a green and sustainable strategy for preparation of silanes.

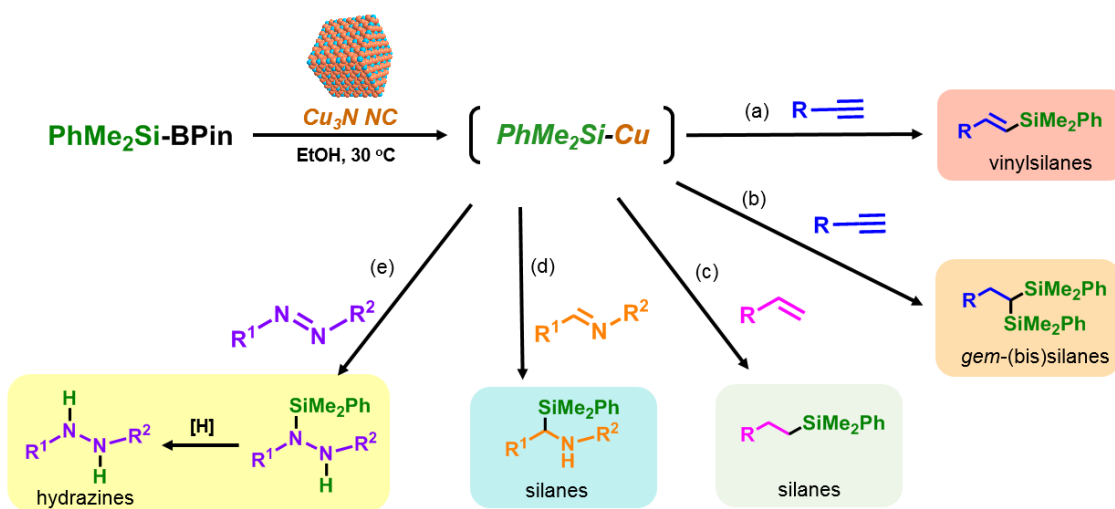


Figure 1-13. $\text{Cu}_3\text{N NC}$ catalyzed-hydrosilylation of unsaturated compounds to silanes.

Finally, the author made a general conclusion of the present thesis and the scope for the further application of the Cu_3N catalyst.

References

1. A. Seaton, D. Godden, W. MacNee, K. Doanldson, *Lancet*, **1995**, *345*, 176–178.
2. P. T. Anastas, J. C. Warner, *Frontiers*, **1998**, *640*.
3. J. A. Dionne, A. Baldi, B. Baum, C. S. Ho, V. Janković, G. V. Naik, T. Narayan, Y. Zhao, *Mrs Bull.*, **2015**, *40*, 1138–1145.
4. R. M. Bullock, J. G. Chen, L. Gagliardi, P. J. Chirik, O. K. Farha, C. H. Hendon, C. W. Jones, J. A. Keith, J. Klosin, S. D. Minter, R. H. Morris, A. T. Radosevich, T. B. Rauchfuss, N. A. Strotman, A. Vojvodic, T. R. Ward, J. Y. Yang, Y. Surendranath, *Science*, **2020**, *369*, eabc3183.
5. M. Sankar, N. Dimitratos, P. J. Miedziak, P. P. Wells, C. J. Kiely, G. J. Hutchings, *Chem. Soc. Rev.*, **2012**, *41*, 8099–8139.
6. K. D. Gilroy, A. Ruditskiy, H. C. Peng, D. Qin, Y. Xia, *Chem. Rev.*, **2016**, *116*, 10414–10472.
7. S. Fujita, K. Nakajima, J. Yamasaki, T. Mizugaki, K. Jitsukawa, T. Mitsudome, *ACS Catal.*, **2020**, *10*, 4261–4267.
8. T. Mitsudome, M. Sheng, A. Nakata, J. Yamasaki, T. Mizugaki, K. Jitsukawa, *Chem. Sci.*, **2020**, *11*, 6682–6689.
9. H. Ishikawa, S. Yamaguchi, A. Nakata, K. Nakajima, S. Yamazoe, J. Yamasaki, T. Mizugaki, T. Mitsudome, *JACS Au*, **2022**, *2*, 419–427.
10. M. Idrees, A. Mukhtar, S. M. Abbas, Q. Zhang, X. Li, *Mater. Today Commun.*, **2021**, *27*, 102363.
11. T. Rao, W. Cai, H. Zhang, W. Liao, *J. Mater. Chem. C*, **2021**, *9*, 5323–5342.
12. K. Schwarz, *Solid State Mater. Sci.*, **1987**, *13*, 211–257.
13. D. T. Tran, T. Kshetri, N. D. Chuong, J. Gautam, H. Van Hien, N. H. Kim, J. H. Lee, *Nano Today*, **2018**, *22*, 100–131.
14. Y. Zhong, X. Xia, F. Shi, J. Zhan, J. Tu, H. J. Fan, *Adv. Sci.*, **2016**, *3*, 1500286.
15. J. Xie, Y. Xie, *Chem. Eur. J.*, **2016**, *22*, 3588–3598.

16. P. Deka, B. J. Borah, H. Saikia, P. Bharali, *Chem. Rec.*, **2019**, *19*, 462–473.
17. A. Kuzmin, A. Anspoks, A. Kalinko, J. Timoshenko, L. Nataf, F. Baudelet, T. Irifune, *Phys. Status Solidi.*, **2018**, *255*, 1800073.
18. J. G. Zhao, S. J. You, L. X. Yang, C. Q. Jin, *Solid State Commun.*, **2010**, *150*, 1521–1524.
19. P. Paredes, E. Rauwel, P. Rauwel, *Nanomaterials*, **2022**, *12*, 2218.
20. A. Jiang, M. Qi, J. Xiao, *J. Mater. Sci. Technol.*, **2018**, *34*, 1467–1473.
21. A. Scigala, E. Szlyk, T. Rerek, M. Wiśniewski, L. Skowronski, M. Trzcinski, R. Szczesny, *Materials*, **2021**, *14*, 603.
22. G. Paniconi, Z. Stoeva, H. Doberstein, R. I. Smith, B. L. Gallagher, D. H. Gregory, *Solid State Sci.*, **2007**, *9*, 907–913.
23. B. S. Lee, M. Yi, S. Y. Chu, J. Y. Lee, H. R. Kwon, K. R. Lee, D. Kang, W. S. Kim, H. B. Lim, J. Lee, H.-J. Youn, D. Y. Chi, N. H. Hu, *Chem. Commun.*, **2010**, *46*, 3935–3937.
24. S. D. Yim, S. J. Kim, J. H. Baik, I. S. Nam, Y. S. Mok, J. H. Lee, K. C. Byong, S. H. Oh, *Ind. Eng. Chem. Res.*, **2004**, *43*, 4856–4863.
25. C. Panda, P. W. Menezes, M. Zheng, S. Orthmann, M. Driess, *ACS Energy Lett.*, **2019**, *4*, 747–754.
26. S. A. Rasaki, B. Zhang, K. Anbalgam, T. Thomas, M. Yang, *Prog. Solid State Chem.*, **2018**, *50*, 1–15.
27. A. K. Tareen, G. S. Priyanga, S. Behara, T. Thomas, M. Yang, *Prog. Solid State Chem.*, **2019**, *53*, 1–26.
28. T. Nakamura, H. Hayashi, T. A. Hanaoka, T. Ebina, *Inorg. Chem.*, **2014**, *53*, 710–715.
29. H. Wu, W. Chen, *J. Am. Chem. Soc.*, **2011**, *133*, 15236–15239.
30. R. Deshmukh, G. Zeng, E. Tervoort, M. Staniuk, D. Wood, M. Niederberger, *Chem. Mater.*, **2015**, *27*, 8282–8288.

31. Z. Yin, C. Yu, Z. Zhao, X. Gou, M. Shen, L. Na, M. Muzzio, J. Li, H. Liu, H. Lin, J. Yin, G. Lu, D. Su, S. Sun, *Nano Lett.*, **2019**, *19*, 8658–8663.
32. C. Y. Su, B. H. Liu, T. J. Lin, Y. M. Chi, C. C. Kei, K. W. Wang, T. P. Perng, *J. Mater. Chem. A*, **2015**, *3*, 18983–18990.
33. Z. Cheng, W. Qi, C. H. Pang, T. Thomas, T. Wu, S. Liu, M. Yang, *Adv. Funct. Mater.*, **2021**, *31*, 2100553.
34. N. Han, P. Liu, J. Jiang, L. Ai, Z. Shao, S. Liu, *J. Mater. Chem. A*, **2018**, *6*, 19912–19933.
35. B. S. Richards, D. Hudry, D. Busko, A. Turshatov, I. A. Howard, *Chem. Rev.*, **2021**, *121*, 9165–9195.
36. R. K. Sithole, L. F. Machogo, M. J. Moloto, S. S. Gqoba, K. P. Mubiayi, J. Van Wyk, N. Moloto, *J. Photochem. Photobiol. A*, **2020**, *397*, 112577.
37. A. Jiang, H. Shao, L. Zhu, S. Ma, J. Xiao, *Materials*, **2020**, *13*, 4325.
38. T. W. van Deelen, C., Hernández Mejía, K. P. de Jong, *Nature Catal.*, **2019**, *2*, 955–970.
39. D. Barman, S. Paul, S. Ghosh, S. K. De, *ACS Appl. Nano Mater.*, **2019**, *2*, 5009–5019.
40. Q. Guo, F. Liang, Z. Sun, Y. Wang, X. B. Li, S. G. Xia, Z. C. Zhang, L. Huang, L. Z. Wu, *J. Mater. Chem. A*, **2020**, *8*, 22601–22606.
41. A. Scigala, E. Szlyk, L. Dobrzanska, D. H. Gregory, R. Szczesny, *Coord. Chem. Rev.*, **2021**, 436, 213791.
42. Z. Liu, M. Zha, Q. Wang, G. Hu, L. Feng, *Chem. Commun.*, **2020**, *56*, 2352–2355.
43. Y. Liu, J. Zhang, Y. Li, Q. Qian, Z. Li, Y. Zhu, G. Zhang, *Nature Commun.*, **2020**, *11*, 1–13.
44. P. Xi, Z. Xu, D. Gao, F. Chen, D. Xue, C. L. Tao, Z. N. Chen, *RSC Adv.*, **2014**, *4*, 14206–14209.
45. M. G. Moreno-Armenta, W. L. Pérez, N. Takeuchi, *Solid State Sci.*, **2007**, *9*, 166–172.
46. N. Lu, A. Ji, Z. Cao, *Sci. Rep.*, **2013**, *3*, 1–6.
47. D. D. Vaughn II, J. Araujo, P. Meduri, J. F. Callejas, M. A. Hickner, R. E. Schaak, *Chem. Mater.*,

- 2014, 26, 6226–6232.
48. J. Jia, X. Hao, Y. Chang, M. Jia, Z. Wen, *J. Colloid Interface Sci.*, **2021**, 586, 491–497.
 49. S. Kim, J. Park, J. Hwang, J. Lee, *EnergyChem*, **2021**, 3, 100054.
 50. S. Mondal, C. R. Raj, *J. Phys. Chem. C*, **2018**, 122, 18468–18475.
 51. H. L. Wang, T. Liu, Z. H. Zhu, J. M. Peng, H. H. Zou, F. P. Liang, *Inorg. Chem. Front.*, **2021**, 8, 2136–2143.
 52. D. Seebach, *Angew. Chem. Int. Ed.*, **1990**, 29, 1320–1367.
 53. S. R. Chemler, *Beilstein J. Org. Chem.*, **2015**, 11, 2252–2253.
 54. S. E. Allen, R. R. Walvoord, R. Padilla-Salinas, M. C. Kozlowski, *Chem. Rev.*, **2013**, 113, 6234–6458.
 55. Y. Guo, B. Qiao, *Chem Catal.*, **2021**, 1, 1362–1365.
 56. Y. Fu, M. Zheng, Q. Li, L. Zhang, S. Wang, V. V. Kondratiev, B. Jiang, *RSC Adv.*, **2020**, 10, 28059–28065.

Chapter II.

*Highly Active Copper Nitride Catalyst
for Hydroxylation of Aryl Halides*

1. Introduction

Phenols as an important class of organic compounds are widely existed in natural compounds, advanced polymers, and pharmaceuticals [1, 2]. The traditional reaction focusing on Pd salts/P ligands-catalyzed coupling of aryl halides with metal hydroxides is a useful approach for the preparation of phenols and attracted high attentions [3–7]. In the last decades, the Cu-based catalytic system has been developed and considered as an alternative to prepare phenols, due to the comparable catalytic activity to palladium systems. For example, in 2011, the Taillefer and You groups have reported the copper iodide (CuI) catalyst for the hydroxylation of aryl iodides using functional nitrogen ligands [8, 9]. More recently, several efficient homogeneous cuprous oxide (Cu₂O)/ligands catalytic systems have also been developed for the hydroxylation of aryl halides [10–12]. Despite the outstanding catalytic performance of reported homogenous Cu catalytic systems, they have some drawbacks, for example, the utilization of organic ligands and non-recyclable Cu catalysts. On the contrary, heterogeneous Cu catalysts (e.g., CuI nanoparticles and supported-copper oxide) showed outstanding reusability in the absence of additive ligands [13, 14]. In 2011, Han et al. disclosed that the functional graphitic carbon nitride (g-C₃N₄) support can serve as a functional N-ligand for Cu species and accelerates the hydroxylation of aryl halides [15]. However, these catalytic systems exhibited low tolerance for bromide substrates. Consequently, the development of heterogeneous Cu catalyst with outstanding efficiency for the hydroxylation of aryl halides is strongly desired.

Nano-sized metal non-oxide compounds have a wide range of applications in several fields [16]. Particularly, metal carbides, metal nitrides, and metal phosphides, which exhibited higher activity, selectivity, and durability in catalysis than those of pure metal NPs [17, 18]. In the last decade, among the metal non-oxide nanoparticles, copper nitride (Cu₃N), which consist of Cu and N atoms, are widely used in photo- and electrocatalysis due to its unique electronic structure [19–21]. The corner-shared Cu–N octahedra in Cu₃N crystal structure are suitable for interaction with organic molecules in organic

synthesis [22, 23]. Moreover, the formal oxidation state of Cu species in Cu_3N is +1, making Cu_3N possesses Lewis acidic property. Therefore, unlike the conventional Cu catalysts, Cu_3N is expected to have high potential in organic synthesis. Inspired by these perspectives, the author paid attention to the application of Cu_3N in hydroxylation of aryl halides.

Herein, in this chapter, the author reported that nano- Cu_3N was prepared through calcination method and utilized as an efficient catalyst for the hydroxylation of aryl halides. The nano- Cu_3N catalyst exhibited high catalytic performance and was comparable to that of conventional Cu catalysts with N ligands, indicating that the N atoms in Cu_3N may serve as functional ligands to accelerate the hydroxylation reaction. Notably, this approach showed broad substrate scope and good functional group tolerance, affording a wide range of phenols. This is the first time that the hydroxylation of aryl chlorides was achieved over a heterogeneous Cu catalyst under additive-free conditions.

2. Experimental section

2.1. General

All organic reagents were purchased from FUJIFILM Wako Pure Chemical Corporation, Sigma–Aldrich, or Tokyo Chemical Industry. Gas chromatography–mass spectrometry (GC-MS) was performed using a Shimadzu GCMS-QP2010 SE instrument equipped with an Inert Cap WAX-HT capillary column (30 m × 0.25 mm i.d. film thickness 0.25 μm). ¹H and ¹³C NMR spectra were acquired at 400 and 100 MHz, respectively, using a JEOL JNM-ESC400 spectrometer. Chemical shifts are reported in parts per million (ppm) relative to the signal (0.00 ppm) for internal tetramethylsilane in CDCl₃ or (CD₃)₂SO. The ¹H NMR spectral data are reported using the following standard chemical shifts: CDCl₃ (7.26 ppm) and (CD₃)₂SO (2.50 ppm). The ¹³C NMR spectral data are reported using the following standard chemical shifts: CDCl₃ (77.16 ppm) and (CD₃)₂SO (39.52 ppm). NMR multiplicities are reported using the following abbreviations: s: singlet, d: doublet, t: triplet, q: quartet, m: multiplet, br: broad, J: coupling constants in hertz. All known compounds described in the paper were characterized by comparison of their ¹H and ¹³C NMR spectra with previously reported data. Scanning electron microscopy (SEM) images were obtained using a Hitachi SU6600 microscope operated at 5.0 kV at the Analytical Instrument Facility, Graduate School of Science, Osaka University. Transmission electron microscopy (TEM) images were obtained using a Hitachi HF-2000 microscope operated at 200 kV at the Research Center for Ultra-High Voltage Electron Microscopy, Osaka University. Cu *K*-edge X-ray absorption spectra (extended X-ray absorption fine structure (EXAFS) and X-ray absorption near edge structure (XANES)) obtained using a Si (111) monochromator were recorded at 25 °C at the BL01B1 and BL14B2 stations, SPring-8, Japan Synchrotron Radiation Research Institute (JASRI), Harima, Japan (promotion numbers: 2020A1487 and 2020A1640). Data analysis was performed using Demeter (ver. 0.9.26). After normalization at edge height, the *k*²-weighted χ spectra were extracted. The *k*²-weighted χ spectra in the *k* range of 3–13 Å⁻¹ was Fourier-

transformed (FT) into the R-space. Curve-fitting analysis was conducted in the R range of 1.0–3.0 Å using the back-scattering amplitude and phase shift functions of Cu–N and Cu–Cu, which were calculated with the FEFF6 program. Powder X-ray diffraction (PXRD) patterns were acquired using a Philips XPert-MPD instrument with Cu-K α radiation.

2.2. Preparation of catalysts

Synthesis of Cu₃N: In a typical synthesis, urea (1.50 g, 25 mmol) and copper (II) acetate (Cu(OAc)₂) (300 mg, 1.5 mmol) were added in two different porcelain boats in a quartz tube. Then, the materials were heated to 300 °C and maintained at the same temperature for 2 h under N₂ flow. After cooling to room temperature, the black solid product (nano-Cu₃N) was collected without further purification.

Synthesis of copper phosphide: The copper phosphide (Cu₃P) was prepared through the reported method [24]. In a typical synthesis, aqueous solutions of copper nitrate (50 mL, 0.05 M) and NaOH (10 mL, 0.25 M) were placed in a flask. The mixture was stirred for 2 h at room temperature. Then, the obtained precipitates (copper hydroxide, Cu(OH)₂) were collected via filtration and dried under vacuum at 60 °C for 6 h. Next, the as-prepared Cu(OH)₂ (0.2 g, 2.0 mmol) and sodium hypophosphite (NaH₂PO₂, 1.0 g, 11.4 mmol) were mixed in a porcelain boat, and the mixtures were calcined at 300 °C for 1 h under N₂ flowing. The obtained black Cu₃P powder was filtered and washed with deionized (DI) water and ethanol three times and dried at 80 °C for 4 h *in vacuo*.

2.3. Reaction procedure

The general reaction procedure for the hydroxylation of aryl halides using nano-Cu₃N was as follows. nano-Cu₃N (5 mg, 11.8 mol%) was placed in a 30 mL pressure tube, followed by addition

of aryl halides (0.5 mmol), cesium hydroxide (CsOH) (6 eq. of aryl halides), and 2 mL of dimethylsulfoxide (DMSO)/H₂O (v/v = 1/1) mixture under argon atmosphere. The reaction mixture was stirred at 100 or 120 °C for 12 or 48 h. After the reaction, the reaction mixture was neutralized with a few drops of aqueous HCl (6 M HCl). Then, the resulting mixture was extracted using ethyl acetate for three times. The combined organic layers were collected and dried over anhydrous MgSO₄, filtered, and concentrated under reduced pressure. Finally, the obtained crude product was purified by flash column chromatography on silica gel (200–300 mesh).

2.4. Product identification

***p*-methoxyphenol**

CAS registry No. [150-76-5], white solid; ¹H NMR (400 MHz, CDCl₃): δ 6.71–6.69 (m, 4H), 5.62 (s, 1H), 3.67 (s, 3H); ¹³C NMR (100 MHz, CDCl₃): δ 153.7, 149.7, 116.2, 115.1, 56.0.

***p*-cresol**

CAS registry No. [106-44-5], colorless liquid; ¹H NMR (400 MHz, CDCl₃): δ 7.03 (d, *J* = 8.0 Hz, 2H), 6.73 (d, *J* = 8.0 Hz, 2H), 4.71 (s, 1 H), 2.27 (s, 3H); ¹³C NMR (100 MHz, CDCl₃): δ 153.4, 130.2, 130.1, 115.2, 20.6.

***m*-methoxyphenol**

CAS registry No. [150-19-6], colorless liquid; ¹H NMR (400 MHz, CDCl₃): δ 7.12 (t, *J* = 8.0 Hz, 1H), 6.51–6.44 (m, 1H), 6.42–6.42 (m, 2H), 5.41 (s, 1H), 3.76 (s, 3H); ¹³C NMR (100 MHz, CDCl₃): δ 161.0, 156.8, 130.3, 108.1, 106.6, 101.7, 55.4.

***m*-cresol**

CAS registry No. [108-39-4], colorless liquid; ¹H NMR (400 MHz, CDCl₃): δ 7.16 (t, *J* = 7.6 Hz, 1H), 6.81–6.77 (m, 1H), 6.70–6.68 (m, 2H), 5.47 (s, 1H), 2.33 (s, 3H); ¹³C NMR (100 MHz, CDCl₃): δ 155.4, 134.0, 129.6, 121.8, 116.2, 112.5, 21.4.

***p*-nitrophenol**

CAS registry No. [100-02-7], yellow solid; ¹H NMR (400 MHz, CDCl₃): δ 8.10 (d, *J* = 8.8 Hz, 2H), 6.86 (d, *J* = 8.4 Hz, 2H), 6.12 (s, 1H); ¹³C NMR (100 MHz, CDCl₃): δ 161.6, 141.8, 126.5, 115.9.

4-hydroxybenzoic acid

CAS registry No. [99-96-7], white solid; ¹H NMR (400 MHz, DMSO): δ 12.41 (s, 1H), 10.22 (s, 1H), 7.79 (d, *J* = 8.8 Hz, 2H), 6.82 (d, *J* = 8.8 Hz, 2H); ¹³C NMR (100 MHz, DMSO): δ 167.2, 161.7, 131.6, 121.4, 115.2.

1-(4-hydroxyphenyl)ethan-1-one

CAS registry No. [99-93-4], white solid; ¹H NMR (400 MHz, CDCl₃): δ 7.92 (d, *J* = 8.8 Hz, 2H), 6.95 (d, *J* = 8.8 Hz, 2H), 2.59 (s, 3H); ¹³C NMR (100 MHz, CDCl₃): δ 199.1, 161.8, 131.4, 129.5, 115.7, 26.4.

biphenyl-4-ol

CAS registry No. [92-69-3], white solid; ¹H NMR (400 MHz, DMSO): δ 9.49 (s, 1H), 7.54–7.51 (m, 2H), 7.45–7.43 (m, 2H), 7.38–7.34 (m, 2H), 7.25–7.21 (m, 1H), 6.84–6.81 (m, 2H); ¹³C NMR (100 MHz, DMSO): δ 157.1, 140.2, 131.9, 128.8, 127.7, 126.3, 125.9, 115.7.

1,2-dihydroxybenzene

CAS registry No. [120-80-9], white solid; ¹H NMR (400 MHz, DMSO): δ 8.80 (s, 2H), 6.79–6.76 (m, 2H), 6.66–6.63 (m, 2H); ¹³C NMR (100 MHz, DMSO): δ 145.3, 119.3, 115.7.

3,5-dimethylphenol

CAS registry No. [108-68-9], white solid; ¹H NMR (400 MHz, CDCl₃): δ 6.50 (s, 1H), 6.38 (s, 2H), 4.79 (s, 1H), 2.18 (s, 6H); ¹³C NMR (100 MHz, CDCl₃): δ 155.5, 139.7, 122.7, 113.2, 21.3.

***o*-methoxyphenol**

CAS registry No. [90-05-1], colorless liquid; ¹H NMR (400 MHz, CDCl₃): δ 6.97–6.94 (m, 1H), 6.90–6.88 (m, 3H), 5.69 (s, 1H), 3.89 (s, 3H); ¹³C NMR (100 MHz, CDCl₃): δ 146.7, 145.8, 121.6, 120.3, 114.7, 110.9, 56.0.

***p*-fluorophenol**

CAS registry No. [371-41-5], colorless liquid; ¹H NMR (400 MHz, CDCl₃): δ 6.86–6.82 (m, 2H), 6.70–6.67 (m, 2H), 5.00 (s, 1H); ¹³C NMR (100 MHz, CDCl₃): δ 158.7, 156.3, 151.6, 116.4.

***p*-chlorophenol**

CAS registry No. [106-48-9], colorless liquid; ¹H NMR (400 MHz, CDCl₃): δ 7.11 (d, *J* = 8.0 Hz, 2H), 6.69 (d, *J* = 8.0 Hz, 2H), 5.08 (s, 1H); ¹³C NMR (100 MHz, CDCl₃): δ 154.2, 129.7, 125.9, 116.8.

***o*-chlorophenol**

CAS registry No. [95-57-8], colorless liquid; ^1H NMR (400 MHz, CDCl_3): δ 7.30 (d, $J = 8.0$ Hz, 1H), 7.17 (t, $J = 8.0$ Hz, 1H), 7.01 (d, $J = 8.0$ Hz, 1H), 6.86 (t, $J = 8.0$ Hz, 1H), 5.57 (s, 1H); ^{13}C NMR (100 MHz, CDCl_3): δ 151.5, 129.1, 128.5, 121.5, 120.0, 116.4.

***p*-bromophenol**

CAS registry No. [106-41-2], colorless liquid; ^1H NMR (400 MHz, CDCl_3): δ 7.26 (d, $J = 8.8$ Hz, 2H), 6.65 (d, $J = 8.8$ Hz, 2H), 4.92 (s, 1H); ^{13}C NMR (100 MHz, CDCl_3): δ 154.8, 132.6, 117.4, 113.1.

phenol

CAS registry No. [108-95-2], colorless liquid; ^1H NMR (400 MHz, CDCl_3): δ 7.26–7.21 (m, 2H), 6.95–6.91 (m, 1H), 6.84–6.82 (m, 2H), 5.00 (s, 1H); ^{13}C NMR (100 MHz, CDCl_3): δ 155.6, 129.8, 121.0, 115.5.

naphthalen-1-ol

CAS registry No. [90-15-3], white solid; ^1H NMR (400 MHz, CDCl_3): δ 8.09–8.07 (m, 1H), 7.72–7.70 (m, 1H), 7.39–7.38 (m, 2H), 7.34 (d, $J = 8.4$ Hz, 1H), 7.17 (t, $J = 7.6$ Hz, 1H), 6.68 (d, $J = 8.4$ Hz, 1H), 5.32 (s, 1H); ^{13}C NMR (100 MHz, CDCl_3): δ 151.5, 134.9, 127.8, 126.6, 126.0, 125.4, 124.5, 121.7, 120.8, 108.8.

3-hydroxypyridine

CAS registry No. [109-00-2], white solid; ^1H NMR (400 MHz, DMSO): δ 9.94 (s, 1H), 8.14 (br, 1H), 8.03 (br, 1H), 7.23–7.14 (m, 2H); ^{13}C NMR (100 MHz, DMSO): δ 153.7, 140.3, 138.0, 124.2, 122.0.

3. Results and discussion

3.1. Characterization of nano-Cu₃N

Firstly, the prepared Cu₃N was analyzed by PXRD measurement and the result was shown in **Figure 2-1** (a), which reveals five diffraction peaks corresponding to phase-pure Cu₃N [25]. SEM and TEM images of nano-Cu₃N validate the cubic morphology with a ranging width from 50 to 200 nm (**Figures 2-1** (b) and (c)). The high-resolution TEM (HR-TEM) images showed the lattice fringes of 0.38 and 0.22 nm, which are attributed to the (100) and (111) planes, respectively, of cubic Cu₃N (**Figure 2-1** (d)). Next, to understand the oxidation state of nano-Cu₃N, X-ray absorption fine structure (XAFS) analysis was conducted. The XANES spectra of nano-Cu₃N and reference Cu compounds (e.g., CuO, Cu₂O, and Cu foil), reveal that the absorption edge energy of nano-Cu₃N close to that of Cu₂O, demonstrates the oxidation state of Cu species in nano-Cu₃N is +1 (**Figure 2-1** (e)) [25]. The EXAFS spectra of nano-Cu₃N in **Figure 2-1** (f) indicated there has two main peaks around 1.8 and 2.3 Å, which are attributed to those from Cu–N and Cu–Cu scattering [26]. Overall, these observations clearly confirmed the successful preparation of phase-pure cubic Cu₃N.

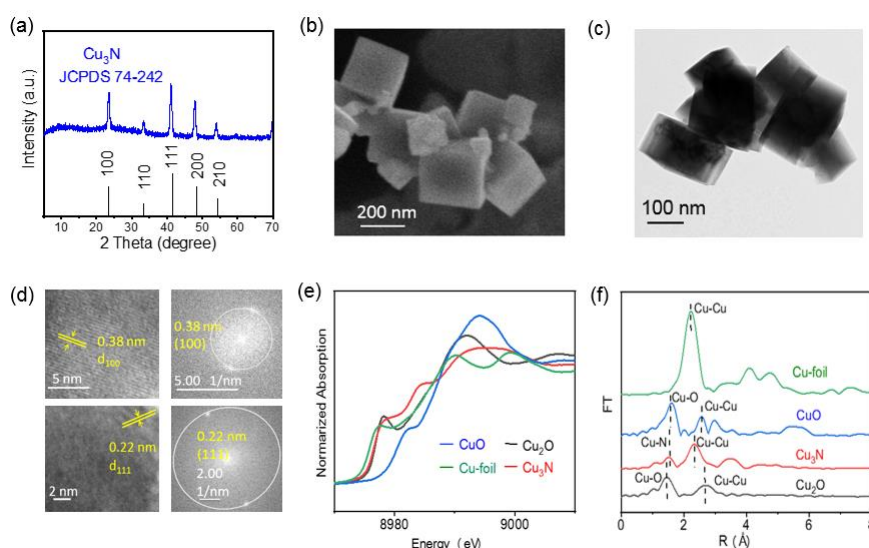


Figure 2-1. (a) PXRD patterns, (b) SEM, (c) TEM, and (d) HR-TEM images of nano-Cu₃N. (e) XANES and (f) EXAFS spectra of nano-Cu₃N, CuO, Cu₂O, and Cu-foil.

3.2. Catalytic activity in hydroxylation of 4-iodoanisole (**1a**)

The catalytic performance of nano-Cu₃N NC was investigated in the hydroxylation of **1a** as the model reaction (**Table 2-1**). It is worth noting that nano-Cu₃N exhibited high activity, and **1a** was efficiently transformed to 4-methoxyphenol (**2a**) in 94% yield without any additive ligands (entry 1). On the contrary, conventional Cu catalysts, e.g., Cu₂O, CuI, CuO, and Cu(OAc)₂, exhibited lower

Table 2-1. Hydroxylation of **1a** over various Cu catalysts.^a

Reaction scheme: **1a** (4-iodoanisole) + **MOH** $\xrightarrow[\text{DMSO/H}_2\text{O}]{\text{Catalyst, Ar}}$ **2a** (4-methoxyphenol)

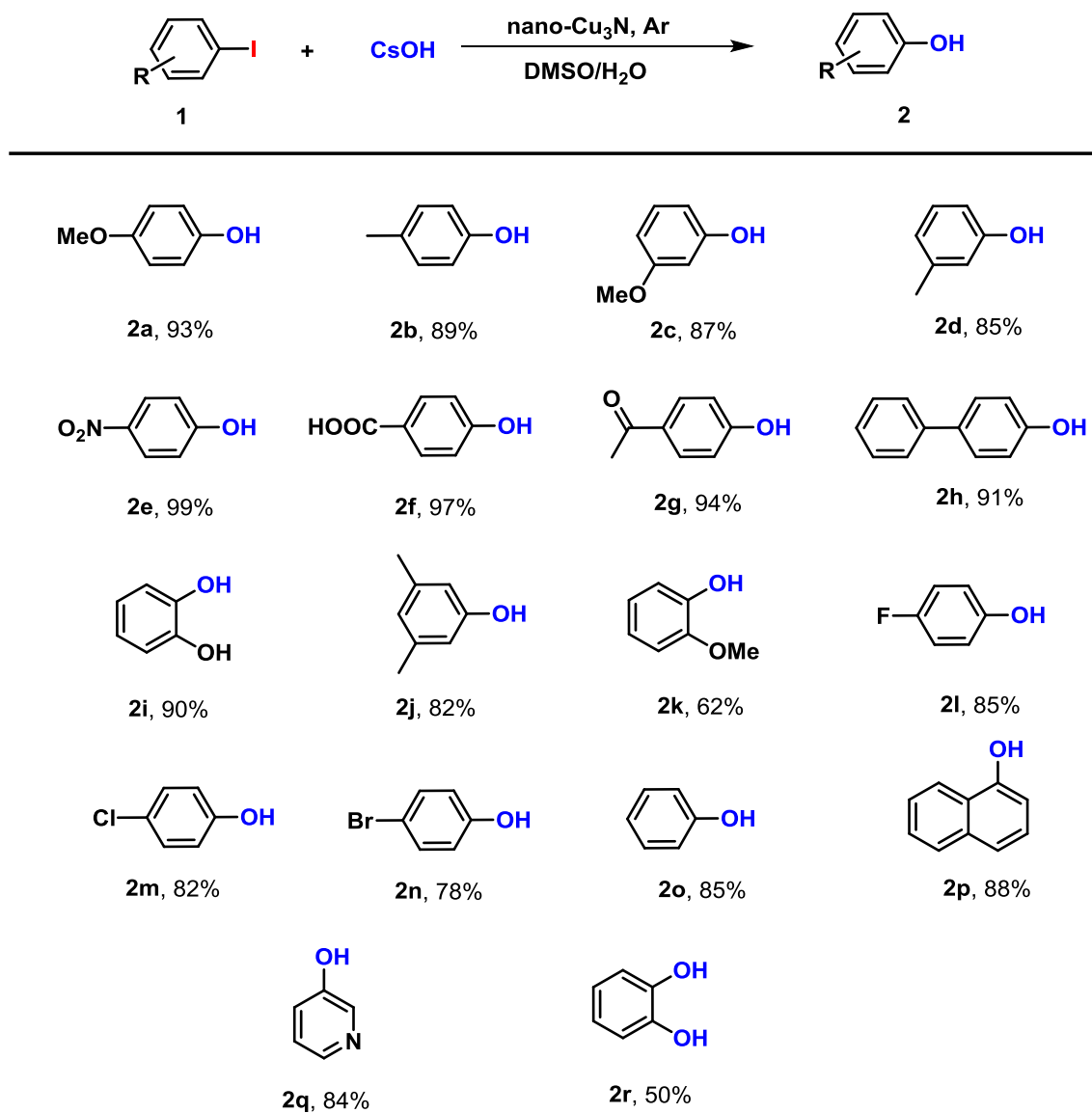
Entry	Catalyst	Base	T (°C)/Time	Yield of 2a ^b (%)
1	nano-Cu ₃ N	NaOH	120/12	94
2	Cu ₂ O	NaOH	120/12	75
3	CuI	NaOH	120/12	63
4	CuO	NaOH	120/12	32
5	Cu(OAc) ₂	NaOH	120/12	26
6 ^c	CuI + Phen	NaOH	120/12	98
7 ^c	Cu ₂ O + Phen	NaOH	120/12	97
8 ^d	Cu ₂ O + TEMDA	NaOH	120/12	86
9	Cu ₃ P	NaOH	120/12	29
10	nano-Cu ₃ N	NaOH	100/12	67
11	nano-Cu ₃ N	KOH	100/12	46
12 ^e	nano-Cu ₃ N	TBAOH	100/12	85
13	nano-Cu ₃ N	CsOH	100/12	99
14	-	CsOH	100/12	0

^a Reaction conditions: **1a** (0.5 mmol), catalyst (Cu: 11.8 mol%), base (3.0 mmol), and H₂O/DMSO = 1 : 1 (2 mL) under Ar. ^b Yields were determined by gas chromatography-mass spectrometry (GC-MS) using naphthalene (0.2 mmol) as an internal standard. ^c Phen = 1,10-phenanthroline (20 mol%). ^d TEMDA = *N,N,N',N'*-tetramethylethylenediamine (20 mol%). ^e TBAOH = tetrabutylammonium hydroxide.

catalytic activity than that of nano-Cu₃N (entries 2–5). To verify the effect of the N atoms in nano-Cu₃N in this reaction, several control experiments were performed. Firstly, when the additional N-ligands for example 1,10-phenanthroline (phen) and *N,N,N',N'*-tetramethyl-ethylenediamine (TMEDA) were added with CuI and Cu₂O, yields of **2a** were comparable to that of nano-Cu₃N (entries 6–8). Moreover, Cu₃P, another Cu–non-metal catalyst, was examined, and only 29% yield of **2a** was obtained (entry 9), demonstrating that the N atoms in nano-Cu₃N plays an essential role in improving the hydroxylation reaction. Moreover, the effect of base on this reaction was investigated. When the cesium hydroxide (CsOH) was used instead of sodium hydroxide (NaOH), **2a** was produced with a 99% yield under a milder reaction condition (entry 13 vs. entries 10–12). The reaction could not proceed under Cu catalyst-free conditions (entry 14). Accordingly, the high catalytic activity of nano-Cu₃N may attribute to the interaction of N atom with Cu species.

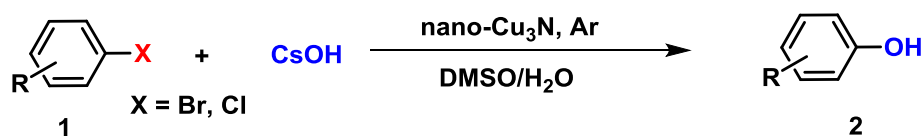
The general applicability for nano-Cu₃N-catalyzed hydroxylation of aryl halides was further investigated. The results were summarized in **Scheme 2-1**. Aryl iodides with electron-donating (–OCH₃ and –CH₃) and electron-withdrawing groups (–NO₂, –COOH, –COCH₃, –Ph, and –OH) exhibited high reactivity, providing the desired phenols in excellent yields (**2a–2i**). Moreover, hydroxylation of aryl iodides with bulky substituents proceeded well to generate **2j** and **2k** in 82% and 62% yields, respectively. 4-Fluoro-1-iodobenzene, 4-chloro-1-iodobenzene, and 4-bromo-1-iodobenzene were also tolerated and provided good yields and regioselectivities of phenols (**2l–2n**). Iodobenzene and 1-iodonaphthalene were also tolerated and afforded the desired products in 85% and 88% yields (**2o** and **2p**). nano-Cu₃N provided excellent yield of a heteroaromatic iodide (**2q**). In Taillefer group's work, 1,2-diiodophenol and o-iodophenol are not suitable substrates for the hydroxylation because of the exclusive formation of phenol [29]. Delightfully, nano-Cu₃N catalytic system is active for the hydroxylation of 1,2-diiodobenzene to 1,2-benzenediol (**2r**) as side-product in 50% yield: this is the first report for the 1,2-benzenediol synthesis from 1,2-dihaloarobenzenes using the

heterogeneous Cu catalysts [27].



Scheme 2-1. Hydroxylation of aryl iodides using nano-Cu₃N catalyst. Reaction conditions: aryl halides (0.5 mmol), nano-Cu₃N (Cu: 11.8 mol%), CsOH (3.0 mmol), H₂O/DMSO = 1/1 (2 mL), 100 °C, 12 h, Ar. Isolated yields.

Table 2-2. nano-Cu₃N catalyzed-hydroxylation of aryl bromides and aryl chlorides.

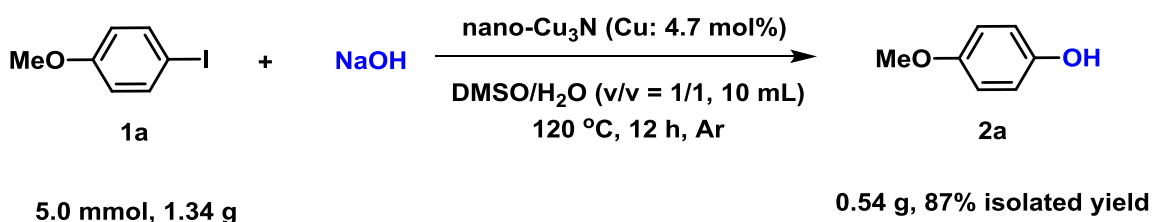


Entry	Substrate	Product	Yield of 2 (%)
1			82
2			76
3			21
4			16
5			32
6			52
7			45

^a Reaction conditions: **1** (0.5 mmol), nano-Cu₃N (Cu: 11.8 mol%), CsOH (3.0 mmol), and H₂O/DMSO = 1 : 1 (2 mL), 140 °C, 48 h, under Ar. Isolated yields.

Furthermore, aryl bromides and chlorides were hydroxylated successfully by nano-Cu₃N catalyst to afford the valuable phenols (**Table 2-2**). Aryl bromides bearing electron-withdrawing groups (e.g., –NO₂ and –COCH₃) were tolerated and provided the desired products in good yields (entries 1 and 2). 4-Bromoanisole and bromobenzene showed low activity to afford only 21% and 16% yields of the corresponding phenols (entries 3 and 4). 1,2-Dibromobenzene was efficiently transformed to the 1,2-benzenediol in a moderate yield (entry 5). Notably, in this method, aryl chlorides with electron-

withdrawing groups (e.g., $-\text{NO}_2$ and $-\text{COCH}_3$) were tolerated, providing phenols in moderate yields (entries 6 and 7). The gram-scale reaction of **1a** (1.34 g, 5.0 mmol) with NaOH (30.0 mmol) was further carried out: the desired product **2a** was obtained in 87% yield (0.54 g) (**Scheme 2-2**), illustrating the good applicability of the nano- Cu_3N catalytic system for large-scale reactions.



Scheme 2-2. Gram scale experiment of hydroxylation of **1a** by nano- Cu_3N catalyst.

Subsequently, the hot filtration experiment was carried out to check whether the hydroxylation proceeded heterogeneously (**Figure 2-2** (a)). The nano- Cu_3N catalyst was removed from the reaction mixture at the 40% yield, and the recovered reaction mixture was further treated under the same reaction conditions. No additional of **2a** was produced, demonstrating that the reaction occurred on the surface of the nano- Cu_3N catalyst. In addition, the nano- Cu_3N was easily recovered via centrifugation and ready to be reused without any treatments. Although the desired **2a** was formed in good yields in the second reuse experiment as shown in **Figure 2-2** (b), the decreased yield of **2a** was observed after the third reuse experiment. To understand the deactivation of recovered nano- Cu_3N , several analyses were performed. The SEM image of reused nano- Cu_3N demonstrates the morphology was not changed after the reaction (**Figure 2-3** (a)). The PXRD patterns and XAFS spectra of recovered nano- Cu_3N reveal that the Cu_3N was gradually converted into Cu_2O during the reaction, which accounts for the deactivation of nano- Cu_3N (**Figures 2-3** (b)–(d)). Overall, the nano- Cu_3N catalyst could be reused for several times and provided satisfied yields of **2a**.

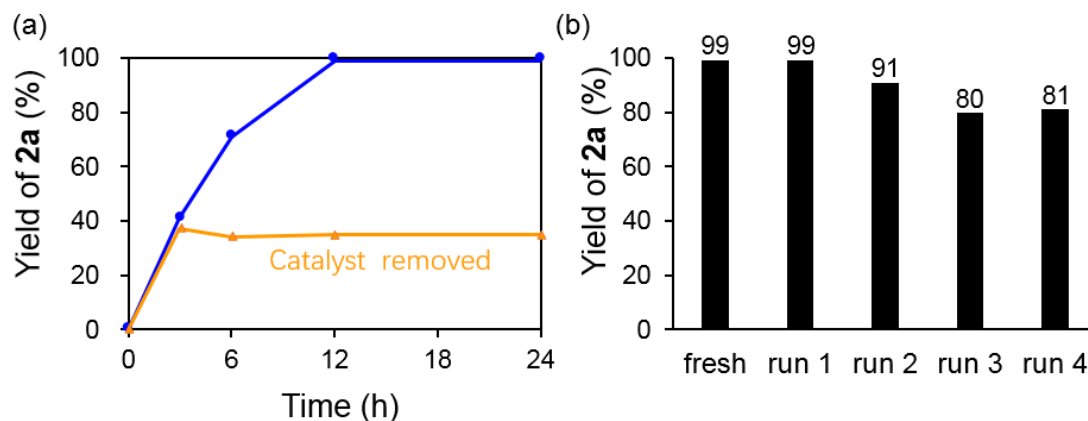


Figure 2-2. (a) Hot filtration experiment of nano-Cu₃N in hydroxylation of **1a**. (b) Reuse experiments of nano-Cu₃N in hydroxylation of **1a**. Reaction conditions: **1a** (0.5 mmol), nano-Cu₃N (Cu: 11.8 mol%), CsOH (3.0 mmol), H₂O/DMSO = 1/1 (2 mL), 100 °C, 12 h, Ar. Yields were determined by GC-MS using naphthalene (0.2 mmol) as an internal standard.

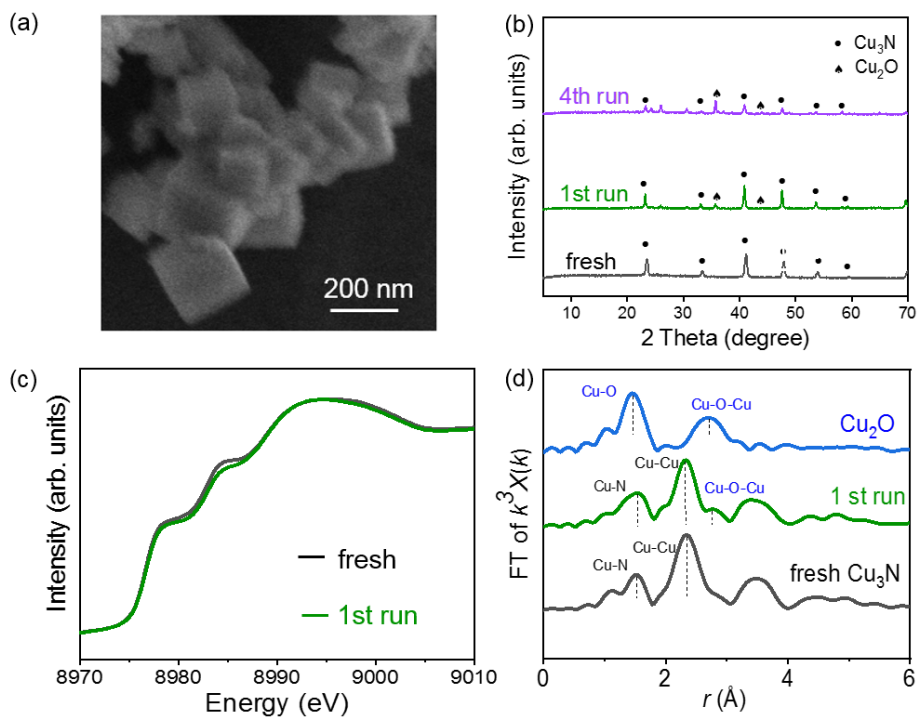
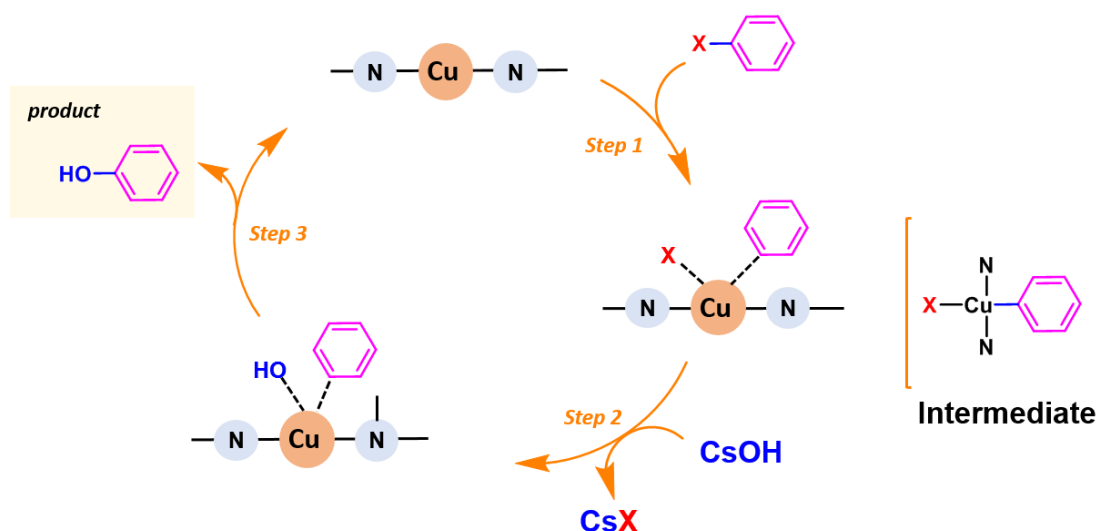


Figure 2-3. (a) SEM image, (b) PXRD patterns, (c) XANES spectra, and (d) XAFS spectra of reused nano-Cu₃N catalyst.

3.3. Proposed mechanism.

According to the reported Cu catalytic systems for this reaction, the proposed mechanism is shown in **Scheme 2-3**. As mentioned in the introduction, Cu_3N crystal structure possesses an open cubic framework of Cu-N octahedra, which can serve as the Cu(I)/N ligand species during the reaction [28–33]. In nano- Cu_3N catalytic system, firstly, a Cu(III) species intermediate is generated through the oxidative addition of aryl halides to nano- Cu_3N . Next, the hydroxylation of the substrate occurs through nucleophilic substitution with $-\text{OH}$ species, affording a Cu species with the ligated product. Finally, via the reductive elimination step, the desired phenol is produced and accompanied by the regeneration of nano- Cu_3N .



Scheme 2-3. Proposed mechanism for the nano- Cu_3N catalyzed hydroxylation of aryl halides.

4. Conclusion

This chapter described that a well-defined nano-Cu₃N was prepared and used an efficient catalyst in the hydroxylation of aryl halides under additive-free conditions. A wide variety of aryl halides, including aryl iodides, bromides, and chlorides reacted well with CsOH or NaOH, generating corresponding phenols in moderate to excellent yields. After the reaction, the nano-Cu₃N can be easily recovered and reused for several times. This study strongly suggests that the N atoms in nano-Cu₃N act as a functional ligand to promote the hydroxylation of aryl halides.

References

- 1 J. H. P. Tyman, *Synthetic and Natural Phenols*, Elsevier, New York, **1996**.
- 2 Z. Rappoport, *The Chemistry of Phenols*, Wiley-VCH, Weinheim, **2003**.
- 3 K. W. Anderson, T. Ikawa, R. E. Tundel, S. L. Buchwald, *J. Am. Chem. Soc.*, **2006**, *128*, 10694–10695.
- 4 M. C. Willis, *Angew. Chem. Int. Ed.*, **2007**, *46*, 3402–3404.
- 5 C. B. Lavery, N. L. Rotta-Loria, R. McDonald, M. Stradiotto, *Adv. Synth. Catal.*, **2013**, *355*, 981–987.
- 6 T. Schulz, C. Torborg, B. Schaffner, J. Huang, A. Zapf, R. Kadyrov, A. Borner, M. Beller, *Angew. Chem. Int. Ed.*, **2009**, *48*, 918–921.
- 7 A. G. Sergeev, T. Schulz, C. Torborg, A. Spannenberg, H. Neumann, M. Beller, *Angew. Chem. Int. Ed.*, **2009**, *48*, 7595–7599.
- 8 A. Tlili, N. Xia, F. Monnier, M. Taillefer, *Angew. Chem., Int. Ed.*, **2009**, *48*, 8725–8728.
- 9 D. Zhao, N. Wu, S. Zhang, P. Xi, X. Su, J. Lan, J. You, *Angew. Chem., Int. Ed.*, **2009**, *48*, 8729–8732.
- 10 D. Yang, H. Fu, *Chem. Eur. J.*, **2010**, *16*, 2366–2370.
- 11 Y. Wang, C. Zhou, R. Wang, *Green Chem.*, **2015**, *17*, 3910–3915.
- 12 X. Liang, H. Li, F. Du, Y. Zhang, J. Dong, X. Bao, Y. Wu, G. Chen, *Tetrahedron Lett.*, **2020**, *61*, 152222.
- 13 H.-J. Xu, Y.-F. Liang, Z.-Y. Cai, H.-X. Qi, C.-Y. Yang, Y.-S. Feng, *J. Org. Chem.*, **2011**, *76*, 2296–2300.
- 14 C.-C. Chan, Y.-W. Chen, C.-S. Su, H.-P. Lin, C.-F. Lee, *Eur. J. Org. Chem.*, **2011**, 7288–7293.
- 15 G. Ding, H. Han, T. Jiang, T. Wu, B. Han, *Chem. Commun.*, **2014**, *50*, 9072–9075.
- 16 J. S. J. Hargreaves, A. R. McFarlane, S. Laassiri, *Alternative Catalytic Materials: Carbides*,

Nitrides, Phosphides and Amorphous Boron Alloys, The Royal Society of Chemistry, **2018**.

- 17 S. Carenco, D. Portehault, C. Boissiere, N. Mezaillies, C. Sanchez, *Chem. Rev.*, **2013**, *113*, 7981–8065.
- 18 D. R. Aireddy, K. Ding, *ACS Catal.*, **2022**, *12*, 4707–4723.
- 19 Z. Yin, C. Yu, Z. Zhao, X. Gou, M. Shen, L. Na, M. Muzzio, J. Li, H. Liu, H. Lin, J. Yin, G. Lu, D. Su, S. Sun, *Nano Lett.*, **2019**, *19*, 8658–8663.
- 20 R. Deshmukh, G. Zeng, E. Tervoort, M. Staniuk, D. Wood, M. Niederberger, *Chem. Mater.*, **2015**, *27*, 8282–8288.
- 21 D. Barman, S. Paul, S. Ghosh, S. K. De, *ACS Appl. Nano Mater.*, **2019**, *8*, 5009–5019.
- 22 F. Gulo, A. Simon, J. Kohler, R. K. Kremer, *Angew. Chem. Int. Ed.*, **2004**, *43*, 2032–2034.
- 23 B. S. Lee, M. Yi, S. Y. Chu, J. Y. Lee, H. R. Kwon, K. R. Lee, D. Kang, W. S. Kim, H. B. Lim, J. Lee, H.-J. Youn, D. Y. Chi, N. H. Hu, *Chem. Commun.*, **2010**, *46*, 3935–3937.
- 24 C. Panda, P. W. Menezes, M. Zheng, S. Orthmann, M. Driess, *ACS Energy Lett.*, **2019**, *4*, 747–754.
- 25 U. Hahn, W. Weber, *Phys. Rev. B*, **1996**, *53*, 12684–12693.
- 26 T. Nakamura, M. Katayama, T. Watanabe, Y. Inada, T. Ebina, A. Yamaguchi, *Chem. Lett.*, **2015**, *44*, 755–757.
- 27 J. Timoshenko, A. Anspoks, A. Kalinko, A. Kuzmin, *Phys. Scr.*, **2016**, *91*, 054003.
- 28 K. G. Thakur, G. Sekar, *Chem. Commun.*, **2011**, *47*, 6692–6694.
- 29 D. D. Vaughn, J. Araujo, P. Meduri, J. F. Callejas, M. A. Hickner, R. E. Schaak, *Chem. Mater.*, **2014**, *26*, 6226–6232.
- 30 S. Bhunia, G. G. Pawar, S. V. Kumar, Y. Jiang, D. Ma, *Angew. Chem. Int. Ed.*, **2017**, *56*, 16136–16179.
- 31 A. Casitas, X. Ribas, *Chem. Sci.*, **2013**, *4*, 2301–2318.

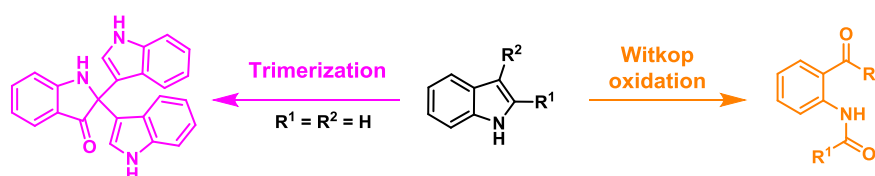
- 32 K. Mullick, S. Biswas, C. Kim, R. Ramprasad, A. M. Angeles-Boza, S. L. Suib, *Inorg. Chem.*, **2017**, *56*, 10290–10297.
- 33 E. Akhavan, S. Hemmati, M. Hekmati, H. Veisi, *New J. Chem.*, **2018**, *42*, 2782–2789.
- 34 H. Veisi, M. Hamelian, S. Hemmati, A. Dalvand, *Tetrahedron Lett.*, **2017**, *58*, 4440–4446.

Chapter III.

***Green Oxidation of Indoles by
Copper Nitride Catalyst***

1. Introduction

Functionalization of indoles is a convenient and practical method for the preparation of several nitrogen-containing compounds [1]. Among them, oxidative trimerization of indoles can directly afford the indolin-3-one derivatives, which are found widely in valuable natural products and pharmaceuticals [2, 3]. Recently, several homogeneous and heterogeneous catalytic systems have been developed for this oxidation reaction. However, the additive oxidants for example *tert*-butyl hydroperoxide (TBHP) [4–6] and oxone [7, 8] were required to complete the reaction in those synthetic methods, which produce large amounts of wastes. Molecular oxygen (O₂) are extensively utilized in oxidative organic conversions since water is theoretically generated as the single co-product [9]. In this context, many researchers have recently focused on the development of greener catalytic trimerization of indoles with O₂ as oxidant. Inada group reported the efficient trimerization of indoles catalyzed by Co(salen) catalyst with sodium dodecylsulfate as surfactant under O₂ bubbling [10]. Liu et al. reported that the 2,2,6,6-tetramethylpiperidine-1-oxyl (TEMPO) was used as an accelerator to achieve the oxidation of indoles with O₂, but benzoic acid was required as co-catalyst [11]. Very recently, photocatalysts, such as ruthenium and natural chlorophyll, have been applied to the trimerization of indoles [12, 13]. Although these catalytic systems showed high efficiency, the requirement of additives and precious metal catalysts leads to large amounts of chemical wastes.



Scheme 3-1. Trimerization and Witkop oxidation of indoles.

The oxidative cleavage of the C2, C3-double bond of indoles, named as Witkop oxidation,

is another interesting and useful oxidative reaction of indoles, which can afford various valuable amide derivatives [14, 15]. Previous synthetic methods usually used the stoichiometric chemical oxidants, such as peroxides [16, 17] and ozone [18]. Recently, some catalytic aerobic oxidation systems have been developed, but they also suffered from the utilization of additive and precious metal catalysts [19, 20]. Hence, from the perspective of practicality and green sustainable chemistry, the development of non-noble metal based-heterogeneous catalytic system for the oxidation of indoles is highly demanded.

This chapter describes that the copper nitride nanocube (Cu_3N NC) exhibits a high catalytic performance for the oxidation of indoles to indolin-3-ones and amide derivatives. A wide range of indoles undergoes this transformation efficiently to generate the desired products in excellent yields. The Cu_3N NC is the first example of a heterogeneous non-precious metal catalyst for synthesizing indolin-3-ones and amide derivatives with O_2 under additive-free conditions.

2. Experimental section

2.1. General information

All organic reagents were purchased from FUJIFILM Wako Pure Chemical Corporation, Sigma–Aldrich, or Tokyo Chemical Industry. The commercial Cu_3N was purchased from KOJUNDO Chemical Lab. Co., Ltd. Gas chromatography-mass spectrometry (GC-MS) was performed using a GCMS-QP2010 SE instrument equipped with an InertCap WAX-HT capillary column (GL Science, 30 m \times 0.25 mm i.d., film thickness 0.25 μm). ^1H and ^{13}C nuclear magnetic resonance (NMR) spectra were acquired at 400 and 100 MHz, respectively, using a JEOL JNM-ESC400 spectrometer. Chemical shifts are reported in parts per million (ppm) relative to the signal (0.00 ppm) for internal tetramethylsilane in CDCl_3 or $(\text{CD}_3)_2\text{SO}$. The ^1H NMR spectral data are reported using the following standard chemical shifts: CDCl_3 (7.26 ppm) and $(\text{CD}_3)_2\text{SO}$ (2.50 ppm). The ^{13}C NMR spectral data are reported using the following standard chemical shifts: CDCl_3 (77.16 ppm) and $(\text{CD}_3)_2\text{SO}$ (39.52 ppm). NMR multiplicities are reported using the following abbreviations: s: singlet, d: doublet, t: triplet, q: quartet, m: multiplet, br: broad, J : coupling constants in hertz. All known compounds described in the paper were characterized by comparison of their ^1H and ^{13}C NMR spectra with previously reported data. Scanning electron microscopy (SEM) image was obtained using a JSM-7600F microscope operated at 15.0 kV at the Analytical Instrument Facility, Graduate School of Science, Osaka University. Transmission electron microscopy (TEM) images were obtained using a Hitachi HF-2000 microscope operated at 200 kV at the Research Center for Ultra-High Voltage Electron Microscopy, Osaka University. Cu K -edge X-ray absorption spectra (extended X-ray absorption near edge structure (XANES)) obtained using a Si (111) monochromator were recorded at 25 °C at the BL01B1 and BL14B2 stations, SPring-8, Japan Synchrotron Radiation Research Institute (JASRI), Harima, Japan. Data analysis was performed using Demeter (ver. 0.9.26). Powder X-ray diffraction (PXRD) patterns were acquired using a Philips XPert-MPD instrument with $\text{Cu-K}\alpha$

radiation. CHN element analysis was performed using a PerkinElmer 2400II CHNS/O.

2.2. Preparation of Cu₃N NC

All reactions were carried out under an Ar atmosphere using standard Schlenk line techniques [21]. In a typical synthesis, 0.5 mmol of Cu(NO₃)₂·3H₂O and octadecylamine (2.5 g) were combined with 2.5 mL of oleylamine in a Schlenk flask. The system was heated to 150 °C and kept for 1 h under Ar. Next, the temperature was increased to 260 °C and maintained for 20 min. After the mixture was cooled to room temperature, the brown product was isolated by precipitation with isopropanol, and redispersion and precipitation cycles using ethanol and toluene were continued until the supernatant liquid was transparent. The obtained material was dried in vacuum.

2.3. Preparation of C2,C3-substitute indoles

The C2,C3-substitute indoles were synthesized according to the reported work [22]. In the general procedure, the substituted phenylhydrazine hydrochloride (3 mmol) was added to AcOH (3 mL) and heated at 50 °C for 30 min. Then, ketones (6 mmol) was added in one portion and the reaction mixture was refluxed for 3 h. After the reaction, AcOH was removed under vacuum and the residue was dissolved in ethyl acetate. The organic phase was washed with water and brine, and then dried over anhydrous Na₂SO₄. After the removal of the solvent, the residue was purified by flash chromatography on silica gel with hexane/ethyl acetate to afford the corresponding C2,C3-substitute indoles. The substrates **3a–3i** and **3l–3o** were also prepared based on this procedure.

2.4. Reaction procedure for the oxidation of indoles using Cu₃N NC

Cu₃N NC powder was placed in a 50-mL stainless steel autoclave with a Teflon inner cylinder. Indole (0.5 mmol) was subsequently added to the mixture of CH₃CN/H₂O (v/v = 2/3, 2 mL).

The reaction mixture was stirred vigorously at 60 °C or 80 °C under 3 bars of O₂. After the reaction, the mixture was cooled to room temperature and concentrated *in vacuo*. The residue was purified by the silica gel flash chromatography with hexane/ethyl acetate to yield the desired products.

2.5. Recycling experiments

In a 50 mL stainless-steel autoclave, **3a** (0.5 mmol) and Cu₃N NC (5 mg, 5 mol% Cu) were added to 2 mL of H₂O/CH₃CN (v/v = 2/3). The autoclave was purged and filled with O₂ (1 bar). After the reaction, Cu₃N NC was removed by centrifugation, and the yield was determined by GC-MS analysis. The spent catalyst was washed with ethanol for the reuse experiments without any other pre-treatments.

2.6. Gram-scale experiment of Witkop reaction

In a 100 mL stainless-steel autoclave, **3a** (1.015 g, 7 mmol) and Cu₃N NC (35 mg, 3 mol% Cu) were added to 10 mL of H₂O/CH₃CN (v/v = 2/3). The autoclave was purged and filled with O₂ until the pressure reached 3 bars. The mixture was then stirred at 60 °C for 24 h and was concentrated *in vacuo*. The residue was purified by the silica gel flash chromatography with hexane/ethyl acetate to yield the desired product **4a**.

2.7. Control experiments

In a 50 mL stainless-steel autoclave, indole (0.5 mmol), Cu₃N NC (5 mg, 5 mol% Cu) and TEMPO (1.0 mmol) were added to 2 mL of H₂O/CH₃CN (v/v = 2/3). The autoclave was purged and filled with O₂ until the pressure reached 3 bars. The mixture was then stirred at 60 °C for 12 h and was concentrated *in vacuo*. The residue was purified by the silica gel flash chromatography with hexane/ethyl acetate to yield the desired products.

2.8. Product identification

[3,2':2',3''-terindolin]-3'-one

CAS registry No. [17646-95-6], yellow solid; ¹H NMR (400 MHz, DMSO-d₆): δ 10.98 (s, 2H), 8.16 (s, 1H), 7.51–7.49 (m, 2H), 7.38–7.32 (m, 4H), 7.12–7.08 (m, 2H), 6.96 (d, *J* = 8.0 Hz, 1H), 6.87–6.83 (m, 2H), 6.75–6.72 (m, 1H); ¹³C NMR (100 MHz, DMSO-d₆): δ 200.9, 160.6, 137.5, 137.0, 125.7, 124.5, 124.1, 121.1, 120.6, 118.4, 117.8, 117.1, 114.0, 111.9, 111.6, 67.7.

5-methoxy-2,2-bis(5-methoxy-1H-indol-3-yl)indolin-3-one

CAS registry No. [214262-54-1], yellow solid; ¹H NMR (400 MHz, DMSO-d₆): δ 10.83 (s, 2H), 7.83 (s, 1H), 7.31–7.26 (m, 3H), 7.10 (d, *J* = 2.4 Hz, 2H), 7.03–6.99 (m, 2H), 6.86 (br, 2H), 6.75 (dd, *J* = 8.8, 2.4 Hz, 2H), 3.77 (s, 3H), 3.59 (s, 6H); ¹³C NMR (100 MHz, DMSO-d₆): δ 201.3, 156.9, 152.6, 151.8, 132.2, 127.8, 126.1, 124.7, 118.1, 113.7, 113.5, 112.1, 110.6, 104.6, 103.1, 68.5, 55.6, 55.1.

5,5',5''-trimethyl-[3,2':2',3''-terindolin]-3'-one

CAS registry No. [1414941-78-8], yellow solid; ¹H NMR (400 MHz, DMSO-d₆): δ 10.79 (s, 2H), 7.81 (s, 1H), 7.36–7.33 (m, 1H), 7.26 (s, 1H), 7.24 (d, *J* = 8.4 Hz, 2H), 7.11 (s, 2H), 7.01 (d, *J* = 2.0 Hz, 2H), 6.90–6.79 (m, 3H), 2.25 (s, 3H), 2.22 (s, 6H); ¹³C NMR (100 MHz, DMSO-d₆): δ 200.8, 159.2, 138.7, 135.3, 126.5, 125.9, 125.8, 124.0, 123.6, 122.6, 120.2, 118.0, 113.7, 112.0, 111.3, 68.0, 21.4, 20.1.

5,5',5''-tribromo-[3,2':2',3''-terindolin]-3'-one

CAS registry No. [95561-75-4], yellow solid; ¹H NMR (400 MHz, DMSO-d₆): δ 11.35 (s, 2H), 8.59 (s, 1H), 7.72–7.68 (m, 2H), 7.45 (s, 2H), 7.41 (d, *J* = 8.8 Hz, 2H), 7.28 (s, 2H), 7.22 (d, *J* = 8.4 Hz, 2H), 7.01 (d, *J* = 8.0 Hz, 1H); ¹³C NMR (100 MHz, DMSO-d₆): δ 199.0, 159.2, 140.1, 135.7, 127.1,

126.7, 125.5, 123.8, 122.3, 119.0, 114.1, 113.9, 112.9, 111.3, 108.4, 67.8.

5,5',5''-trichloro-[3,2':2',3''-terindolin]-3'-one

CAS registry No. [2400913-11-1], yellow solid; ¹H NMR (400 MHz, DMSO-d₆): δ 11.30 (s, 2H), 8.51 (s, 1H), 7.56 (dd, *J* = 8.8, 2.4 Hz, 1H), 7.50 (d, *J* = 2.0 Hz, 1H), 7.41 (d, *J* = 8.8 Hz, 2H), 7.25–7.24 (m, 4H), 7.05 (dd, *J* = 8.8, 2.4 Hz, 2H), 7.01 (d, *J* = 8.8 Hz, 1H); ¹³C NMR (100 MHz, DMSO-d₆): δ 199.3, 159.0, 137.6, 135.5, 126.5, 125.6, 123.6, 123.2, 121.3, 121.2, 119.3, 118.3, 113.7, 113.4, 113.0, 67.9.

5,5',5''-trifluoro-[3,2':2',3''-terindolin]-3'-one

CAS registry No. [1414941-76-6], yellow solid; ¹H NMR (400 MHz, CDCl₃): δ 8.24 (s, 2H), 7.34 (dd, *J* = 7.2, 2.8 Hz, 1H), 7.31–7.26 (m, 1H), 7.21 (dd, *J* = 9.2, 4.8 Hz, 2H), 7.10 (d, *J* = 2.4 Hz, 1H), 7.01 (dd, *J* = 10.0, 2.4 Hz, 2H), 6.90–6.85 (m, 3H), 5.28 (s, 1H); ¹³C NMR (100 MHz, CDCl₃): δ 201.2 (d, *J* = 3.0 Hz), 157.8 (d, *J* = 234.0 Hz), 157.1, 157.0 (d, *J* = 239.0 Hz), 133.6, 126.2 (d, *J* = 25.0 Hz), 125.8 (d, *J* = 10.0 Hz), 125.7, 120.3 (d, *J* = 7.0 Hz), 114.6 (d, *J* = 5.0 Hz), 114.5 (d, *J* = 7.0 Hz), 112.4 (d, *J* = 10.0 Hz), 111.0 (d, *J* = 27.0 Hz), 110.3 (d, *J* = 25.0 Hz), 105.3 (d, *J* = 25.0 Hz), 69.2.

6,6',6''-trimethyl-[3,2':2',3''-terindolin]-3'-one

CAS registry No. [2413003-66-2], yellow solid; ¹H NMR (400 MHz, DMSO-d₆): δ 10.76 (s, 2H), 7.97 (s, 1H), 7.34 (d, *J* = 7.6 Hz, 1H), 7.18 (d, *J* = 8.4 Hz, 2H), 7.12 (s, 2H), 6.98–6.97 (m, 2H), 6.72 (s, 1H), 6.65 (d, *J* = 8.4 Hz, 1H), 6.63 (d, *J* = 8.0 Hz, 1H), 2.33 (s, 3H), 2.32 (s, 6H); ¹³C NMR (100 MHz, DMSO-d₆): δ 200.0, 160.9, 148.1, 137.3, 130.0, 124.2, 123.6, 123.3, 120.4, 120.1, 118.7, 115.7, 114.2, 111.5, 111.3, 67.9, 22.1, 21.3.

6,6',6''-trichloro-[3,2':2',3''-terindolin]-3'-one

CAS registry No. [1585169-26-1], yellow solid; ¹H NMR (400 MHz, DMSO-d₆): δ 11.20 (s, 2H), 8.48 (s, 1H), 7.50 (d, *J* = 8.0 Hz, 1H), 7.42 (d, *J* = 2.0 Hz, 2H), 7.23 (d, *J* = 8.4 Hz, 2H), 7.18 (d, *J* = 2.4 Hz, 2H), 6.95 (d, *J* = 1.6 Hz, 2H), 6.90 (dd, *J* = 8.8, 2.0 Hz, 2H), 6.75 (dd, *J* = 8.0, 1.6 Hz, 1H); ¹³C NMR (100 MHz, DMSO-d₆): δ 199.1, 160.7, 142.5, 137.4, 126.4, 126.0, 125.2, 124.2, 121.5, 119.0, 117.7, 116.3, 113.6, 111.3, 111.1, 67.8.

6,6',6''-trifluoro-[3,2':2',3''-terindolin]-3'-one

CAS registry No. [1414941-88-0], yellow solid; ¹H NMR (400 MHz, DMSO-d₆): δ 11.10 (s, 2 H), 8.52 (s, 1H), 7.56 (dd, *J* = 8.4, 6.0 Hz, 1H), 7.26 (dd, *J* = 8.8, 5.6 Hz, 2H), 7.16–7.14 (m, 4H), 6.78–6.75 (m, 2H), 6.65 (dd, *J* = 10.4, 2.0 Hz, 1H), 6.57–6.53 (m, 1H); ¹³C NMR (100 MHz, DMSO-d₆): δ 198.6, 168.9 (d, *J* = 250.0 Hz), 161.8 (d, *J* = 15.0 Hz), 158.7 (d, *J* = 234.0 Hz), 136.8 (d, *J* = 12.0 Hz), 127.4 (d, *J* = 13.0 Hz), 124.6 (d, *J* = 4.0 Hz), 122.3, 121.3 (d, *J* = 10.0 Hz), 114.5, 113.8, 107.2 (d, *J* = 24.0 Hz), 105.7 (d, *J* = 25.0 Hz), 97.6 (d, *J* = 26.0 Hz), 97.3 (d, *J* = 27.0 Hz), 68.1.

7,7',7''-trimethoxy-[3,2':2',3''-terindolin]-3'-one

CAS registry No. [1585169-27-2], yellow solid; ¹H NMR (400 MHz, DMSO-d₆): δ 11.02 (s, 2H), 7.80 (s, 1H), 7.12–7.06 (m, 2H), 6.95–6.92 (m, 4H), 6.78–6.68 (m, 3H), 6.62–6.59 (m, 2H), 3.89 (s, 3H), 3.88 (s, 3H), 3.86 (s, 3H); ¹³C NMR (100 MHz, DMSO-d₆): δ 200.7, 151.6, 146.1, 145.8, 127.1, 126.9, 124.0, 118.9, 118.4, 117.4, 116.4, 115.7, 114.4, 113.6, 101.5, 99.5, 68.2, 55.5, 55.1.

7,7',7''-tribromo-[3,2':2',3''-terindolin]-3'-one

CAS registry No. [2400913-12-2], yellow solid; ¹H NMR (400 MHz, DMSO-d₆): δ 11.33 (s, 2H), 8.42 (s, 1H), 7.81 (dd, *J* = 8.0, 1.2 Hz, 1H), 7.55–7.53 (m, 1H), 7.33–7.30 (m, 4H), 7.15 (d, *J* = 2.4 Hz, 2H),

6.85 (t, $J = 8.0$ Hz, 2H), 6.74 (t, $J = 7.6$ Hz, 1H); ^{13}C NMR (100 MHz, DMSO- d_6): δ 199.9, 157.5, 140.1, 135.1, 127.0, 126.0, 124.1, 123.9, 120.2, 120.1, 119.5, 118.9, 114.3, 104.4, 104.4, 68.2.

***N*-(2-acetylphenyl)acetamide**

CAS registry No. [5234-26-4], white solid; ^1H NMR (400 MHz, CDCl_3): δ 11.69 (s, 1H), 8.74 (dd, $J = 8.4, 1.2$ Hz, 1H), 7.89 (d, $J = 8.0, 1.6$ Hz, 1H), 7.57–7.53 (m, 1H), 7.13–7.09 (m, 1H), 2.67 (s, 3H), 2.23 (s, 3H); ^{13}C NMR (100 MHz, CDCl_3): δ 202.9, 169.6, 141.1, 135.2, 131.7, 122.4, 121.8, 120.8, 28.8, 25.7.

***N*-(2-acetyl-4-methoxyphenyl)acetamide**

CAS registry No. [52417-34-2], white solid; ^1H NMR (400 MHz, CDCl_3): δ 11.32 (s, 1H), 8.65 (d, $J = 9.2$ Hz, 1H), 7.36 (d, $J = 2.8$ Hz, 1H), 7.12 (dd, $J = 9.2, 2.8$ Hz, 1H), 3.84 (s, 3H), 2.64 (s, 3H), 2.20 (s, 3H); ^{13}C NMR (100 MHz, CDCl_3): δ 202.6, 169.2, 154.3, 134.5, 123.0, 122.4, 120.2, 116.8, 55.8, 28.7, 25.5.

***N*-(2-acetyl-4-methylphenyl)acetamide**

CAS registry No. [38968-47-7], brown solid; ^1H NMR (400 MHz, CDCl_3): δ 11.56 (s, 1H), 8.61 (d, $J = 8.0$ Hz, 1H), 7.66 (s, 1H), 7.36 (d, $J = 8.0$ Hz, 1H), 2.64 (s, 3H), 2.35 (s, 3H), 2.21 (s, 3H); ^{13}C NMR (100 MHz, CDCl_3): δ 202.9, 169.4, 138.7, 135.9, 131.9, 121.8, 120.7, 28.7, 25.6, 20.9.

***N*-(2-acetyl-4-isopropylphenyl)acetamide**

CAS registry No. [2640316-79-4], yellow solid; ^1H NMR (400 MHz, CDCl_3): δ 11.56 (s, 1H), 8.63 (d, $J = 8.4$ Hz, 1H), 7.70 (d, $J = 2.4$ Hz, 1H), 7.43 (dd, $J = 8.8, 2.0$ Hz, 1H), 2.95–2.88 (m, 1H), 2.67 (s, 3H), 2.21 (s, 3H), 1.27 (s, 3H), 1.26 (s, 3H); ^{13}C NMR (100 MHz, CDCl_3): δ 203.0, 169.4, 140.9,

138.9, 133.3, 129.3, 122.0, 121.0, 33.6, 28.7, 25.6, 24.0.

***N*-(2-acetyl-4-bromophenyl)acetamide**

CAS registry No. [29124-64-9], brown solid; ¹H NMR (400 MHz, CDCl₃): δ 11.57 (s, 1H), 8.67 (d, *J* = 9.2 Hz, 1H), 7.97 (d, *J* = 2.4 Hz, 1H), 7.63 (dd, *J* = 9.6, 2.4 Hz, 1H), 2.66 (s, 3H), 2.22 (s, 3H); ¹³C NMR (100 MHz, CDCl₃): δ 201.8, 169.6, 140.2, 137.9, 134.2, 123.2, 122.6, 114.6, 28.8, 25.7.

***N*-(2-acetyl-4-chlorophenyl)acetamide**

CAS registry No. [52263-95-3], white solid; ¹H NMR (400 MHz, CDCl₃): δ 11.57 (s, 1H), 8.73 (d, *J* = 8.8 Hz, 1H), 7.83 (s, 1H), 7.49 (d, *J* = 8.8 Hz, 1H), 2.66 (s, 3H), 2.23 (s, 3H); ¹³C NMR (100 MHz, CDCl₃): δ 201.9, 169.5, 139.6, 134.9, 131.2, 127.3, 122.9, 122.3, 28.8, 25.6.

***N*-(2-acetyl-4-fluorophenyl)acetamide**

CAS registry No. [2794-54-9], colorless oil; ¹H NMR (400 MHz, CDCl₃): δ 11.47 (s, 1H), 8.74 (dd, *J* = 9.2, 5.2 Hz, 1H), 7.55 (dd, *J* = 9.6, 2.4 Hz, 1H), 7.30–7.25 (m, 1H), 2.65 (s, 3H), 2.22 (s, 3H); ¹³C NMR (100 MHz, CDCl₃): δ 201.8, 169.5, 157.1 (d, *J* = 240.0 Hz), 137.4, 122.8–122.7 (m), 122.2 (d, *J* = 21.0 Hz), 117.4 (d, *J* = 23.0 Hz), 28.7, 25.5.

***N*-(2-acetyl-4-nitrophenyl)acetamide**

CAS registry No. [41019-20-9], colorless solid; ¹H NMR (400 MHz, DMSO-*d*₆): δ 11.48 (s, 1H), 8.74 (s, 1H), 8.54–8.47 (m, 2H), 2.77 (s, 3H), 2.25 (s, 3H); ¹³C NMR (100 MHz, DMSO-*d*₆): δ 201.2, 169.6, 144.0, 141.5, 128.7, 126.7, 124.3, 120.9, 28.7, 24.9.

***N*-(2-acetyl-5-methylphenyl)acetamide**

CAS registry No. [127396-17-2], colorless solid; ¹H NMR (400 MHz, CDCl₃): δ 11.75 (s, 1H), 8.57

(s, 1H), 7.77 (d, $J = 8.4$ Hz, 1H), 6.91 (d, $J = 8.4$ Hz, 1H), 2.63 (s, 3H), 2.40 (s, 3H), 2.22 (s, 3H); ^{13}C NMR (100 MHz, CDCl_3): δ 202.5, 169.7, 146.7, 141.2, 131.8, 123.4, 121.0, 119.5, 28.6, 25.7, 22.3.

***N*-(1-formylnaphthalen-2-yl)acetamide**

CAS registry No. [42900-57-2], white solid; ^1H NMR (400 MHz, DMSO-d_6): δ 9.97 (s, 1H), 8.00–7.95 (m, 2H), 7.79 (d, $J = 8.8$ Hz, 1H), 7.58–7.49 (m, 3H), 2.53 (s, 3H), 2.09 (s, 3H); ^{13}C NMR (CDCl_3 , 100 MHz): δ 203.1, 169.0, 132.1, 130.9, 129.8, 128.9, 128.2, 127.3, 125.7, 124.8, 124.2, 31.5, 23.1.

***N*-(2-acetylphenyl)formamide**

CAS registry No. [5257-06-7], yellow solid; ^1H NMR (400 MHz, CDCl_3): δ 11.63 (s, 1H), 8.75 (d, $J = 8.4$ Hz, 1H), 8.50 (s, 1H), 7.93–7.91 (m, 1H), 7.60–7.56 (m, 1H), 7.20–7.16 (m, 1H), 2.68 (s, 3H); ^{13}C NMR (100 MHz, CDCl_3): δ 202.9, 160.0, 140.0, 135.3, 131.8, 123.2, 122.1, 121.7, 28.7.

***N*-(2-propionylphenyl)acetamide**

CAS registry No. [52457-99-5], yellow solid; ^1H NMR (400 MHz, CDCl_3): δ 11.75 (s, 1H), 8.76–8.72 (m, 1H), 7.96–7.91 (m, 1H), 7.57–7.52 (m, 1H), 7.14–7.08 (m, 1H), 3.05 (q, $J = 7.2$ Hz, 2H), 2.24 (s, 3H), 1.22 (t, $J = 7.2$ Hz, 3H); ^{13}C NMR (100 MHz, CDCl_3): δ 205.5, 169.6, 141.1, 134.9, 130.7, 122.4, 121.6, 120.9, 33.3, 25.7, 8.5.

***N*-(4-methyl-2-propionylphenyl)acetamide**

CAS registry No. [640316-83-0], yellow solid; ^1H NMR (400 MHz, CDCl_3): δ 11.61 (s, 1H), 8.60 (d, $J = 8.4$ Hz, 1H), 7.70 (s, 1H), 7.35 (d, $J = 8.8$ Hz, 1H), 3.02 (q, $J = 7.2$ Hz, 2H), 2.35 (s, 3H), 2.22 (s, 3H), 1.21 (t, $J = 7.2$ Hz, 3H); ^{13}C NMR (100 MHz, CDCl_3): δ 205.5, 169.4, 138.6, 135.6, 131.8, 130.8, 121.6, 120.9, 33.2, 25.6, 20.9, 8.5.

***N*-(2-acetylphenyl)benzamide**

CAS registry No. [6011-26-3], yellow solid; ¹H NMR (400 MHz, CDCl₃): δ 12.67 (s, 1H), 9.00–8.94 (m, 1H), 8.05–8.03 (m, 2H), 7.95–7.91 (m, 1H), 7.60–7.48 (m, 4H), 7.14–7.10 (m, 1H), 2.68 (s, 3H); ¹³C NMR (100 MHz, CDCl₃): δ 203.4, 166.3, 141.6, 135.5, 135.0, 132.1, 132.0, 129.0, 127.6, 122.6, 122.2, 121.0, 28.7.

***N*-(2-acetyl-4-methylphenyl)benzamide**

CAS registry No. [41019-19-6], yellow solid; ¹H NMR (400 MHz, CDCl₃): δ 12.56 (s, 1H), 8.84 (d, *J* = 8.8 Hz, 1H), 8.05–8.03 (m, 2H), 7.69 (s, 1H), 7.53–7.47 (m, 3H), 7.39 (d, *J* = 8.8 Hz, 1H), 2.67 (s, 3H), 2.35 (s, 3H); ¹³C NMR (100 MHz, CDCl₃): δ 203.4, 166.0, 139.1, 136.2, 135.0, 132.1, 132.0, 128.8, 127.5, 122.0, 120.8, 28.7, 20.9.

spiro[cyclopentane-1,2'-indolin]-3'-one

CAS registry No. [4669-18-5], yellow solid; ¹H NMR (400 MHz, CDCl₃): δ 7.61 (d, *J* = 7.6 Hz, 1H), 7.53–7.41 (m, 1H), 6.84–6.79 (m, 2H), 4.83 (s, 1H), 2.11–2.04 (m, 2H), 1.99–1.95 (m, 2H), 1.86–1.82 (m, 2H), 1.74–1.69 (m, 2H); ¹³C NMR (100 MHz, CDCl₃): δ 205.3, 160.1, 137.0, 124.7, 120.8, 118.9, 112.4, 74.6, 38.2, 25.6.

3. Results and discussion

3.1. Characterization of Cu₃N NC

The crystal structure of Cu₃N NC was verified using PXRD analysis (**Figure 3-1** (a)). The diffraction peaks located at 23.1, 33.2, 40.9, 47.6, and 53.7° can be assigned to the (100), (110), (111), (200), and (210) planes of Cu₃N (JCPDS No. 47-1088). The morphology of prepared Cu₃N was investigated through the TEM and SEM analysis, suggesting that the nanoalloy has a cubic morphology with an average edge length of 67 nm (**Figures 3-1** (b) and (c)). Then, the XAFS analysis was carried out to investigate the oxidation state of Cu species in the Cu₃N NC. The Cu *K*-edge XANES spectrum revealed that the absorption edge energy of Cu₃N NC is close to that of Cu₂O, demonstrating the oxidation state of Cu species in the Cu₃N NC is +1 (**Figures 3-1** (d)).

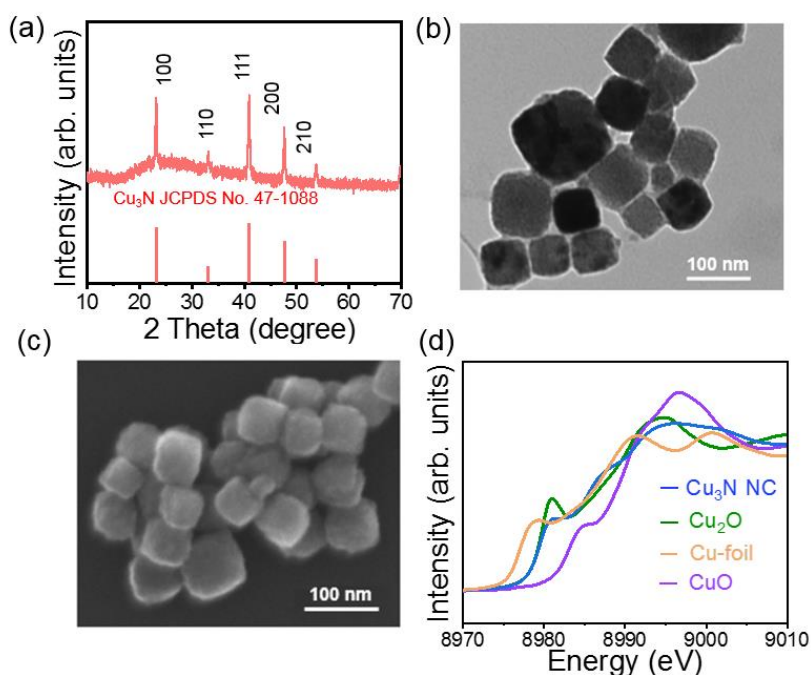
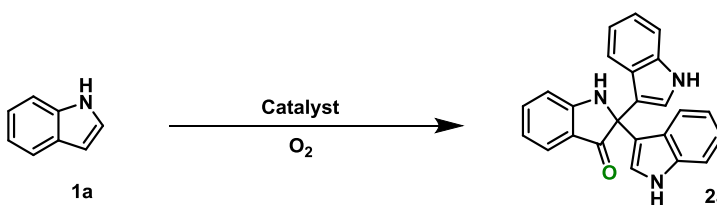


Figure 3-1. (a) PXRD patterns, (b) TEM, and (c) SEM images of the Cu₃N NC. (d) Cu *K*-edge XANES spectra of the Cu₃N NC and the reference Cu compounds.

3.2. Catalytic performance of Cu₃N NC in trimerization of indoles

The trimerization of indole (**1a**) was selected as a model reaction to investigate the catalytic performance of the Cu₃N NC. The reaction was performed in an aqueous CH₃CN solution (H₂O/CH₃CN, v/v = 2/3) under 3 bars of O₂ atmosphere at 60 °C for 12 h (**Table 3-1**). Notably, the Cu₃N NC showed outstanding activity to afford the [3,2':2',3''-terindolin]-3'-one (**2a**) in 84% yield (entry 1). Notably, the O₂-mediated trimerization of indole under additive-free conditions is achieved for the first time with Cu₃N NC catalyst (**Table 3-2**). On the other hand, other Cu compounds, Cu₃N, Cu₂O, CuCl, CuO, and Cu₃P, showed lower catalytic performance compared to the Cu₃N NC (entries 2–6 vs 1). No desired product was obtained with another oxidant (TBHP) instead of O₂, revealing that the O₂ are essential for this reaction (entry 7). The oxidative reaction was not occurred under catalyst- and oxidant-free conditions (entries 8 and 9), confirming the irreplaceable roles of O₂ and Cu₃N NC catalyst in this conversion.

Table 3-1. Trimerization of **1a** using Cu catalysts



The reaction scheme shows indole (**1a**) reacting with O₂ in the presence of a catalyst to form the trimeric product [3,2':2',3''-terindolin]-3'-one (**2a**).

Entry	Catalyst	O ₂ (bar)	Yield of 2a (%)
1	Cu ₃ N NC	3	84
2	Cu ₃ N (commercial)	3	28
3	Cu ₂ O	3	26
4	CuCl	3	23
5	CuO	3	18
6	Cu ₃ P	3	18
7 ^{b,c}	Cu ₃ N NC	-	N. R.
8 ^b	Cu ₃ N NC	-	N. R.
9	-	3	N. R.

^a Reaction conditions: **1a** (0.5 mmol), catalyst (5 mol% Cu), H₂O/CH₃CN (v/v = 2/3, 2 mL), 60 °C, 12 h, isolated yields. ^b Ar (3 bar). ^c TBHP (2.0 eq.). The abbreviation N. R. indicates No Reaction.

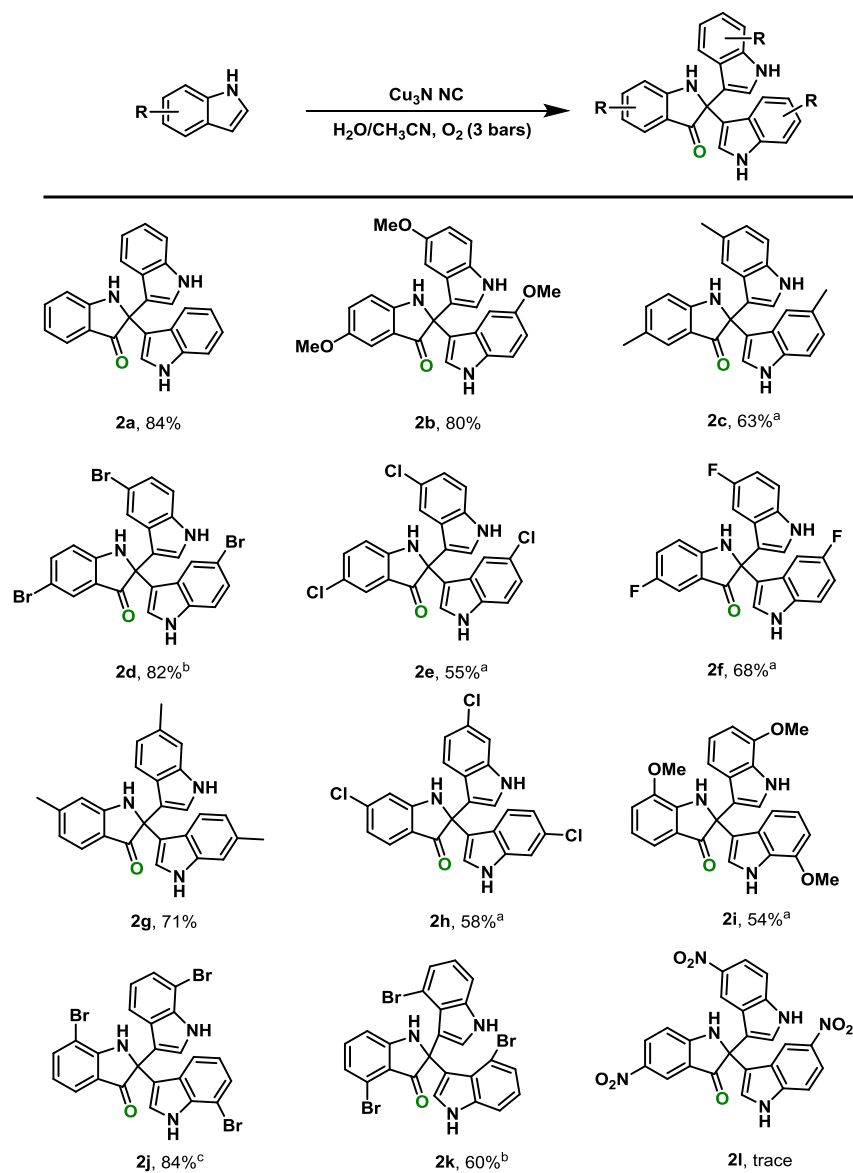
Table 3-2. Comparison of Cu₃N NC catalytic system and reported catalytic systems for trimerization of indole

Entry	Catalyst	Reaction condition	Yield [%]	Ref.
1	Cu ₃ N NC	O ₂ (3 bars), H ₂ O/CH ₃ CN, 60 °C, 12 h	84	<i>This work</i>
2	c-Chl	O ₂ , White LED, K ₃ PO ₄ , SDS, H ₂ O, rt, 48 h	87	13
3	Ru(bpy) ₃ Cl ₂ ·6H ₂ O	O ₂ , Blue LED, H ₂ O/CH ₃ CN, rt, 7 h	76	12
4	Co(salen)	O ₂ (bubbling), SDS, MeOH, rt, 24 h	44	10
5	-	TEMPO ⁺ BF ⁻ (with O ₂), THF, rt, 6 h	90	23
6	CuCl ₂	TEMPO (with O ₂), Benzoic acid, CH ₃ CN, 60 °C, 6 h	83	11
7	-	TEMPO (with O ₂), Benzoic acid, CH ₃ CN, 65 °C, 72 h	80	24
8	PdCl ₂ /MnO ₂	TBHP, CH ₃ CN, 60 °C, 5 h	90	4
9	I ₂	TBHP, Cyclohexanone, rt, 8 h	87	5
10	-	TBHP, 100 °C, 3 h	84	6
11	Nano Au-Pd-rGO	Oxone, H ₂ O, rt, 12 h	90	7
12	Fe ₂ O ₃ -Zeolite-Y	Oxone, MeCN, rt, 0.25 h	90	8

Note: SDS = sodium dodecyl sulfate

The Cu₃N NC system could be applied to the oxidative trimerization of a wide range of indoles with O₂ as oxidant (**Scheme 3-2**). Indoles bearing electron-donating groups (–OMe and –Me) at the C5 position were tolerated and smoothly transformed to the desired products in 82% and 63% isolated yields (**2b** and **2c**). Moreover, indoles bearing electron-withdrawing groups (–Br, –Cl, and –F) exhibited high activity, affording the oxidative products in good yields (**2d–2f**). The other position-substituted indoles could also be used as the reaction partner to produce the good yields of

trimerization products (**2g–2k**). When indole with a strong electron-withdrawing group ($-\text{NO}_2$) was treated under standard reaction conditions, no reaction was occurred (**2l**). These results demonstrate that the $\text{Cu}_3\text{N NC}$ functions as an efficient catalyst for the trimerization of indoles with O_2 as oxidant with a wide substrate scope.

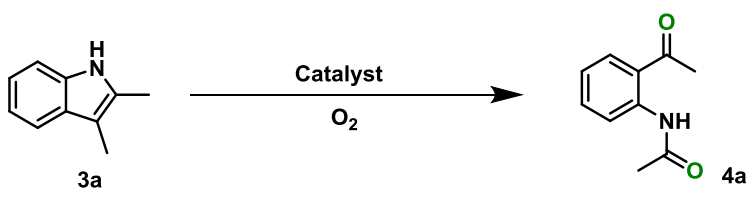


Scheme 3-2. Reaction conditions: **1** (0.5 mmol), $\text{Cu}_3\text{N NC}$ (5 mg, 5 mol% Cu), $\text{H}_2\text{O}/\text{CH}_3\text{CN}$ (v/v = 2/3, 2 mL), 60 °C, 12 h, isolated yield. ^a 60 °C, 24 h. ^b 80 °C, 12 h. ^c 80 °C, 24 h.

3.3. Catalytic performance of Cu₃N NC in Witkop reaction of indoles

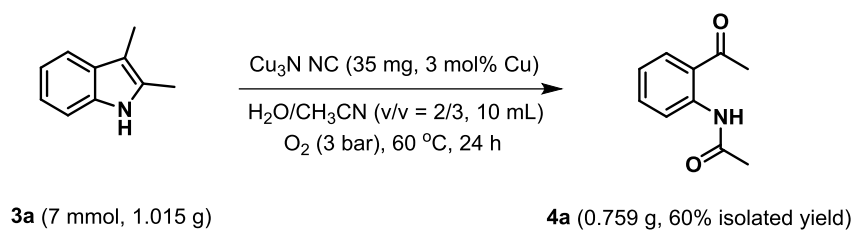
To further extend the generality of the oxidation catalysis of Cu₃N NC, the oxidative cleavage reaction of the C2-C3 C=C double bond of indoles was investigated. The oxidation of 2,3-dimethylindole (**3a**) was selected as a model reaction, and the results were summarized in **Table 3-3**. The Cu₃N NC catalyst efficiently promoted the Witkop oxidation of **3a** to *N*-(2-acetylphenyl)acetamide (**4a**) in 72% isolated yield under 1 bar of O₂ without additives in an aqueous CH₃CN solvent, while other Cu catalysts exhibited lower activities (entry 1 vs entries 2–6). When the pressure of O₂ was increased to 3 bars, the yield of **4a** was 79% (entry 7). The reaction was not occurred in the absence of Cu₃N NC catalyst (entry 8). This Cu₃N NC–O₂ catalyst system was also applicable to the gram-scale synthesis, and **3a** (7.0 mmol) was converted to **4a** in 60% isolated yield (0.76 g) (**Scheme 3-3**).

Table 3-3. Witkop oxidation of **3a** using Cu catalysts



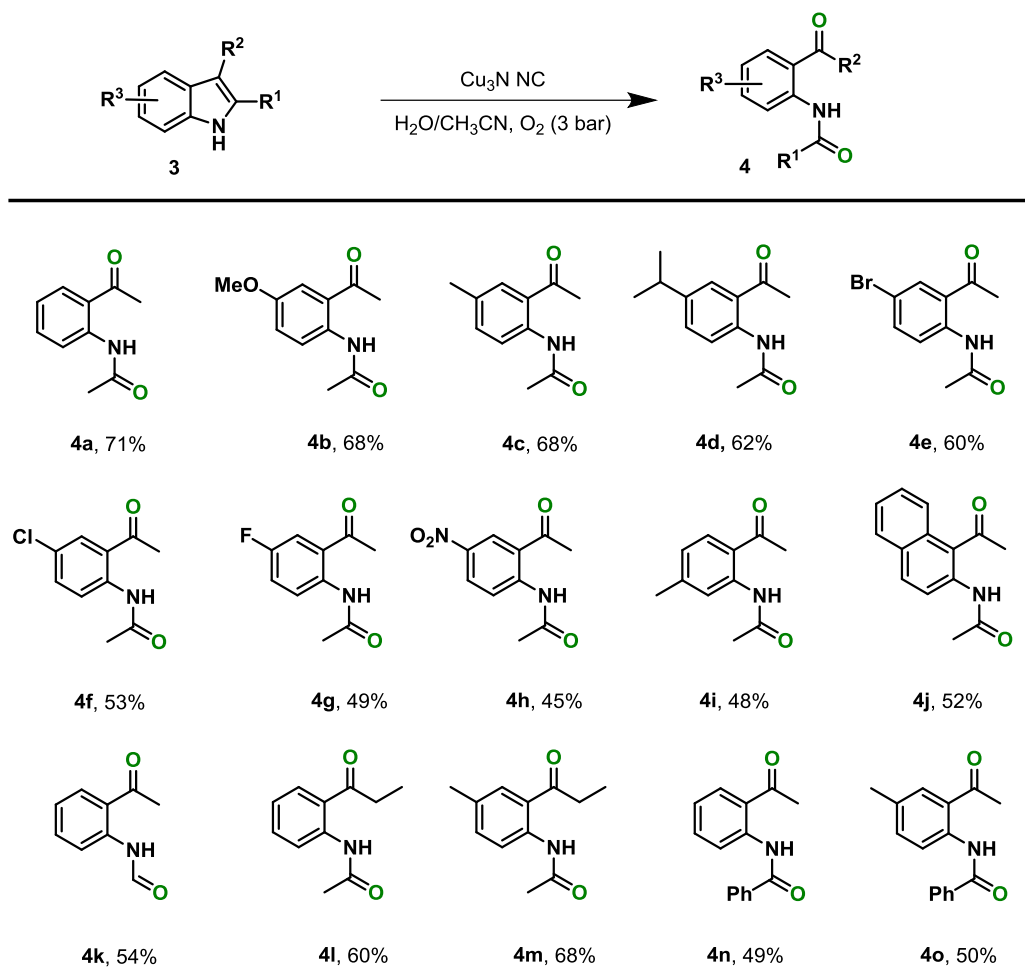
Entry	Catalyst	O ₂ (bar)	Yield of 4a (%)
1	Cu ₃ N NC	1	72
2	Cu ₂ O	1	50
3	CuI	1	41
4	CuCl	1	26
5	CuO	1	23
6	CuCl ₂	1	21
7	Cu ₃ N NC	3	79
8	-	3	2

^a Reaction conditions: **3a** (0.5 mmol), catalyst (5 mol% Cu), H₂O/CH₃CN (v/v = 2/3, 2 mL), 60 °C, 12 h. Yields were calculated by GC-MS analysis using naphthalene as an internal standard.



Scheme 3-3. Gram-scale experiment of the Witkop reaction of **3a** using $\text{Cu}_3\text{N NC}$.

Furthermore, a wide range of 2,3-dimethylindole derivatives with different groups, such as $-\text{OMe}$, $-\text{Me}$, $-\text{Br}$, $-\text{Cl}$, and $-\text{F}$, at the C5 position were smoothly transformed into the corresponding oxygenated products in good yields (**4b–4g**). 5-Nitro-substituted dimethylindole, 2,3-dimethyl-5-nitroindole, was also tolerated (**4h**). Other position-substituted indoles were utilized as efficient substrates in this catalytic system and provided **4i** and **4j** in 46% and 52% yields, respectively. The oxidation of 3-methylindole also proceeded efficiently to generate the desired product **4k** in 54% yield. Additionally, when other C2, C3-disubstituted indoles were used in this reaction, the corresponding Witkop cleavage products (**4l–4o**) were obtained in acceptable yields (49–68%). These results revealed that the $\text{Cu}_3\text{N NC}$ catalytic system is applicable to the additive-free Witkop oxidation with a broad substrate scope (**Table 3-4**).



Scheme 3-4. Substrate scope of the Witkop oxidation of indoles. Reaction conditions: **3** (0.5 mmol), Cu₃N NC (5 mg, 5 mol% Cu), H₂O/CH₃CN (v/v = 2/3, 2 mL), 60 °C, 12 h, isolated yield.

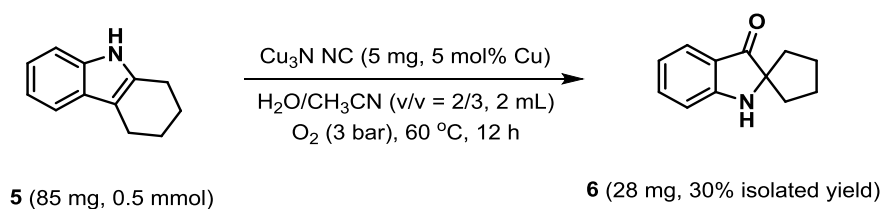
Table 3-4. Comparison of Cu₃N NC catalytic system and reported catalytic systems for Witkop oxidation

Entry	Catalyst	Reaction conditions	Yield [%]	Ref.
1	Cu ₃ N NC	O ₂ (3 bars), H ₂ O/CH ₃ CN, 60 °C, 12 h	71	<i>This work</i>
2	Cu-X zeolite	O ₂ , DCE/CH ₃ CN, 50 °C, 3 h	84	25
3	CuBr	O ₂ , L3 /Na ₂ CO ₃ , THF, 50 °C, 24 h	55	19

4	Rose bengal	O ₂ , Blue LED, K ₃ PO ₄ , H ₂ O/DMF, rt, 45 h	82	26
5	c-Chl	O ₂ , White LED, K ₃ PO ₄ , H ₂ O/SDS, rt, 18 h	79	12
6	Fe ^{III} (O ₂ ⁻)(TPP)	O ₂ n, DMF, -40 °C, 2 h	49	27
7	FeCl ₃	O ₂ , BiPy/Py, THF, 25 °C, 20 h	37	28
8	[(B)(Por)Fe ^{III} (O ₂ ⁻)]	O ₂ , THF/DCM, -40 °C, 2 h	31	29
9	-	H ₂ O ₂ or UHP, CH ₃ CN or HFIP, 45 °C, 24 h	77 or 81	16
10	CaCl ₂	H ₂ O ₂ , MeOH, reflux, 4 h	50	30
11	KCl	Oxone, H ₂ O/HFIP, rt, 24 h	76	18

Note: **L3** = 2,2'-(propane-2,2-diyl)bis(5-(tert-butyl)benzo[d]oxazole), SDS = sodium dodecyl sulfate; BiPy = 2,2'-bipyridine; Py = pyridine; UHP = urea hydrogen peroxide; HFIP = 1,1,1,3,3,3-hexafluoroisopropanol.

Then, to investigate the applicability of the Cu₃N NC catalytic system, the oxidative rearrangement of C2-C3 cyclic-substituted indole, 2,3,4,9-tetrahydro-1*H*-carbazole (**5**) was conducted (**Scheme 3-5**). The previously reported reaction systems required additional acid or base [31], while the Cu₃N NC catalyst provided the desired rearrangement product spiro-[cyclopentane-1,2'-indolin]-3'-one (**6**) in 30% yield.



Scheme 3-5. Cu₃N NC catalyzed-oxidative rearrangement of **5**.

3.4. Reusability of Cu₃N NC

Recycling experiments of Cu₃N NC were conducted in the Witkop oxidation of **3a**. After the reaction, the Cu₃N NC was recovered from the reaction solution. As shown in **Figure 3-2** (a), Cu₃N NC catalyst maintained its activity up to the second reuse experiment (run 2), generating an approximately 60% yield of **4a** for 0.5 h. For the third run, a slight decrease of **4a** yield was observed. To clarify the reason for this, several analyses of reused Cu₃N NC were carried out. The PXRD patterns and TEM image of the reused Cu₃N NC catalyst suggested that the cubic morphology of Cu₃N NC was gradually transformed to amorphous during the reaction (**Figures 3-2** (b) and (c)). The deactivation of Cu₃N NC in the third run may be caused by the morphology change. Overall, the Cu₃N NC catalyst could be reused for several times without significant loss of its original activity.

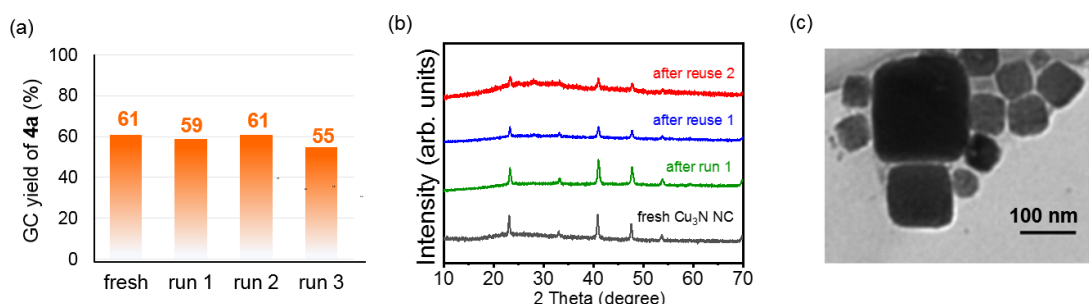
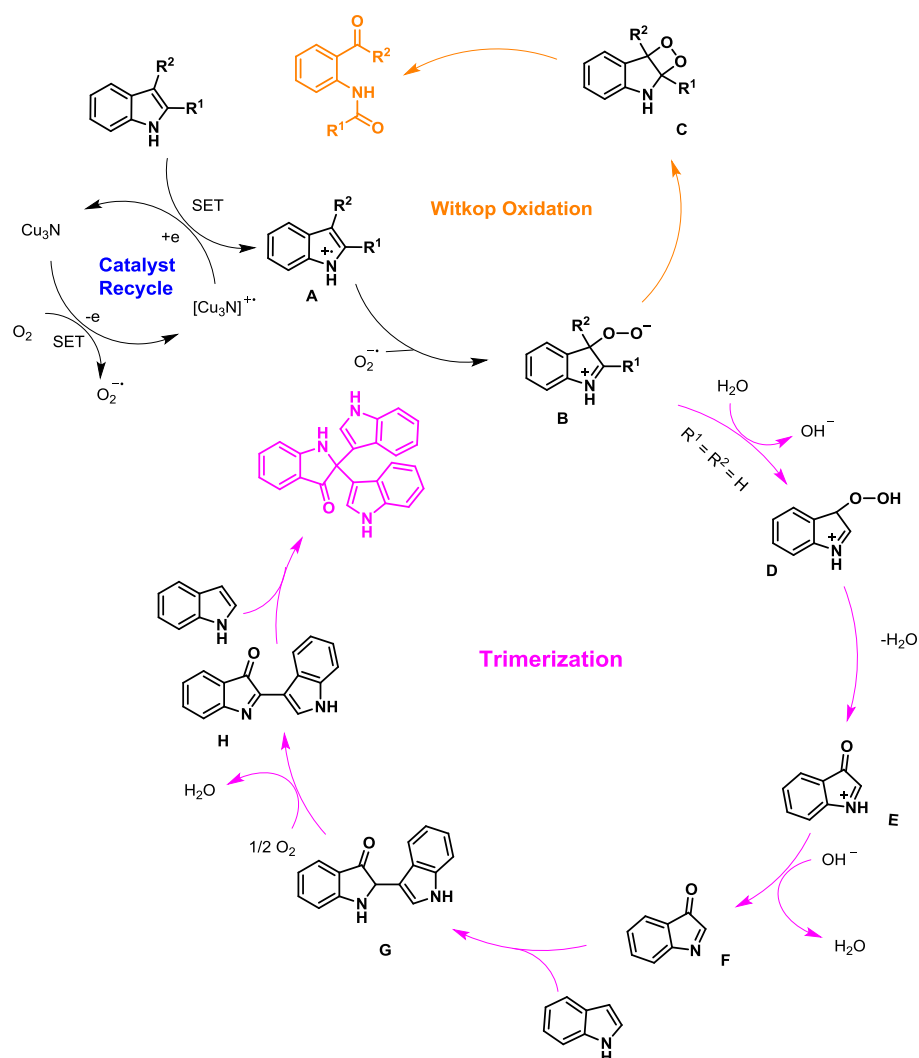


Figure 3-2. (a) Reuse experiments of Cu₃N NC for Witkop oxidation (0.5 h); Reaction conditions: **3a** (0.5 mmol), Cu₃N NC (5 mg, 5 mol% Cu), H₂O/CH₃CN (v/v = 2/3, 2 mL), O₂ (1 bar), 60 °C, 0.5 h. Yields were calculated by GC-MS analysis using naphthalene as an internal standard. (b) PXRD patterns of fresh and recovered Cu₃N NC. (c) TEM images of reused Cu₃N NC (after run 1).

3.5. Proposed mechanism

The proposed mechanism for Cu₃N NC-catalyzed oxidation of indoles is presented in **Scheme 3-7** [11–13, 16–20]. Firstly, O₂ and indoles are converted to O₂^{•-} and a radical-cation intermediate **A**, respectively, through the single-electron-transfer (SET) process mediated by Cu₃N. Subsequently, the

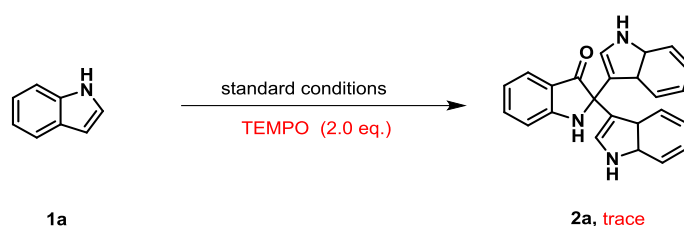
radical cation **A** reacted with $O_2^{\cdot-}$ to give the peroxide species **B**, which follows the intermolecular hydrogen transfer process and affords the peroxide **C**. Next, the intermediate **C** undergoes the dehydration and provides the imine **D**, which reacts with indole to form the nucleophilic addition product **E**. Finally, the intermediate **F** is generated through the oxidation of **E** and further reacts with indole to afford the trimerization product. For the Witkop reaction, **B** is transformed into the dioxetane **C** via intermolecular cyclization, which is further produce the Witkop oxidation product via rearrangement process.



Scheme 3-7. Proposed mechanism for the Cu_3N NC catalyzed-oxidation of indoles.

This mechanism is supported by the control experiments: 1) The TEMPO was added as a

radical scavenger under the standard reaction condition, and the trimerization of **1a** was prohibited, demonstrating a free radical process was involved in the Cu₃N NC-catalyzed trimerization reaction (Scheme 3-6) [32, 33]. 2) The results of GC-MS analysis clearly confirmed the formation of intermediates **G** and **H** during the trimerization of **1a** (Figures 3-3 and 3-4). Hence, these observations verified the conversion of O₂ to superoxide species was activated by Cu₃N NC, which processes arranged N–Cu–N structure on surface.



Scheme 3-6. Control experiment in the reaction of **1a** using TEMPO under O₂.

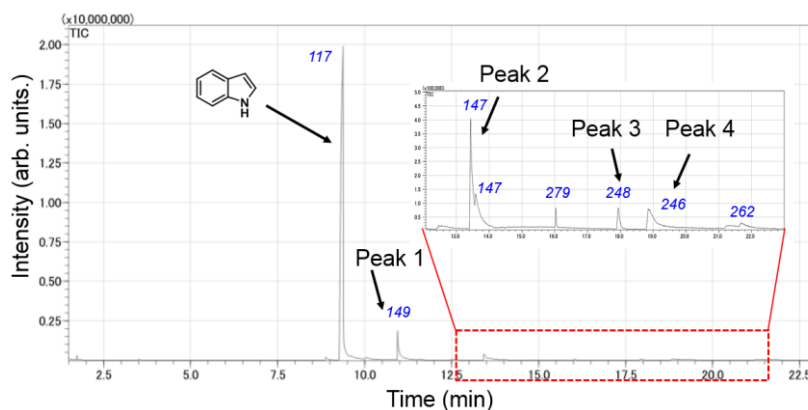


Figure 3-3. GC-MS chromatogram for the trimerization of **1a** using Cu₃N NC. Reaction conditions: **1a** (0.5 mmol), Cu₃N NC (5 mg, 5 mol% Cu), H₂O/CH₃CN (v/v = 2/3, 2 mL), O₂ (3 bars), 60 °C, 6 h.

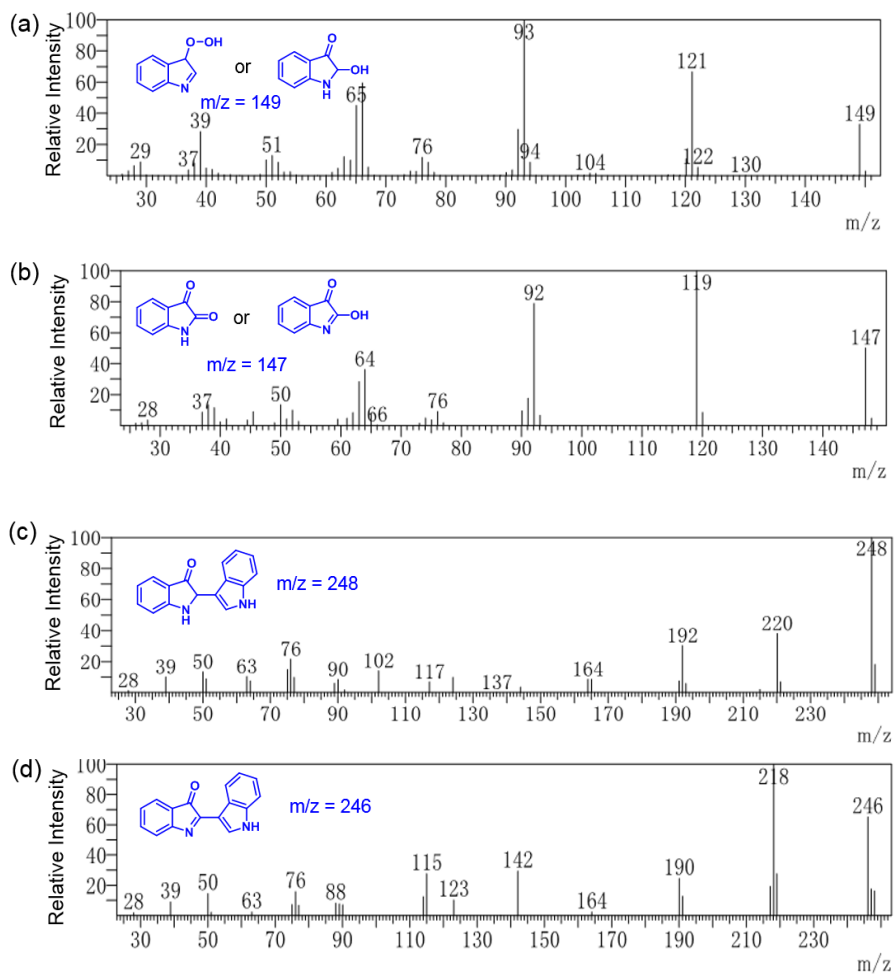


Figure 3-4. EI-MS spectra of (a) Peak 1, (b) Peak 2, (c) Peak 3, and (d) Peak 4 in **Figure 3-3** detected in the trimerization of **1a**.

4. Conclusion

This chapter demonstrated that the Cu₃N NC is an efficient heterogeneous catalyst for green oxidative conversion of indoles with O₂ as a sole oxidant under additive-free conditions. The catalytic activity of Cu₃N NC outperformed other Cu compounds in oxidative trimerization and Witkop oxidation of indoles. A wide range of indoles can be converted to the corresponding products in moderate to good yields. This is the first application of the Cu₃N NC to oxidative reactions. The high catalytic activity of Cu₃N NC may be attributed to the essential regularly arranged N–Cu–N structure, which promotes the transformation of O₂ to superoxide species.

References

- 1 K. Urbina, D. Tresp, K. Sipps, M. Szostak, *Adv. Synth. Catal.*, **2021**, *363*, 2723–2739.
- 2 K. McClay, S. Mehboob, J. Yu, B. D. Santarsiero, J. Deng, J. L. Cook, H. Jeong, M. E. Johnson, R. J. Steffan, *AMB Express*, **2015**, *5*, 38.
- 3 C. Wu, Y. Liu, Y. Yang, P. Zhang, W. Zhong, Y. Wang, Q. Wang, Y. Xu, M. Li, X. Li, M. Zheng, L. Chen, H. Li, *Acta Pharm. Sin. B.*, **2020**, *10*, 766–788.
- 4 S. K. Guchhait, V. Chaudhary, V. A. Rana, G. Priyadarshani, S. Kandekar, M. Kashyap, *Org. Lett.*, **2016**, *18*, 1534–1537.
- 5 B. Deka, M. L. Deb, R. Thakuria, P. K. Baruah, *Catal. Commun.*, **2018**, *106*, 68–72.
- 6 J. Kothandapani, S. M. K. Reddy, S. Thamotharan, S. M. Kumar, K. Byrappa, S. S. Ganesan, *Eur. J. Org. Chem.*, **2018**, *2018*, 2762–2767.
- 7 S. B. Gohain, M. Basumatary, P. K. Boruah, M. R. Das, A. J. Thakur, *Green Chem.*, **2020**, *22*, 170–179.
- 8 M. J. Baruah, A. Dutta, S. Biswas, G. Gogoi, N. Hoque, P. K. Bhattacharyya, K. K. Bania, *ACS Appl. Nano Mater.*, **2022**, *5*, 1446–1459
- 9 Z. Shi, C. Zhang, C. Tang, N. Jiao, *Chem. Soc. Rev.*, **2012**, *41*, 3381–3430.
- 10 A. Inada, Y. Nakamura, Y. Morita, *Chem. Pharm. Bull.*, **1988**, *36*, 462–464.
- 11 Y. B. Kong, J.-Y. Zhu, Z.-W. Chen, L.-X. Liu, *Can. J. Chem.*, **2014**, *92*, 269–273.
- 12 L.-T. Cheng, S.-Q. Luo, B.-C. Hong, C.-L. Chen, W.-S. Li, G.-H. Lee, *Org. Biomol. Chem.*, **2020**, *18*, 6247–6252.
- 13 S. Banu, S. Choudhari, G. Patel, P. P. Yadav, *Green Chem.*, **2021**, *23*, 3039–3047.
- 14 M. Mentel, R. Breinbauer, *Curr. Org. Chem.*, **2007**, *11*, 159–176.
- 15 J. A. Homer, J. Sperry, *J. Nat. Prod.*, **2017**, *80*, 2178–2187.
- 16 N. Llopis, P. Gisbert, A. Baeza, *Adv. Synth. Catal.*, **2021**, *363*, 3245–3249.

- 17 P. Astolfi, L. Greci, C. Rizzoli, P. Sgarabotto, G. Marrosu, *J. Chem. Soc., Perkin Trans. 2*, **2001**, 1634.
- 18 J. Xu, L. Liang, H. Zheng, Y. R. Chi, R. Tong, *Nat. Commun.*, **2019**, *10*, 4754–4765.
- 19 J. Shi, R.-A. Wang, W. Wu, J.-R. Song, Q. Chi, W.-D. Pan, H. Ren, *Org. Lett.*, **2022**, *24*, 3358–3362.
- 20 Z. Yuan, L. Lu, M. Liu, X. Liu, C. Liu, D. Yin, Y. Zhang, Y. Rao, *Green Chem.*, **2022**, *24*, 3277–3283.
- 21 Z. Yin, C. Yu, Z. Zhao, X. Gou, M. Shen, L. Na, M. Muzzio, J. Li, H. Liu, H. Lin, J. Yin, G. Lu, D. Su, S. Sun, *Nano Lett.*, **2019**, *19*, 8658–8663.
- 22 B. Robinson, *Chem. Rev.*, **1963**, *63*, 373–401.
- 23 X. Yan, Y.-D. Tang, C.-S. Jiang, X. Liu, H. Zhang, *Molecules*, **2020**, *25*, 419–441.
- 24 W.-B. Qin, Q. Chang, Y.-H. Bao, N. Wang, Z.-W. Chen, L.-X. Liu, *Org. Biomol. Chem.*, **2012**, *10*, 8814–8821.
- 25 K. Ebitani, K. Nagashima, T. Mizugaki, K. Kaneda, *Chem. Commun.*, **2000**, 869–870.
- 26 W. Schilling, Y. Zhang, D. Riemer, S. Das, *Chem. Eur. J.*, **2020**, *26*, 390–395.
- 27 J. J. D. Sacramento, D. P. Goldberg, *Chem. Commun.*, **2020**, *56*, 3089–3092.
- 28 K. Ohkubo, M. Iwabuchi, K. Takano, *J. Mol. Catal.*, **1985**, *32*, 285–290.
- 29 P. Mondal, G. Wijeratne, *J. Am. Chem. Soc.*, **2020**, *142*, 1846–1856.
- 30 P. Astolfi, L. Greci, C. Rizzoli, P. Sgarabotto, G. Marrosu, *J. Chem. Soc., Perkin Trans. 2*, **2001**, 1634.
- 31 C. A. Mateo, A. Urrutia, J. G. Rodriguez, I. Fonseca, F. H. Cano, *J. Org. Chem.*, **1996**, *61*, 810–812.
- 32 S. E. Allen, R. R. Walvoord, R. Padilla-Salinas, M. C. Kozlowski, *Chem. Rev.*, **2013**, *113*, 6234–6458.

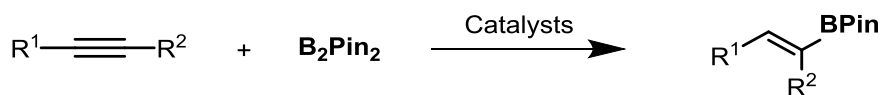
33 X.-X. Liu, X.-L. Luo, Z.-Y. Wu, X.-F. Cui, X.-Q. Zhou, Y.-Q. He, G.-S. Huang, *J. Org. Chem.*, **2017**, 82, 2107–2113.

Chapter I V.

***Efficient Hydroboration of Alkynes to Vinyl Boronates
by Copper Nitride Nanocube***

1. Introduction

Vinyl boronate esters have been widely used in organic and medicinal chemistry as well as functional materials [1–3]. The hydroboration of alkynes with pinacolborane (HBPin) is considered as an efficient protocol for synthesizing the vinyl boronate esters [4]. Nevertheless, HBPin is difficult to handle due to its moisture and oxygen sensitivities [5]. In last decades, the hydroboration of alkynes with bis(pinacolato)diboron (B_2Pin_2) has captured much attention because B_2Pin_2 reagent is highly water resistant and oxygen insensitive (**Scheme 4-1**) [6]. Hitherto, several efficient catalytic systems based on noble metals such as Pt, Pd, and Au [7–9] have been developed for this reaction, but these constituent metals are expensive, rare, and inherently toxic. Although cheap, earth-abundant, and low-toxic homogeneous Cu catalysts, e.g., CuCl or CuSO₄, have been adopted for the hydroboration of alkynes with B_2Pin_2 , they have the problems in terms of difficulty of separation and recycling of the catalysts [10–15]. To overcome these drawbacks, heterogeneous copper catalysts such as Cu powder, Cu-CuFe₂O₄, and Cu-SNC sponge, have been developed [16–25]. However, the reported works required the utilization of additives to furnish high yields and selectivity. Recently, the hydroboration of alkynes under additive-free conditions were achieved with single atom copper catalysts [26, 27], but the thermal conditions are still required. Therefore, developing an efficient and environmentally benign catalytic system operating under mild and additive-free conditions would significantly advance the utility for the hydroboration of alkynes.



Scheme 4-1. Hydroboration of alkynes with B_2Pin_2 to vinyl boronates.

In this chapter, the highly efficient hydroboration of alkynes to vinyl boronate esters was achieved over a copper nitride nanocube ($\text{Cu}_3\text{N NC}$) catalyst under additive-free and mild reaction conditions. The catalytic activity of $\text{Cu}_3\text{N NC}$ was superior to those of the other Cu catalysts, and good functional group tolerance was observed, affording a wide range of vinyl boronate esters in excellent yields. Furthermore, the $\text{Cu}_3\text{N NC}$ provided an outstanding turnover number (912) in the hydroboration of alkynes. This is the first time for the hydroboration of alkynes under mild and additive-free conditions with a heterogeneous catalyst.

2. Experimental section

2.1. General information

All organic reagents were purchased from FUJIFILM Wako Pure Chemical Corporation, Sigma–Aldrich, or Tokyo Chemical Industry. Gas chromatography-mass spectrometry (GC-MS) was performed using a GCMS-QP2010 SE instrument equipped with an InertCap WAX-HT capillary column (GL Science, 30 m × 0.25 mm i.d., film thickness 0.25 μm). ¹H and ¹³C nuclear magnetic resonance (NMR) spectra were acquired at 400 and 100 MHz, respectively, using a JEOL JNM-ESC400 spectrometer. Chemical shifts are reported in parts per million (ppm) relative to the signal (0.00 ppm) for internal tetramethylsilane in CDCl₃. The ¹³C NMR spectral data are reported using the following standard chemical shift: CDCl₃ (77.16 ppm). NMR multiplicities are reported using the following abbreviations: s: singlet, d: doublet, t: triplet, q: quartet, m: multiplet, br: broad, *J*: coupling constants in hertz. All known compounds described in the paper were characterized by comparison of their ¹H and ¹³C NMR spectra with previously reported data. Scanning electron microscopy (SEM) image was obtained using a JSM-7600F microscope operated at 15.0 kV at the Analytical Instrument Facility, Graduate School of Science, Osaka University. Transmission electron microscopy (TEM) images were obtained using a Hitachi HF-2000 microscope operated at 200 kV at the Research Center for Ultra-High Voltage Electron Microscopy, Osaka University. Cu *K*-edge X-ray absorption spectra (extended X-ray absorption near edge structure (XANES)) obtained using a Si (111) monochromator were recorded at 25 °C at the BL01B1 and BL14B2 stations, SPring-8, Japan Synchrotron Radiation Research Institute (JASRI), Harima, Japan. Data analysis was performed using Demeter (ver. 0.9.26). Powder X-ray diffraction (PXRD) patterns were acquired using a Philips XPert-MPD instrument with Cu-*K*_α radiation. The X-ray photoelectron spectroscopies (XPS) spectra of samples were obtained using a KRATOS AXIS ULTRA HAS spectrometer, and the binding energy referred to the C 1s peak (284.4 eV). Fourier-transform infrared (FT-IR) spectra were recorded using a JASCO FT-IR 4100

spectrometer equipped with a mercury cadmium telluride detector. Temperature-programmed desorption (TPD) data were obtained using a BELCAT-A instrument (BEL Japan Inc.) equipped with a mass spectrometer (BELMass-S, BEL Japan, Inc.).

2.2. Preparation of Cu₂O NC

The Cu₂O NC was prepared by a facile wet chemical approach [28]. In a typical reaction, 0.075 mol L⁻¹ of NaOH (10 mL) was added dropwise to 0.5 mol L⁻¹ of CuSO₄ aqueous solution (5 mL) under stirring at pH = 10.5. Subsequently, the 0.1 mol L⁻¹ of ascorbic acid (13 mL) was added dropwise into the solution and was continuously stirred at room temperature for 1 h. Then, a yellow precipitate was obtained (pH = 4.0–4.5). Redispersion and precipitation cycles were repeated using a water and ethanol to afford the yellow powder.

2.3. Reaction procedure for the hydroboration of alkynes

General reaction procedure for the hydroboration of alkynes using Cu₃N NC was as follows. Cu₃N NC (5 mg) was placed in a 50 mL stainless-steel autoclave with a Teflon inner cylinder, followed by addition of alkynes (0.5 mmol), diboron reagents (0.6 mmol), and EtOH (2 mL). The reaction mixture was stirred at 30 °C under Ar. After the reaction, the reaction solution was analyzed by GC-MS or ¹H NMR to determine the reaction selectivity. The mixture was concentrated to yield the crude product, which was further purified by silica gel flash chromatography (hexane/ethyl acetate) to give the desired products.

2.4. Gram scale experiment

Cu₃N NC (2 mg, 0.01 mmol of Cu) was placed in a 50 mL stainless-steel autoclave with a Teflon inner cylinder, followed by addition of phenylacetylene (1.02 g, 10.0 mmol), B₂Pin₂ (3.03 g,

12.0 mmol), and EtOH (10 mL). The reaction mixture was stirred at 30 °C under Ar for 12 h. After the reaction, the reaction mixture was concentrated to yield the crude product, which was further purified by silica gel flash chromatography (hexane/ethyl acetate, v/v = 30/1) to give the (*E*)-4,4,5,5-tetramethyl-2-styryl-1,3,2-dioxaborolane (2.09 g).

2.5. Recycling experiments

Cu₃N NC (5 mg) was placed in a 50 mL stainless-steel autoclave with a Teflon inner cylinder, followed by addition of phenylacetylene (0.5 mmol), B₂Pin₂ (0.6 mmol), and EtOH (2 mL). After the reaction mixture was stirred at 30 °C for 1 h under Ar, Cu₃N NC were recovered by filtration. The catalyst was washed with ethanol and dried at room temperature *in vacuo* without further purification or reactivation before reuse.

2.6. Product identification

(E)-4,4,5,5-tetramethyl-2-styryl-1,3,2-dioxaborolane

CAS registry No. [83947-56-2], white solid; ^1H NMR (400 MHz, CDCl_3): δ 7.51–7.48 (m, 2H), 7.40 (d, $J = 18.4$ Hz, 1H), 7.36–7.26 (m, 3H), 6.17 (d, $J = 18.4$ Hz, 1H), 1.31 (s, 12H); ^{13}C NMR (100 MHz, CDCl_3): δ 149.7, 137.7, 129.1, 128.7, 127.2, 83.5, 25.0.

(E)-2-(4-methoxystyryl)-4,4,5,5-tetramethyl-1,3,2-dioxaborolane

CAS registry No. [149777-83-3], colorless liquid; ^1H NMR (400 MHz, CDCl_3): δ 7.43 (d, $J = 8.0$ Hz, 2H), 7.36 (d, $J = 18.4$ Hz, 1H), 6.85 (d, $J = 8.0$ Hz, 2H), 6.01 (d, $J = 18.4$ Hz, 1H), 3.78 (s, 3H), 1.30 (s, 12H); ^{13}C NMR (100 MHz, CDCl_3): δ 160.4, 149.1, 130.4, 128.5, 114.0, 83.2, 55.3, 24.9.

(E)-4,4,5,5-tetramethyl-2-(4-methylstyryl)-1,3,2-dioxaborolane

CAS registry No. [149777-84-4], yellow liquid; ^1H NMR (400 MHz, CDCl_3): δ 7.42–7.32 (m, 3H), 7.13 (d, $J = 8.0$ Hz, 2H), 6.11 (d, $J = 18.8$ Hz, 1H), 2.33 (s, 3H), 1.30 (s, 12H); ^{13}C NMR (100 MHz, CDCl_3): δ 149.6, 139.0, 134.9, 129.4, 127.1, 83.3, 24.9, 21.4.

(E)-4-(2-(4,4,5,5-tetramethyl-1,3,2-dioxaborolan-2-yl)vinyl)aniline

CAS registry No. [2159091-30-0], yellow solid; ^1H NMR (400 MHz, CDCl_3): δ 7.35–7.24 (m, 3H), 6.62 (d, $J = 8.4$ Hz, 2H), 5.93 (d, $J = 18.4$ Hz, 1H), 3.79 (s, 2H), 1.30 (s, 12H); ^{13}C NMR (100 MHz, CDCl_3): δ 149.7, 147.5, 128.6, 128.1, 114.9, 83.1, 24.8.

(E)-2-(4-bromostyryl)-4,4,5,5-tetramethyl-1,3,2-dioxaborolane

CAS registry No. [1242770-51-9], white solid; ^1H NMR (400 MHz, CDCl_3): δ 7.46 (d, $J = 8.8$ Hz, 2H), 7.42–7.28 (m, 3H), 6.15 (d, $J = 18.4$ Hz, 1H), 1.31 (s, 12H); ^{13}C NMR (100 MHz, CDCl_3): δ

148.2, 136.5, 131.9, 128.6, 123.0, 83.6, 24.9.

(E)-2-(4-chlorostyryl)-4,4,5,5-tetramethyl-1,3,2-dioxaborolane

CAS registry No. [223919-54-8], white solid; ¹H NMR (400 MHz, CDCl₃): δ 7.40 (d, *J* = 8.4 Hz, 2H), 7.38–7.29 (m, 3H), 6.13 (d, *J* = 18.4 Hz, 1H), 1.31 (s, 12H); ¹³C NMR (100 MHz, CDCl₃): δ 148.1, 136.1, 134.7, 128.9, 128.3, 83.5, 24.9.

(E)-2-(4-fluorostyryl)-4,4,5,5-tetramethyl-1,3,2-dioxaborolane

CAS registry No. [504433-86-7], colorless liquid; ¹H NMR (400 MHz, CDCl₃): δ 7.51–7.42 (m, 2H), 7.36 (d, *J* = 18.4 Hz, 1H), 7.01 (t, *J* = 8.8 Hz, 2H), 6.08 (d, *J* = 18.4 Hz, 1H), 1.31 (s, 12H); ¹³C NMR (100 MHz, CDCl₃): δ 163.2 (d, *J* = 248.0 Hz), 148.2, 133.8 (d, *J* = 4.0 Hz), 128.7 (d, *J* = 8.0 Hz), 115.6 (d, *J* = 22.0 Hz), 83.5, 24.9.

(E)-4,4,5,5-tetramethyl-2-(4-nitrostyryl)-1,3,2-dioxaborolane

CAS registry No. [149777-86-6], white solid; ¹H NMR (400 MHz, CDCl₃): δ 8.20 (d, *J* = 8.8 Hz, 2H), 7.61 (d, *J* = 8.8 Hz, 2H), 7.42 (d, *J* = 18.4 Hz, 1H), 6.33 (d, *J* = 18.4 Hz, 1H), 1.33 (s, 12H); ¹³C NMR (100 MHz, CDCl₃): δ 147.8, 146.7, 143.7, 127.7, 124.1, 83.9, 24.9.

(E)-4,4,5,5-tetramethyl-2-(2-methylstyryl)-1,3,2-dioxaborolane

CAS registry No. [1294009-26-9], yellow liquid; ¹H NMR (400 MHz, CDCl₃): δ 7.65 (d, *J* = 18.4 Hz, 1H), 7.57–7.53 (m, 1H), 7.20–7.12 (m, 3H), 6.08 (d, *J* = 18.4 Hz, 1H), 2.42 (s, 3H), 1.31 (s, 12H); ¹³C NMR (100 MHz, CDCl₃): δ 147.2, 136.8, 136.4, 130.5, 128.7, 126.2, 125.9, 83.4, 24.9, 19.9.

(E)-4,4,5,5-tetramethyl-2-(3-methylstyryl)-1,3,2-dioxaborolane

CAS registry No. [1421061-31-5], yellow liquid; ^1H NMR (400 MHz, CDCl_3): δ 7.37 (d, $J = 18.4$ Hz, 1H), 7.33–7.26 (m, 2H), 7.24–7.18 (m, 1H), 7.09 (d, $J = 7.2$ Hz, 1H), 6.15 (d, $J = 18.4$ Hz, 1H), 2.33 (s, 3H), 1.30 (s, 12H); ^{13}C NMR (100 MHz, CDCl_3): δ 149.7, 138.1, 137.5, 129.8, 128.5, 127.8, 124.3, 83.3, 24.9, 21.4.

(E)-2-(2-chlorostyryl)-4,4,5,5-tetramethyl-1,3,2-dioxaborolane

CAS registry No. [1355094-04-0], yellow liquid; ^1H NMR (400 MHz, CDCl_3): δ 7.79 (d, $J = 18.4$ Hz, 1H), 7.62 (d, $J = 7.6$ Hz, 1H), 7.42–7.32 (m, 1H), 7.31–7.18 (m, 2H), 6.17 (d, $J = 18.4$ Hz, 1H), 1.31 (s, 12H); ^{13}C NMR (100 MHz, CDCl_3): δ 145.0, 135.7, 133.9, 129.9, 129.8, 127.1, 126.9, 83.5, 24.9.

(E)-2-(3-chlorostyryl)-4,4,5,5-tetramethyl-1,3,2-dioxaborolane

CAS registry No. [871125-84-7], yellow liquid; ^1H NMR (400 MHz, CDCl_3): δ 7.45 (s, 1H), 7.34–7.24 (m, 4H), 6.17 (d, $J = 18.4$ Hz, 1H), 1.31 (s, 12H); ^{13}C NMR (100 MHz, CDCl_3): δ 147.9, 139.4, 134.7, 129.9, 128.8, 127.0, 125.3, 83.6, 24.9.

(E)-2-(2-(4,4,5,5-tetramethyl-1,3,2-dioxaborolan-2-yl)vinyl)pyridine

CAS registry No. [161395-83-1], yellow oil; ^1H NMR (400 MHz, CDCl_3): δ 8.60 (d, $J = 4.8$ Hz, 1H), 7.69–7.62 (m, 1H), 7.46 (d, $J = 18.0$ Hz, 1H), 7.40 (d, $J = 7.6$ Hz, 1H), 7.23–7.16 (m, 1H), 6.63 (d, $J = 18.0$ Hz, 1H), 1.31 (s, 12H); ^{13}C NMR (100 MHz, CDCl_3): δ 155.6, 149.8, 148.9, 136.6, 123.2, 122.3, 83.6, 24.9.

(E)-4,4,5,5-tetramethyl-2-(2-(thiophen-3-yl)vinyl)-1,3,2-dioxaborolane

CAS registry No. [736987-75-0], colorless oil; ^1H NMR (400 MHz, CDCl_3): δ 7.38 (d, $J = 18.4$ Hz, 1H), 7.32–7.28 (m, 2H), 7.27–7.24 (m, 1H), 5.94 (d, $J = 18.4$ Hz, 1H), 1.30 (s, 12H); ^{13}C NMR (100

MHz, CDCl₃): δ 143.3, 141.4, 126.2, 125.2, 125.0, 83.4, 24.9.

(E)-2-methyl-4-(4,4,5,5-tetramethyl-1,3,2-dioxaborolan-2-yl)but-3-en-2-ol

CAS registry No. [581802-26-8], colorless oil; ¹H NMR (400 MHz, CDCl₃): δ 6.72 (d, *J* = 18.4 Hz, 1H), 5.61 (d, *J* = 18.4 Hz, 1H), 1.62 (s, 1H), 1.31 (s, 6H), 1.28 (s, 12H); ¹³C NMR (100 MHz, CDCl₃): δ 159.9, 83.4, 71.9, 29.2, 24.9.

(E)-4,4,5,5-tetramethyl-2-(oct-1-en-1-yl)-1,3,2-dioxaborolane

CAS registry No. [83947-55-1], colorless oil; ¹H NMR (400 MHz, CDCl₃): δ 6.64 (dt, *J* = 18.0, 6.4 Hz, 1H), 5.42 (d, *J* = 18.0, 1H), 2.21–2.09 (m, 2H), 1.45–1.29 (m, 2H), 1.29–1.25 (m, 18H), 0.88 (t, *J* = 5.2 Hz, 3H); ¹³C NMR (100 MHz, CDCl₃): δ 155.0, 83.1, 36.0, 31.9, 29.1, 28.3, 24.9, 22.7, 14.2.

4,4-Bis(4,4,5,5-tetramethyl-1,3,2-dioxaborolan-2-yl)butan-2-one

CAS registry No. [1175712-38-5], yellow oil; ¹H NMR (400 MHz, CDCl₃): δ 2.74 (d, *J* = 8.0 Hz, 2H), 2.11 (s, 3H), 1.24 (s, 12H), 1.21 (s, 12H), 0.97 (t, *J* = 8.0 Hz, 1H); ¹³C NMR (100 MHz, CDCl₃): δ 209.1, 83.2, 40.7, 29.1, 24.8, 24.6.

(Z)-2-(1,2-diphenylvinyl)-4,4,5,5-tetramethyl-1,3,2-dioxaborolane

CAS registry No. [264144-59-4], white solid; ¹H NMR (400 MHz, CDCl₃): δ 7.36 (s, 1H), 7.31–7.23 (m, 2H), 7.22–7.14 (m, 3H), 7.13–7.09 (m, 3H), 7.07–7.03 (m, 2H), 1.31 (s, 12H); ¹³C NMR (100 MHz, CDCl₃): δ 143.3, 140.6, 137.1, 130.1, 129.0, 128.4, 128.0, 127.7, 126.4, 83.9, 24.9.

(Z)-4,4,5,5-tetramethyl-2-(1-phenylprop-1-en-2-yl)-1,3,2-dioxaborolane

CAS registry No. [141091-35-2], colorless oil; ¹H NMR (400 MHz, CDCl₃): δ 7.41–7.29 (m, 4H),

7.26–7.19 (m, 2H), 1.99 (d, $J = 1.7$ Hz, 3H), 1.31 (s, 12H); ^{13}C NMR (100 MHz, CDCl_3): δ 142.5, 138.1, 129.6, 128.2, 127.2, 83.7, 25.0, 16.1.

(*E*)-2-(3-(4,4,5,5-tetramethyl-1,3,2-dioxaborolan-2-yl)allyl)isoindoline-1,3-dione

CAS registry No. [581802-29-1], white solid; ^1H NMR (400 MHz, CDCl_3): 7.95–7.83 (m, 2H), 7.80–7.71 (m, 2H), 6.55 (dt, $J = 18.0, 4.4$ Hz, 1H), 5.49 (d, $J = 18.0$ Hz, 1H), 4.38 (s, 2H), 1.24 (s, 12H); ^{13}C NMR (100 MHz, CDCl_3): 167.8, 145.3, 134.1, 132.1, 123.4, 83.4, 41.0, 24.8.

(8*R*,9*S*,13*S*,14*S*,17*R*)-13-methyl-17-((*E*)-2-(4,4,5,5-tetramethyl-1,3,2-dioxaborolan-2-yl)vinyl)-7,8,9,11,12,13,14,15,16,17-decahydro-6*H*-cyclopenta[*a*]phenanthrene-3,17-diol

CAS registry No. [2661398-14-5], white solid; ^1H NMR (400 MHz, CDCl_3): 7.01–6.86 (m, 3H), 6.64–6.54 (m, 2H), 5.67 (d, $J = 18.0$ Hz, 1H), 2.85–2.61 (m, 2H), 2.05–1.59 (m, 6H), 1.34 (s, 12H), 1.27–1.14 (m, 8H), 0.86 (s, 3H); ^{13}C NMR (100 MHz, CDCl_3): 158.7, 154.2, 138.5, 132.5, 126.1, 115.6, 112.2, 85.1, 84.1, 49.3, 47.3, 42.4, 39.0, 37.3, 32.4, 29.8, 27.3., 25.9, 25.0, 24.8, 23.5, 14.3.

(*E*)-5,5-dimethyl-2-styryl-1,3,2-dioxaborinane

CAS registry No. [202864-71-9], colorless oil; ^1H NMR (400 MHz, CDCl_3): δ 7.46 (d, $J = 8.0$ Hz, 2H), 7.39–7.20 (m, 4H), 6.11 (d, $J = 18.4$ Hz, 1H), 3.69 (s, 4H), 0.99 (s, 6H); ^{13}C NMR (100 MHz, CDCl_3): δ 147.2, 137.9, 128.6, 127.1, 72.3, 31.9, 22.0.

(*E*)-2-(4-Methoxystyryl)-5,5-dimethyl-1,3,2-dioxaborinane

CAS registry No. [905966-49-6], colorless oil; ^1H NMR (400 MHz, CDCl_3): δ 7.42 (d, $J = 6.8$ Hz, 2H), 7.28 (d, $J = 18.4$ Hz, 1H), 6.84 (d, $J = 6.8$ Hz, 2H), 5.95 (d, $J = 18.4$ Hz, 1H), 3.77 (s, 3H), 3.67 (s, 4H), 0.98 (s, 6H); ^{13}C NMR (100 MHz, CDCl_3): δ 160.1, 146.7, 130.8, 128.4, 114.0, 72.2, 55.3,

31.9, 21.90.

(E)-2-(4-Methylstyryl)-5,5-dimethyl-1,3,2-dioxaborinane

CAS registry No. [938080-15-0], colorless oil; ^1H NMR (400 MHz, CDCl_3): δ 7.38 (d, $J = 8.0$ Hz, 2H), 7.30 (d, $J = 18.0$ Hz, 1H), 7.13 (d, $J = 8.0$ Hz, 2H), 6.04 (d, $J = 18.0$ Hz, 1H), 3.69 (s, 4H), 2.34 (s, 3H), 1.00 (s, 6H); ^{13}C NMR (100 MHz, CDCl_3): δ 147.2, 138.7, 135.2, 129.4, 127.1, 72.3, 32.0, 22.0, 21.4.

(E)-2-(4-chlorostyryl)-5,5-dimethyl-1,3,2-dioxaborinane

CAS registry No. [2493295-76-2], white solid; ^1H NMR (400 MHz, CDCl_3): δ 7.45–7.37 (m, 2H), 7.32–7.26 (m, 3H), 6.07 (d, $J = 18.0$ Hz, 1H), 3.70 (s, 4H), 1.00 (s, 6H); ^{13}C NMR (100 MHz, CDCl_3): δ 145.8, 136.4, 134.3, 128.9, 128.3, 72.4, 32.0, 22.0.

(E)-4-(5,5-dimethyl-1,3,2-dioxaborinan-2-yl)-2-methylbut-3-en-2-ol

Colorless liquid; ^1H NMR (400 MHz, CDCl_3): δ 6.64 (d, $J = 18.0$ Hz, 1H), 5.52 (d, $J = 18.0$ Hz, 1H), 3.65 (s, 4H), 1.31 (s, 6H), 0.98 (s, 6H); ^{13}C NMR (100 MHz, CDCl_3): δ 157.4, 72.2, 71.8, 31.9, 29.3, 22.0. IR (ATR): $\nu_{\text{max}} = 3470, 2964, 1640, 1423, 1312, 1250, 1083, 755, 638 \text{ cm}^{-1}$. HRMS (ESI): m/z Calculated for $\text{C}_{10}\text{H}_{19}\text{BO}_3$ $[\text{M}]^+$: 198.1427, found 198.1429.

(Z)-2-(1,2-diphenylvinyl)-5,5-dimethyl-1,3,2-dioxaborinane

CAS registry No. [1942884-64-1], white solid; ^1H NMR (400 MHz, CDCl_3): δ 7.34 (s, 1H), 7.30–7.24 (m, 2H), 7.23–7.15 (m, 1H), 7.14–7.06 (m, 5H), 7.04–6.97 (m, 2H), 3.69 (s, 4H), 1.00 (s, 6H); ^{13}C NMR (100 MHz, CDCl_3): δ 141.4, 141.2, 137.4, 130.1, 128.9, 128.4, 127.9, 127.4, 126.1, 72.6, 31.8, 22.0.

(E)-2-Phenylvinylboronic acid

CAS registry No. [4363-35-3], white solid; ^1H NMR (400 MHz, CDCl_3): δ 7.78 (d, $J = 18.0$ Hz, 1H), 7.62 (d, $J = 8.0$ Hz, 2H), 7.46–7.33 (m, 3H), 6.35 (d, $J = 18.4$ Hz, 1H); ^{13}C NMR (100 MHz, CDCl_3): δ 152.4, 137.3, 129.6, 128.8, 127.7.

(E)-(4-methoxystyryl)boronic acid

CAS registry No. [214907-25-2], white solid; ^1H NMR (400 MHz, CDCl_3): δ 7.72 (d, $J = 18.0$ Hz, 1H), 7.56 (d, $J = 8.8$ Hz, 2H), 6.92 (d, $J = 8.8$ Hz, 1H), 6.18 (d, $J = 18.0$ Hz, 1H), 3.84 (s, 3H); ^{13}C NMR (100 MHz, CDCl_3): δ 160.9, 151.8, 130.3, 129.2, 127.5, 114.2, 55.5.

3. Results and discussion

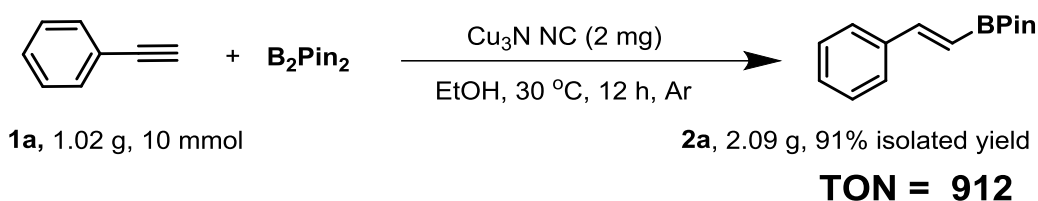
3.1. Catalytic activity of Cu₃N NC

Initially, the catalytic performance of Cu₃N NC for hydroboration of **1a** with B₂Pin₂ in EtOH was investigated (**Table 4-1**). The Cu₃N NC efficiently promoted the hydroboration of **1a** to afford **2a** in quantitative yield (entry 1), which presents the first example of a heterogeneous Cu catalyst for the hydroboration of **1a** with B₂Pin₂ under additive-free and mild conditions (**Table 4-2**). In sharp contrast, other metal–non-metal heterogeneous Cu catalysts, for example Cu₂O and CuO, were inactive under such mild reaction conditions. Moreover, the Cu₂O nanocube (Cu₂O NC) with the same morphology and size as Cu₃N NC was prepared and used in the hydroboration of **1a**, but the reaction was not proceeded. A scale-up experiment using 1.02 g of **1a** was then conducted, and an outstanding turnover number (TON = 912) was obtained (**Scheme 4-2**). These results demonstrated the excellent catalytic performance of Cu₃N NC in the hydroboration of **1a**.

Table 4-1. Hydroboration of **1a** using with B₂Pin₂ various Cu catalysts

Entry	Catalyst	Yield of 2a
1	Cu ₃ N NC	99%
2	Cu ₂ O	<1%
3	CuO	<1%
4	Cu ₂ O NC	<1%

Reaction conditions: **1a** (0.5 mmol), catalyst (5 mol% of Cu), and EtOH (2 mL) under Ar. Yield was determined by ¹H NMR analysis using 1,4-dinitrobenzene (0.1 mmol) as an internal standard.



Scheme 4-2. Gram-scale experiment of the hydroboration of **1a** to **2a** using $\text{Cu}_3\text{N NC}$.

Table 4-2. Comparison of $\text{Cu}_3\text{N NC}$ catalytic system and reported Cu catalytic systems for hydroboration of **1a** with B_2Pin_2

Entry	Catalyst	Additives	Solvent	Temp. (°C)	TON	Ref.
1	$\text{Cu}_3\text{N NC}$	-	EtOH	30	912	<i>This work</i>
2	Cu-3D-MOF	K_2CO_3	$\text{CH}_3\text{CN}/\text{H}_2\text{O}$	rt	41734	25
3	Cu-TiC	H_2O	Toluene	80	612	27
4	Cu-NPs/rGO	MeONa	MeOH/ 1,4-dioxane	50	14	24
5	PCN-222(Cu)	3-methylpyridine	EtOH/ H_2O	80	66	23
6	Cu-MOF	MeONa	EtOH	25	310	22
7	Cu- CeO_2	-	EtOH	90	192	26
8	Cu_2O RD	PPh_3	1,4-dioxane	60	14	21
9	Cu- CuFe_2O_4	MeONa	MeOH	rt	190	19
10	Nano-Cu@Si	MeONa	EtOH	rt	10	18
11	CuFe_2O_4	<i>t</i> -BuOK	MeOH	50	180	29
12	micro copper powder	MeONa	MeOH	rt	9	17
13	Basic CuCO_3	PPh_3	H_2O	27	16	30
14	Cu/MgO	PPh_3	Toluene	45	23	16

Note: rt = room temperature.

Subsequently, the recycling experiments of Cu₃N NC were carried out. The Cu₃N NC was easily recoverable by centrifugation and used without a loss of its original activity even after three times (**Figure 4-1** (a)). The structure of recovered Cu₃N NC was analyzed by PXRD, TEM, and XAFS measurements. The PXRD patterns of recovered Cu₃N NC display five peaks, which are same as those of fresh Cu₃N NC (**Figure 4-2** (a)). From the TEM analysis, the author found that the size of recovered Cu₃N NC was not obviously changed after the reaction (**Figure 4-2** (b)). The results of XANES spectrum revealed that the absorption edge energy of the reused Cu₃N NC is almost similar to that of fresh Cu₃N NC (**Figure 4-2** (c)). These observations demonstrate the high durability of Cu₃N NC catalyst. The author further investigated the hot filtration experiment to check the leaching of metal species during the reaction. After the Cu₃N NC catalyst was removed, no additional product was generated in the filtrate (**Figure 4-1** (b)), indicating the hydroboration of **1a** proceeded on the Cu₃N NC surface.

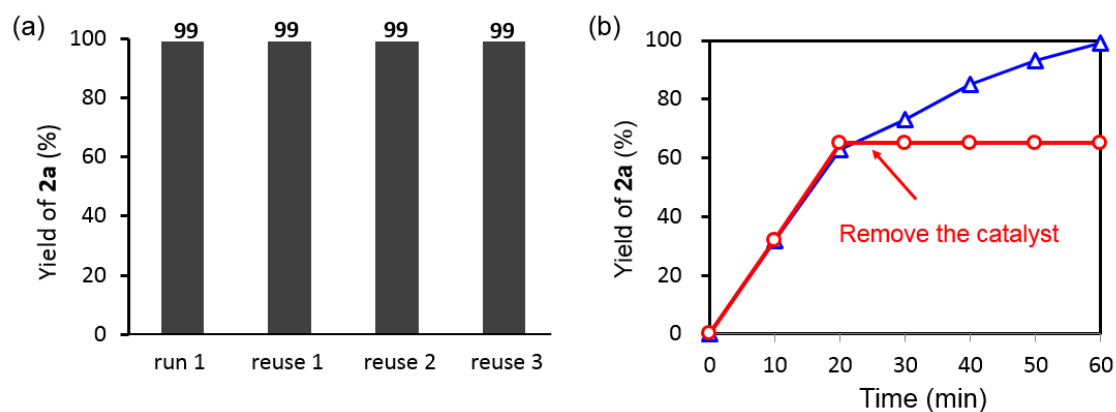


Figure 4-1. (a) Reuse experiments of Cu₃N NC in the hydroboration of **1a** to **2a** for 1 h. (b) Hot filtration experiment of Cu₃N NC in the hydroboration of **1a** to **2a**: without catalyst removal (blue line) and with catalyst removal (red line). Reaction conditions: Cu₃N NC (5 mg), **1a** (0.5 mmol), B₂Pin₂ (0.6 mmol), EtOH (2 mL), 30 °C, Ar. Yields were calculated by ¹H NMR analysis using 1,4-nitrobenzene as an internal standard.

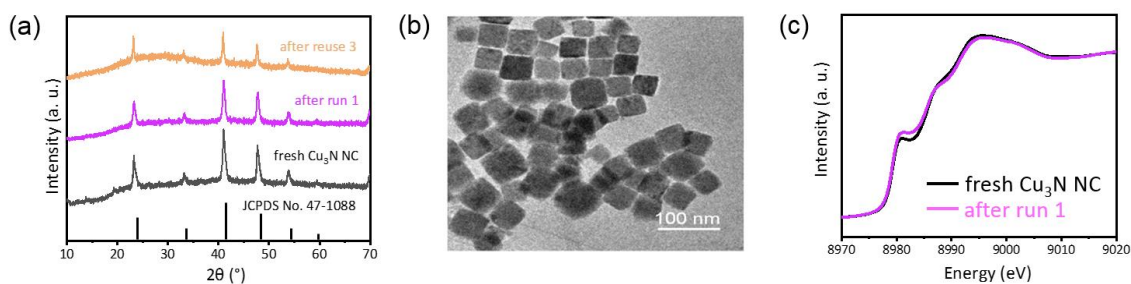
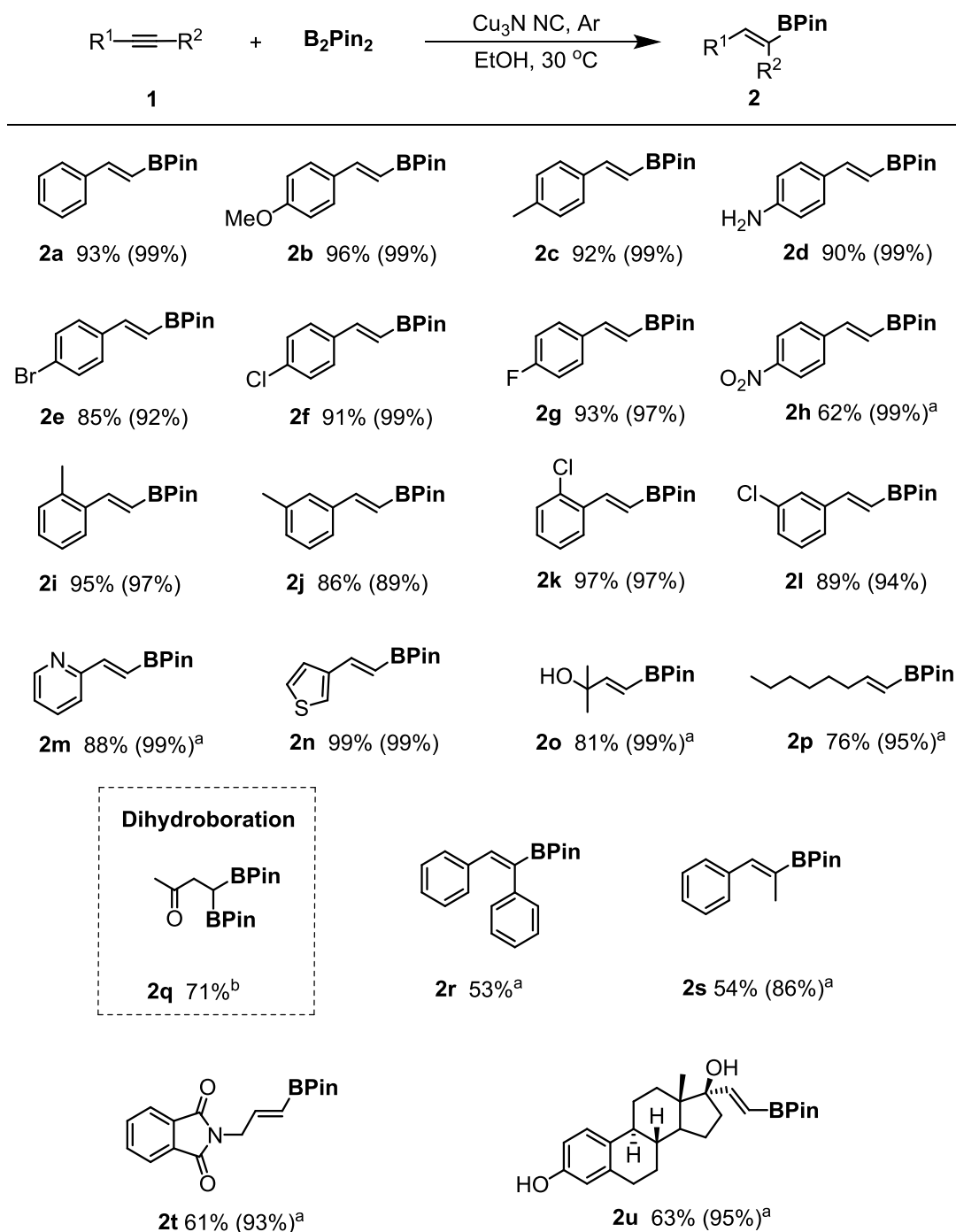


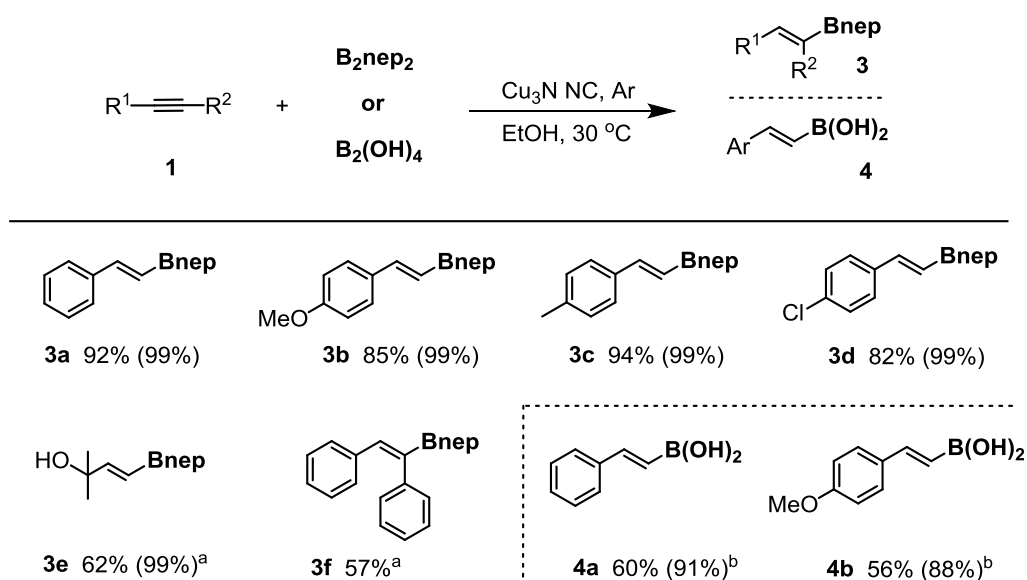
Figure 4-2. (a) PXRD patterns of fresh and reused Cu_3N NC. (b) TEM image of Cu_3N NC (after run 1). (c) Cu K-edge XANES spectra of fresh and reused Cu_3N NC.

The wide applicability of the Cu_3N NC was further demonstrated through the hydroboration of alkynes with various functional groups (**Scheme 4-3**). A variety of 1-ethynylbenzene derivatives were tolerated, affording the desired boronate esters in good to excellent isolated yields (**2b–2h**). The hydroboration of other position substituted 1-ethynylbenzenes proceeded smoothly to generate the corresponding products in 86–97% yields (**2i–2l**). 2-Ethylpyridine and 3-ethylthiophene successfully converted to **2m** and **2n** in 88% and 88% yields. Notably, aliphatic terminal alkynes could also be borylated, giving **2o** and **2p** in 81% and 76% yields. Cu_3N NC catalyst exhibited outstanding catalytic performance in the dihydroboration of alkynes to 1,1-diborylalkanes, which are useful in organic and pharmaceutical chemistry [31]. When the amount of B_2Pin_2 increased to 2.5 eq., dihydroboration product **2q** was obtained in 71% isolated yield, which is the first example of the heterogeneous metal catalyst for the dihydroboration of alkynes with B_2Pin_2 under additive-free conditions [32]. In addition, internal alkynes underwent the hydroboration reaction to produce the corresponding products in 53% and 54% yields (**2s** and **2t**). The bioactive phthalimide (**2t**) and steroid (**2u**) derivatives were obtained in moderate isolated yields, respectively, through this method. Overall, these results demonstrated a high utility of Cu_3N NC for fine chemical synthesis.



Scheme 5-2. Hydroboration of various alkynes with B₂Pin₂. Reaction conditions: **1** (0.5 mmol), B₂Pin₂ (0.6 mmol), Cu₃N NC (5 mg, 5 mol% of Cu), EtOH (2 mL), Ar, 30 °C, 1 h. Isolated yields. Regioselectivity in parentheses was determined by GC-MS analysis. ^a 12 h. ^b But-3-yn-2-one (0.2 mmol), B₂Pin₂ (2.5 eq.), Cu₃N NC (2 mg), EtOH (1 mL) 80 °C, 1 h.

The hydroboration of alkynes with bis(neopentylglycolato)diboron (B_2nep_2) was also performed (**Scheme 4-3**). Various alkynes bearing both electron-donating ($-OMe$ and $-Me$) and -withdrawing ($-Cl$) groups on the phenyl ring efficiently reacted with B_2nep_2 , generating the corresponding products in 82–94% yields (**3a–3d**). The hydroboration of aliphatic alkyne and internal alkyne with B_2nep_2 proceeded to yield the desired products in good yields (**3e** and **3f**). Next, the hydroboration of alkynes with $B_2(OH)_4$ to vinyl boronic acids, which are crucial intermediates for organic transformations, was also achieved using Cu_3N NC catalytic system [33]. The reported system required multi-steps, while this Cu_3N NC catalyst efficiently promoted the hydroboration of alkynes to the desired vinyl boronic acids in 56–50% yields (**4a** and **4b**).



Scheme 5-3. Hydroboration of various alkynes with B_2nep_2 or $B_2(OH)_4$. Reaction conditions: **1** (0.5 mmol), B_2nep_2 or $B_2(OH)_4$ (0.6 mmol), Cu_3N NC (5 mg, 5 mol% of Cu), EtOH (2 mL), Ar, 30 °C, 1 h. Isolated yields. Regioselectivity in parentheses was determined by 1H NMR analysis of crude reaction solution. ^a 12 h. ^b 3 h.

3.2. Origin of high catalytic activity of Cu₃N NC

Several spectroscopic analyses for Cu₃N NC and Cu₂O NC were conducted to investigate the origin of the high catalytic activity of Cu₃N NC. In **Figure 4-3** (a), the FT-IR spectrum of the Cu₃N NC after pyridine absorption showed three peaks at 1594, 1576, and 1442 cm⁻¹, which are attributed to the pyridine coordination to Lewis acid sites (purple line) [34]. In addition, the results of CO₂-TPD measurement clearly revealed that Cu₃N NC possesses the base sites on surface (**Figure 4-3** (b), purple line). In contrary, there are no absorption peaks in the FT-IR and CO₂-TPD spectra of Cu₂O NC (**Figure 4-3**, red line). Furthermore, the author performed the XPS analysis of Cu₃N NC and Cu₂O NC. In the Cu 2p spectra of Cu₃N NC, the peak of Cu 2p_{3/2} was located at 932.3 eV, while the binding energy of Cu species in Cu₂O NC was lower than that in Cu₃N NC (**Figure 4-5** (a)) [35]. It is caused by the electron transfer from Cu to N atoms in Cu₃N NC, leading to the Lewis acid sites on Cu₃N NC [36]. Moreover, the N 1s peak of Cu₃N NC displayed two contributions, which were corresponded to the residual surface amines (398.3 eV) and the Cu–N (396.2 eV) species, respectively (**Figure 4-5** (b)) [37, 38]. The lower binding energy of Cu–N species revealed the presence of electron-rich N atoms, which serve as Lewis-base sites efficiently [39]. Thus, the co-existence of Lewis acid-base sites may account for the outstanding catalytic performance of Cu₃N NC [40].

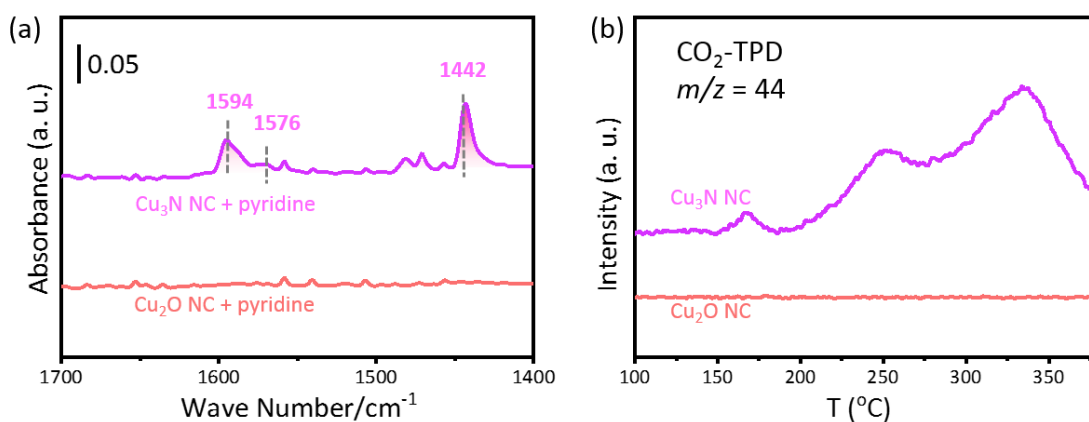


Figure 4-3. (a) FT-IR spectra of pyridine absorbed on Cu₃N NC (purple line) and Cu₂O NC (red line). (b) CO₂-TPD signals of Cu₃N NC (purple line) and Cu₂O NC (red line) monitored at $m/z = 44$.

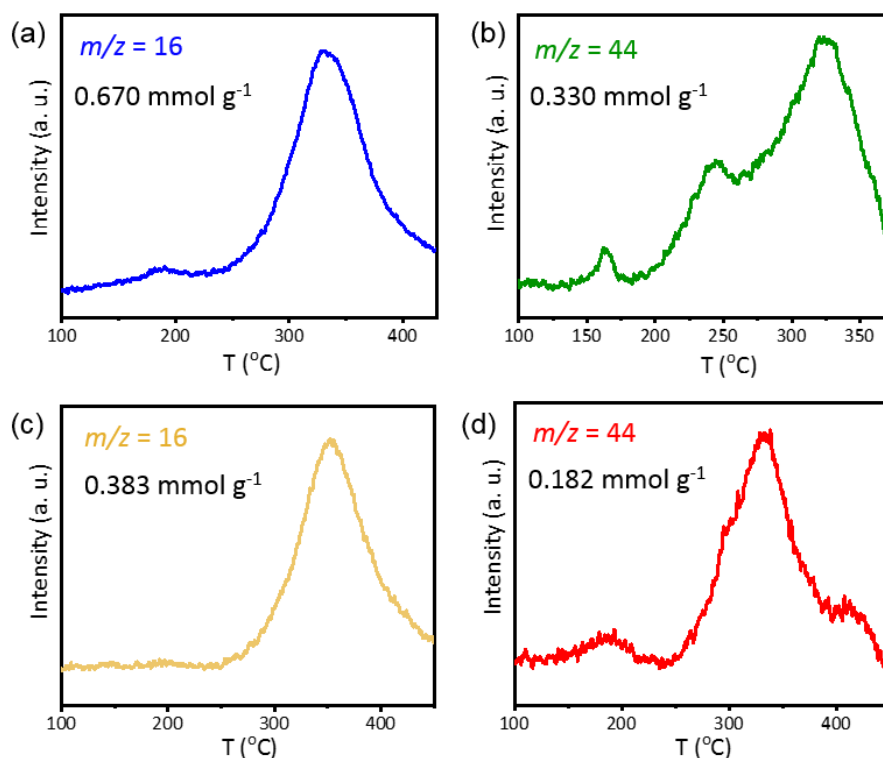


Figure 4-4. (a) NH₃-TPD and (b) CO₂-TPD signals of Cu₃N NC monitored at m/z 16 and 44. (c) NH₃-TPD and (d) CO₂-TPD signals of Cu₃N NC (without NH₃ or CO₂ pretreatment) monitored at m/z 16 and 44.

Table 4-3. The amount of Lewis acid and base

	Lewis acid site amount (mmol g ⁻¹)	Lewis base site amount (mmol g ⁻¹)
Cu ₃ N NC	0.287	0.148

Note: The NH₃ and CO₂-TPD spectra of Cu₃N NC show the amounts of Lewis acid-base sites of Cu₃N NC, which are 0.670 and 0.330 mmol g⁻¹, respectively (**Figure 4-4** (a) and (b)). Furthermore, the experiments using Cu₃N NC without NH₃ or CO₂ pre-treatment were performed, and the amounts of Lewis acid-base sites were calculated to be 0.383 and 0.182 mmol g⁻¹, respectively (**Figure 4-4** (c) and (d)). Based on these results, the exact amount of Lewis acid-base sites of Cu₃N NC except for the other components are estimated as shown in **Table 4-3**.

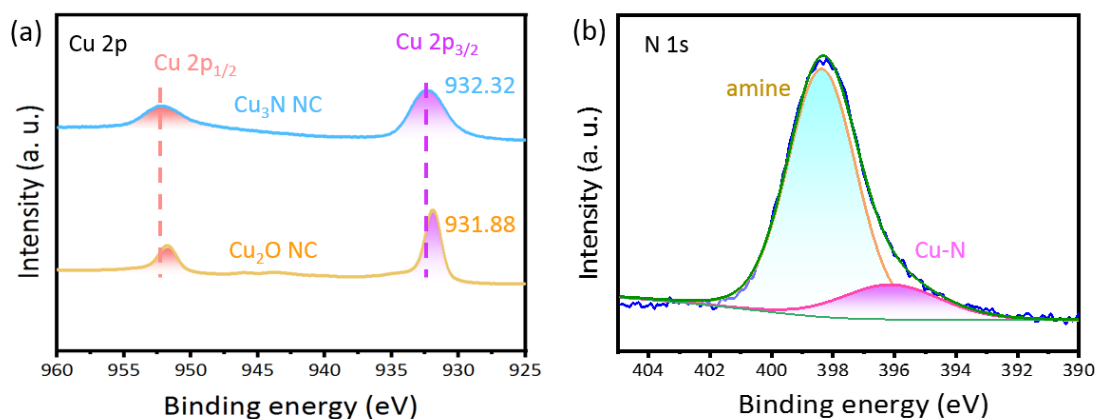


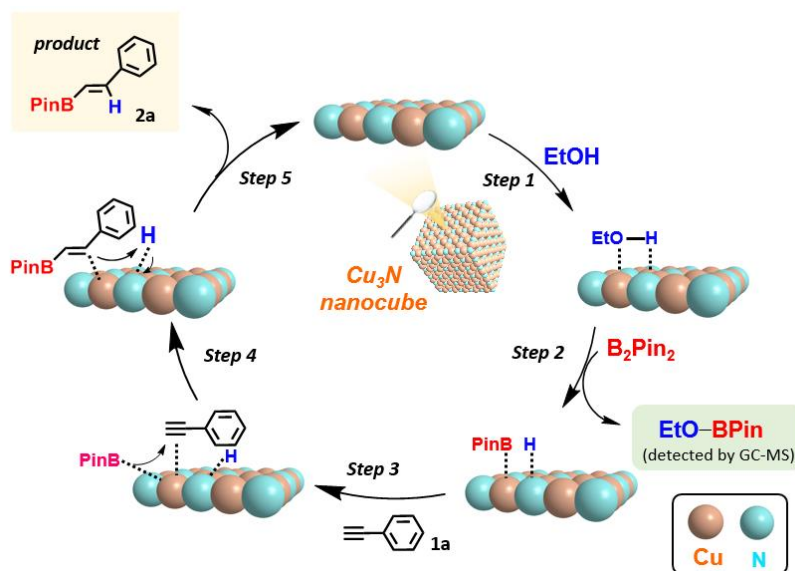
Figure 4-5. (a) Cu 2p XPS spectra of Cu₃N NC and Cu₂O NC. (b) N 1s XPS spectrum of Cu₃N NC.

3.3. Proposed reaction mechanism

According to the above observations and previous works [41], the proposed mechanism is shown in Scheme 4-5. Firstly, Cu and N atoms in Cu₃N NC acted as Lewis acid and base sites to activate the EtOH (step 1) [42, 43]. Then, the B₂Pin₂ molecule reacts with activated EtOH to generate the EtO–BPin and Cu–BPin (step 2). Subsequently, **1a** was absorbed on the Cu sites at the parallel position (step 3) and further reacted with Cu–BPin intermediate to afford the linear addition intermediate (step 4). Finally, the desired product **2a** was formed via the hydrogen transfer to the copper intermediate, and the Cu₃N catalyst was regenerated (step 5). Therefore, the cooperative catalysis of Cu₃N NC combining its Lewis acid-base property is key factor to the efficient hydroboration of alkynes.

The proposed mechanism was stand by the following experimental results: 1) The generation of EtO–BPin was confirmed by GC-MS analysis (Figure 4-6). 2) When the hydroboration of **1a** was carried out in monodeuterized ethanol (EtOD), the monodeuterized **2a** (**2a-d**) was formed as the major product (Scheme 4-6 (a)). 3) The EtOH/EtOD kinetic isotope effect (KIE) in the borylation of **1a** was observed (KIE: 3.2) (Scheme 4-6 (b)). Therefore, the excellent catalytic activity

of Cu_3N NC should be attributed to cooperative catalysis of Lewis acid-base sites for simultaneous activation of EtOH , B_2Pin_2 , and alkyne [43].



Scheme 4-5. Proposed mechanism of the hydroboration of **1a** catalyzed by Cu_3N NC.

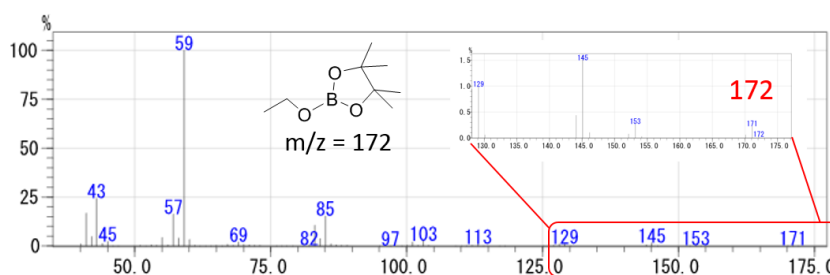
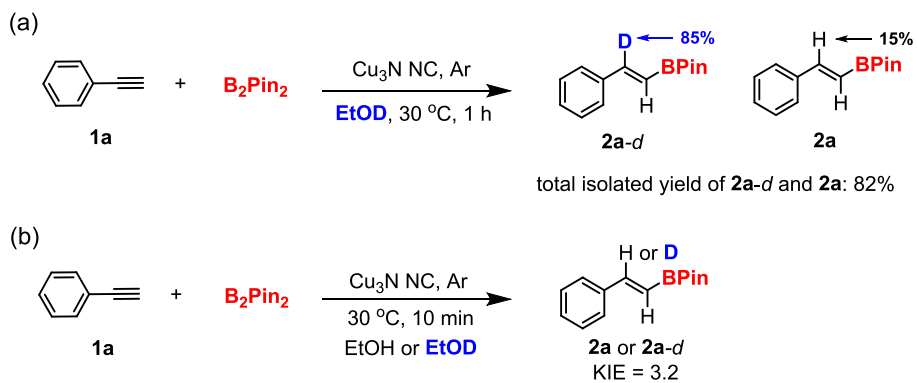


Figure 4-6. EI-MS spectrum of 2-ethoxy-4,4,5,5-tetramethyl-1,3,2-dioxaborolane.



Scheme 4-6. The deuterium-labeling experiments of hydroboration of **1a** using Cu_3N NC.

4. Conclusion

This chapter demonstrated the highly efficient hydroboration of alkynes with the heterogeneous $\text{Cu}_3\text{N NC}$ catalyst. A variety of alkynes was efficiently boronated to afford the desired vinyl boronate esters in good yields. The $\text{Cu}_3\text{N NC}$ was also applicable to gram-scale production with an excellent TON (912) and reusable several times without a loss of activity and selectivity. This is the first time that the hydroboration of alkynes is achieved over a heterogeneous Cu catalyst under additive-free and mild reaction conditions. Furthermore, the selective hydroboration of alkynes with $\text{B}_2(\text{OH})_4$ to vinyl boronic acids was promoted by $\text{Cu}_3\text{N NC}$ catalyst. The excellent catalytic activity of $\text{Cu}_3\text{N NC}$ in the hydroboration of alkynes is attributed to the cooperative effect of Lewis acid-base sites on $\text{Cu}_3\text{N NC}$.

References

- 1 J. W. B. Fyfe, A. J. B. Watson, *Chem*, **2017**, *3*, 31–55.
- 2 K. Yang, Q. Song, *Acc. Chem. Res.*, **2021**, *54*, 2298–2312.
- 3 N. Miyaura, A. Suzuki, *Chem. Rev.*, **1995**, *95*, 2457–2483.
- 4 J. Hu, M. Ferger, Z. Shi, T. B. Marder, *Chem. Soc. Rev.*, **2021**, *50*, 13129–13188.
- 5 J. F. Li, Z. Z. Wei, Y. Q. Wang, M. Ye, *Green Chem.*, **2017**, *19*, 4498–4502.
- 6 S. K. Bose, L. Mao, L. Kuehn, U. Radius, J. Nekkunda, W. L. Santos, A. W. Stephen, G. S. Patrick, T. B. Marder, *Chem. Rev.*, **2021**, *121*, 13238–13341.
- 7 J. Ramírez, E. Fernandez, *Synthesis*, **2005**, *10*, 1698–1700.
- 8 D. P. Ojha, K. R. Prabhu, *Org. Lett.*, **2016**, *18*, 432–435.
- 9 Q. Chen, J. Zhao, Y. Ishikawa, N. Asao, Y. Yamamoto, T. Jin, *Org. Lett.*, **2013**, *15*, 5766–5769.
- 10 J. E. Lee, J. Kwon, J. Yun, *Chem. Commun.*, **2008**, 733–734.
- 11 G. Stavber, Z. Časar, *Appl. Organometal. Chem.*, **2013**, *27*, 159–165.
- 12 H. Yoshida, Y. Takemoto, K. Takaki, *Chem. Comm.*, **2014**, *50*, 8299–8302.
- 13 Y. E. Kim, D. Li, J. Yun, *Dalton Trans.*, **2015**, *44*, 12091–12093.
- 14 Q. Feng, K. Yang, Q. Song, *Chem. Commun.*, **2015**, *51*, 15394–15397.
- 15 A. K. Nelson, C. L. Peck, S. M. Rafferty, W. L. Santos, *J. Org. Chem.*, **2016**, *81*, 4269–4279.
- 16 A. Grirrane, A. Corma, H. Garcia, *Chem. Eur. J.*, **2011**, *17*, 2467–2478.
- 17 J. Zhao, Z. Niu, H. Fu, Y. Li, *Chem. Comm.*, **2014**, *50*, 2058–2060.
- 18 L. Xu, B. Xu, *Tetrahedron Lett.*, **2017**, *58*, 2542–2546.
- 19 X. Zeng, C. Gong, H. Guo, H. Xu, J. Zhang, J. Xie, *New J. Chem.*, **2018**, *42*, 17346–17350.
- 20 C. Zhang, M. Zhou, S. Liu, B. Wang, Z. Mao, H. Xu, Y. Zhong, L. Zhang, B. Xu, X. Sui, *Carbohydr. Polym.*, **2018**, *191*, 17–24.
- 21 H. Y. Tsai, M. Madasu, M. H. Huang, *Chem. Eur. J.*, **2019**, *25*, 1300–1303.

- 22 Z. L. Wu, X. Lan, N. Gao, X. Kang, Z. Wang, T. Hu, B. Zhao, *J. Catal.*, **2021**, *404*, 250–257.
- 23 L. J. Zhang, J. C. Yuan, L. J. Ma, Z. Y. Tang, X. M. Zhang, *J. Catal.*, **2021**, *401*, 63–69.
- 24 B. Wang, L. Gao, H. Yang, G. Zheng, *ACS Appl. Mater. Interfaces*, **2021**, *13*, 47530–47540.
- 25 R. J. Wei, P. Y. You, H. Duan, M. Xie, R. Q. Xia, X. Chen, X. Zhao, G.-H. Ning, A. I. Cooper, D. Li, *J. Am. Chem. Soc.*, **2022**, *144*, 17487–17495.
- 26 J. Zhang, Z. Wang, W. Chen, Y. Xiong, W. C. Cheong, L. Zheng, W. Yan, L. Gu, C. Chen, C. Peng, P. Hu, D. Wang, Y. Li, *Chem*, **2020**, *6*, 725–737.
- 27 W. H. Li, J. Yang, H. Jing, J. Zhang, Y. Wang, J. Li, J. Zhao, D. Wang, Y. Li, *J. Am. Chem. Soc.*, **2021**, *143*, 15453–15461.
- 28 A. M. Elseman, M. S. Selim, L. Luo, C. Y. Xu, G. Wang, Y. Jiang, D. B. Liu, L. P. Liao, Z. Hao, Q. L. Song, *ChemSusChem*, **2019**, *12*, 3808–3816.
- 29 B. Mohan, K. H. Park, *Appl. Catal. A-Gen.*, **2016**, *519*, 78–84.
- 30 G. Stavber, Z. Časar, *Appl. Organometal. Chem.*, **2013**, *27*, 159–165.
- 31 K. Endo, M. Hirokami, T. Shibata, *J. Org. Chem.*, **2010**, *75*, 3469–3472.
- 32 M. Gao, S. B. Thorpe, W. L. Santos, *Org. Lett.*, **2009**, *11*, 3478–3481.
- 33 D. G. Hall, *Chem. Soc. Rev.*, **2019**, *48*, 3475–3496.
- 34 V. S. Escribano, C. del Hoyo Martínez, E. F. López, J. G. Amores, G. Busca, *Catal. Commun.*, **2009**, *10*, 861–864.
- 35 Z. Yin, C. Yu, Z. Zhao, X. Gou, M. Shen, N. Li, M. Muzzio, J. Li, H. Liu, H. Lin, J. Yin, G. Lu, D. Su, S. Sun, *Nano Lett.*, **2019**, *19*, 8658–8663.
- 36 X. H. Li, M. Antonietti, *Chem. Soc. Rev.*, **2013**, *42*, 6593–6604.
- 37 R. K. Sithole, L. F. E. Machogo, M. A. Airo, S. S. Gqoba, M. J. Moloto, P. Shumbula, J. Van Wyk, N. Moloto, *New J. Chem.*, **2018**, *42*, 3042–3049;
- 38 M. Parvizian, A. D. Balsa, R. Pokratath, C. Kalha, S. Lee, D. Van den Eynden, M. Ibanez, A. Regoutz, J. De Roo, *Angew. Chem., Int. Ed.*, **2022**, *134*, e202207013.

- 39 Y.-X. Liu, H.-H. Wang, T.-J. Zhao, B. Zhang, H. Su, Z.-H. Xue, X.-H. Li, J.-S. Chen, *J. Am. Chem. Soc.*, **2019**, *141*, 38–41.
- 40 S. Furukawa, M. Ieda, K. Shimizu, *ACS Catal.*, **2019**, *9*, 5096–5103.
- 41 P. Zhang, J. Meijide Suárez, T. Driant, E. Dera, Y. Zhang, M. Ménand, S. Roland, M. Sollogoub, *Angew. Chem., Int. Ed.*, **2017**, *56*, 10821–10825.
- 42 K. Shimizu, K. Kon, K. Shimura, S. S. M. A. Hakim, *J. Catal.*, **2013**, *300*, 242–250;
- 43 G. S. Foo, F. Polo-Garzon, V. Fung, D.-E. Jiang, S. H. Overbury, Z. Wu, *ACS Catal.*, **2017**, *7*, 4423–4434.

Chapter V.

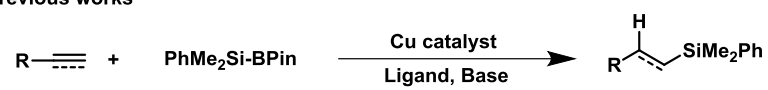
*A Green and Efficient Method for Silanes Synthesis via
Hydrosilylation of Unsaturated Compounds*

1. Introduction

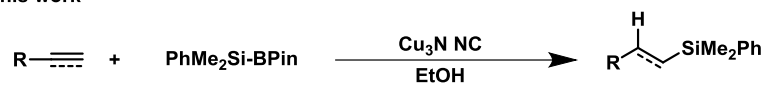
Transition metal-catalyzed cross-coupling reaction for carbon–silicon bond formation is one of the most straightforward and useful methods for synthesizing organosilane compounds, which are of great importance as versatile building blocks in organic synthesis and advanced materials [1, 2]. In this context, copper (Cu) catalyzed-hydrosilylation of unsaturated compounds to silanes has gained high attention [3–5]. Several studies demonstrated that the outstanding efficiency of this method is attributed to the unique chemical property of silylcopper (Cu–Si) species, which serves as a soft silicon nucleophile and easily reacts with soft electrophiles to afford silanes [6]. Recently, the (dimethylphenylsilyl)boronic acid pinacol ester (PhMe₂Si-Bpin), a commercially available and moisture-stable silicon source [7], has been widely used in the Cu catalyzed-hydrosilylation of unsaturated compounds including olefins, alkynes, and imines (**Scheme 5-1** (a)) [8–10]. However, the reported systems required organic ligands to activate the Cu species and the use of base additives to assist in the formation of essential Cu–Si species. Moreover, most of the Cu catalytic systems suffered from the low reaction applicability. Up to now, a facile method for the synthesis of silanes through the hydrosilylation of unsaturated compounds under base- and ligand-free conditions, has not been reported. Therefore, the development of an efficient heterogeneous catalytic system for the hydrosilylation of various types of unsaturated compounds under environmentally friendly reaction conditions is highly desired and is still a challenge in silicon chemistry.

This chapter represents an efficient method for the preparation of various silanes through the hydrosilylation of unsaturated compounds with copper nitride nanocube (Cu₃N NC) catalyst (**Scheme 5-1** (b)). A wide range of substrates, including alkynes, alkenes, imines, and azobenzenes, were efficiently converted to the desired products under base- and ligand-free, and mild reaction conditions. Moreover, the Cu₃N NC catalytic system was applicable to the gram scale experiment, and the Cu₃N NC catalyst could be reused several times without loss of its original catalytic activity.

(a) Previous works



(b) This work



Scheme 5-1. Synthesis of silanes through the hydrosilylation of unsaturated compounds.

2. Experimental section

2.1 General information

All organic reagents were purchased from FUJIFILM Wako Pure Chemical Corporation, Sigma–Aldrich, or Tokyo Chemical Industry. Gas chromatography-mass spectrometry (GC-MS) was performed using a GCMS-QP2010 SE instrument equipped with an InertCap WAX-HT capillary column (GL Science, 30 m × 0.25 mm i.d., film thickness 0.25 μm). ¹H and ¹³C nuclear magnetic resonance (NMR) spectra were acquired at 400 and 100 MHz, respectively, using a JEOL JNM-ESC400 spectrometer. Chemical shifts are reported in parts per million (ppm) relative to the signal (0.00 ppm) for internal tetramethylsilane in CDCl₃. The ¹H NMR spectral data are reported using the following standard chemical shift: CDCl₃ (7.26 ppm). The ¹³C NMR spectral data are reported using the following standard chemical shift: CDCl₃ (77.16 ppm). NMR multiplicities are reported using the following abbreviations: s: singlet, d: doublet, t: triplet, q: quartet, m: multiplet, br: broad, *J*: coupling constants in hertz. All known compounds described in the paper were characterized by comparison of their ¹H and ¹³C NMR spectra with previously reported data. FT-IR attenuated total reflectance (ATR) spectra were recorded using a SHIMADZU IRSprit-T spectrometer.

2.2. Reaction procedure

The general reaction procedure for the oxidation of indoles using Cu₃N NC was as follows. Cu₃N NC powder was placed in a 50 mL stainless steel autoclave with a Teflon inner cylinder. Unsaturated compounds (0.25 mmol), PhMe₂Si-BPin (0.375 mmol), Cu₃N NC (5 mol%), and EtOH (0.1 mL) were subsequently added. The reaction mixture was vigorously stirred at 30 °C under Ar. After the reaction, the mixture was concentrated *in vacuo*. The residue was subjected to the silica gel flash chromatography with hexane/ethyl acetate to yield the desired products.

2.3. Gram-scale experiment

Cu₃N NC (2 mg, 0.01 mmol of Cu) was placed in a 50 mL stainless-steel autoclave with a Teflon inner cylinder, followed by addition of phenylacetylene (1.02 g, 10.0 mmol), PhMe₂Si-BPin (3.93 g, 15.0 mmol), and EtOH (4 mL). After being stirred at 30 °C under Ar for 24 h, the reaction mixture was concentrated to yield the crude product, which was further purified by silica gel flash chromatography (hexane) to give the product (2.13 g).

2.4. Recycling experiment

Cu₃N NC (5 mg) was placed in a 50 mL stainless-steel autoclave with a Teflon inner cylinder, followed by addition of phenylacetylene (0.5 mmol), PhMe₂Si-BPin (0.75 mmol), and EtOH (2.0 mL). The reaction mixture was stirred at 30 °C for 1 h under Ar, and Cu₃N NC were then recovered by filtration. The catalyst was washed with ethanol and dried at room temperature *in vacuo* without further purification or reactivation before reuse.

2.5. Product identification

(*E*)-dimethyl(phenyl)(styryl)silane

CAS registry No. [64788-85-8], colorless oil; ¹H NMR (400 MHz, CDCl₃): δ 7.60–7.55 (m, 2H), 7.45–7.42 (m, 2H), 7.38–7.27 (m, 5H), 7.30–7.22 (m, 1H), 6.94 (d, *J* = 19.2 Hz, 1H), 6.62 (d, *J* = 19.2 Hz, 1H), 0.43 (s, 6H); ¹³C NMR (100 MHz, CDCl₃): δ 145.5, 138.7, 138.3, 134.1, 129.2, 128.7, 128.3, 128.0, 127.2, 126.6, -2.4.

(*E*)-(4-methoxystyryl)dimethyl(phenyl)silane

CAS registry No. [264189-26-6], colorless oil; ¹H NMR (400 MHz, CDCl₃): δ 7.60–7.53 (m, 2H), 7.42–7.33 (m, 5H), 6.94–6.83 (m, 3H), 6.40 (d, *J* = 19.2 Hz, 1H), 3.78 (s, 3H), 0.42 (s, 6H); ¹³C NMR

(100 MHz, CDCl₃): δ 159.8, 144.9, 139.0, 134.1, 131.3, 129.1, 127.9, 127.9, 124.3, 114.0, 55.4, -2.3.

(E)-dimethyl(4-methylstyryl)(phenyl)silane

CAS registry No. [264189-27-7], colorless oil; ¹H NMR (400 MHz, CDCl₃): δ 7.59–7.54 (m, 2H), 7.37–7.31 (m, 5H), 7.12 (d, *J* = 8.0 Hz, 2H), 6.91 (d, *J* = 19.2 Hz, 1H), 6.51 (d, *J* = 19.2 Hz, 1H), 2.32 (s, 3H), 0.42 (s, 6H); ¹³C NMR (100 MHz, CDCl₃): δ 145.4, 138.9, 138.2, 135.7, 134.1, 129.4, 129.1, 127.9, 126.6, 125.8, 21.4, -2.3.

(E)-4-(2-(dimethyl(phenyl)silyl)vinyl)aniline

CAS registry No. [2607809-66-3], brown oil; ¹H NMR (400 MHz, CDCl₃): δ 7.61–7.53 (m, 2H), 7.38–7.32 (m, 3H), 7.29–7.24 (m, 2H), 6.84 (d, *J* = 19.2 Hz, 1H), 6.62 (d, *J* = 8.8 Hz, 2H), 6.32 (d, *J* = 19.2 Hz, 1H), 3.69 (br, 2H), 0.40 (s, 6H); ¹³C NMR (100 MHz, CDCl₃): δ 145.3, 139.3, 134.1, 133.9, 129.3, 129.1, 128.0, 127.9, 122.2, 115.1, -2.2.

(E)-(4-chlorostyryl)dimethyl(phenyl)silane

CAS registry No. [264189-29-9], colorless oil; ¹H NMR (400 MHz, CDCl₃): δ 7.62–7.53 (m, 2H), 7.48–7.26 (m, 7H), 6.87 (d, *J* = 19.2 Hz, 1H), 6.55 (d, *J* = 19.2 Hz, 1H), 0.43 (s, 6H); ¹³C NMR (100 MHz, CDCl₃): δ 144.0, 138.4, 136.8, 134.0, 133.9, 129.3, 128.8, 128.3, 128.0, 127.8, -2.5.

(E)-(4-fluorostyryl)dimethyl(phenyl)silane

CAS registry No. [264189-28-8], colorless oil; ¹H NMR (400 MHz, CDCl₃): δ 7.60–7.53 (m, 2H), 7.42–7.31 (m, 5H), 7.00 (t, *J* = 8.8 Hz, 2H), 6.88 (d, *J* = 19.2 Hz, 1H), 6.48 (d, *J* = 19.2 Hz, 1H), 0.43 (s, 6H); ¹³C NMR (100 MHz, CDCl₃): δ 162.8 (d, *J* = 246.0 Hz), 144.1, 138.6, 134.6 (d, *J* = 3.0 Hz), 134.0, 129.2, 128.2 (d, *J* = 9.0 Hz), 128.0, 127.0 (d, *J* = 3.0 Hz), 115.6 (d, *J* = 22.0 Hz), -2.4.

(E)-dimethyl(4-nitrostyryl)(phenyl)silane

CAS registry No. [2676952-59-1], brown oil; ¹H NMR (400 MHz, CDCl₃): δ 8.16 (d, *J* = 8.8 Hz, 2H), 7.62–7.51 (m, 4H), 7.44–7.36 (m, 3H), 6.96 (d, *J* = 19.2 Hz, 1H), 6.80 (d, *J* = 19.2 Hz, 1H), 0.47 (s, 6H); ¹³C NMR (100 MHz, CDCl₃): δ 147.4, 144.2, 142.8, 137.6, 134.0, 129.5, 128.1, 127.1, 124.0, -2.7.

(E)-dimethyl(2-methylstyryl)(phenyl)silane

CAS registry No. [1440971-96-9], & **dimethyl(phenyl)(1-(o-tolyl)vinyl)silane** : CAS registry No. [2058243-82-4], yellow oil; ¹H NMR (400 MHz, CDCl₃): δ 7.62–7.46 (m, 4.16H), 7.39–7.31 (m, 4.23H), 7.22–7.01 (m, 5.70H), 6.79–6.75 (m, 0.32H), 6.48 (d, *J* = 18.8 Hz, 1H), 5.73 (d, *J* = 3.2 Hz, 0.35H), 5.72 (d, *J* = 3.2 Hz, 0.33H), 2.34 (s, 3H), 2.06 (s, 1.10H), 0.44 (s, 6H), 0.35 (s, 1.96H); ¹³C NMR (100 MHz, CDCl₃) δ: 152.5, 143.3, 138.8, 137.8, 137.6, 135.5, 134.2, 134.1, 130.5, 130.1, 129.7, 129.2, 129.2, 128.1, 128.0, 127.8, 127.8, 126.2, 126.0, 125.5, 125.2, 20.3, 19.7, -2.3, -2.8.

(E)-dimethyl(3-methylstyryl)(phenyl)silane

CAS registry No. [1283747-54-5], colorless oil; ¹H NMR (400 MHz, CDCl₃): δ 7.59–7.54 (m, 2H), 7.37–7.34 (m, 3H), 7.24–7.17 (m, 3H), 7.09–7.04 (m, 1H), 6.91 (d, *J* = 19.2 Hz, 1H), 6.57 (d, *J* = 19.2 Hz, 1H), 2.33 (s, 3H), 0.42 (s, 6H); ¹³C NMR (100 MHz, CDCl₃): δ 145.6, 138.8, 138.3, 138.2, 134.1, 129.2, 129.1, 128.6, 128.0, 127.3, 127.0, 123.9, 21.5, -2.4.

1-Chloro-2-[2-(dimethylphenylsilyl)ethenyl]benzene

CAS registry No. [1523444-01-0], colorless oil; ¹H NMR (400 MHz, CDCl₃): δ 7.66–7.55 (m, 2H), 7.40–7.31 (m, 3H), 7.25–7.13 (m, 3H), 6.58 (d, *J* = 19.2 Hz, 1H), 0.45 (s, 6H); ¹³C NMR (100 MHz, CDCl₃): δ 141.2, 138.4, 136.3, 133.4, 131.0, 129.8, 129.3, 128.0, 126.9, -2.5.

(E)-(3-chlorostyryl)dimethyl(phenyl)silane

CAS registry No. [1523443-97-1], colorless oil; ¹H NMR (400 MHz, CDCl₃): δ 7.58–7.53 (m, 2H), 7.45–7.34 (m, 4H), 7.30–7.18 (m, 3H), 6.84 (d, *J* = 19.2 Hz, 1H), 6.59 (d, *J* = 19.2 Hz, 1H), 0.43 (s, 6H); ¹³C NMR (100 MHz, CDCl₃): δ 143.9, 140.1, 138.2, 134.7, 134.0, 129.9, 129.4, 129.3, 128.1, 128.0, 126.5, 124.9, -2.5.

(E)-dimethyl(phenyl)(2-(thiophen-3-yl)vinyl)silane

CAS registry No. [1440972-00-8], colorless oil; ¹H NMR (400 MHz, CDCl₃): δ 7.69–7.56 (m, 2H), 7.50–7.20 (m, 6H), 7.93 (d, *J* = 19.2 Hz, 1H), 6.35 (d, *J* = 19.2 Hz, 1H), 0.41 (s, 6H); ¹³C NMR (100 MHz, CDCl₃): δ 139.2, 134.1, 129.2, 128.0, 126.9, 126.1, 125.1, 123.1, -2.4.

(E)-3-(2-(dimethyl(phenyl)silyl)vinyl)pyridine

CAS registry No. [773121-47-4], brown oil; ¹H NMR (400 MHz, CDCl₃): δ 8.62 (s, 1H), 8.46 (d, *J* = 3.2 Hz, 1H), 7.77–7.72 (m, 1H), 7.59–7.52 (m, 2H), 7.40–7.35 (m, 3H), 7.28–7.20 (m, 1H), 6.91 (d, *J* = 19.2 Hz, 1H), 6.68 (d, *J* = 19.2 Hz, 1H), 0.45 (s, 6H); ¹³C NMR (100 MHz, CDCl₃): δ 149.1, 148.8, 141.7, 138.0, 134.0, 133.7, 132.9, 130.6, 129.3, 128.0, 123.5, -2.6.

(E)-4-(dimethyl(phenyl)silyl)-2-methylbut-3-en-2-ol

CAS registry No. [56539-57-2], colorless oil; ¹H NMR (400 MHz, CDCl₃): δ 7.57–7.45 (2H, m), 7.45–7.28 (3H, m), 6.23 (d, *J* = 18.8 Hz, 1H), 5.95 (d, *J* = 18.8 Hz, 1H), 1.30 (6H, s), 0.34 (6H, s); ¹³C NMR (100 MHz, CDCl₃): δ 155.2, 138.8, 133.9, 129.1, 127.9, 122.6, 72.2, 29.5, -2.4.

(E)-1-dimethylphenylsilyl-1-octene

CAS registry No. [116488-00-7] & **dimethyl(1-methyleneheptyl)silyl]benzene** CAS registry No. [87437-03-4], colorless oil; ¹H NMR (400 MHz, CDCl₃): δ 7.54–7.48 (m, 2.7H), 7.36–7.31 (m, 4.2H), 6.12 (dt, 1H, *J* = 18.4, *J* = 6.4 Hz), 5.75 (dt, 1H, *J* = 18.4 Hz, *J* = 1.6 Hz), 5.68–5.65 (m, 1.1H), 5.4–5.3 (m, 1.1H), 2.19–2.05 (m, 2.76H), 1.37–1.14 (m, 10.7H), 0.92–0.81 (m, 4H), 0.36 (s, 6H), 0.31 (s, 2.1H). ¹³C NMR (100 MHz, CDCl₃): δ 150.7, 149.7, 139.6, 138.7, 134.1, 134.0, 129.0, 128.9, 127.8, 127.3, 125.8, 37.0, 36.2, 31.9, 29.3, 29.0, 28.8, 22.8, 14.2, -2.3, -2.8.

(E)-(1,2-diphenylvinyl)dimethyl(phenyl)silane

CAS registry No [65149-25-9], colorless oil; ¹H NMR (400 MHz, CDCl₃): δ 7.79–7.70 (m, 2H), 7.58–7.52 (d, *J* = 4.0 Hz, 3H), 7.45–7.34 (m, 3H), 7.30–7.23 (m, 3H), 7.18–7.05 (m, 4H), 7.01 (s, 1H), 0.58 (s, 6H). ¹³C NMR (100MHz, CDCl₃): δ 145.1, 142.4, 139.3, 137.8, 137.4, 134.4, 129.7, 129.3, 128.7, 128.0, 127.9, 127.2, 127.3, 125.8, -2.9.

(E)-2-(3-(dimethyl(phenyl)silyl)allyl)isoindoline-1,3-dione

Colorless oil, ¹H NMR (400 MHz, CDCl₃): δ 7.87–7.83 (m, 2H), 7.72–7.68 (m, 2H), 7.49–7.45 (m, 2H), 7.46 (d, *J* = 7.0 Hz, 1H), 7.35–7.30 (m, 1H), 6.10 (dt, *J* = 18.4, 4.8 Hz, 1H), 5.94 (dt, *J* = 18.4, 1.6 Hz, 1H), 4.36 (dd, *J* = 16, 4.8 Hz, 2H), 0.31 (s, 6H); ¹³C NMR (100 MHz, CDCl₃): 168.0, 140.5, 138.2, 134.1, 134.0, 132.2, 130.3, 129.2, 127.9, 123.5, 42.1, -2.5. IR (ATR): 1712, 1389, 904, 818, 718 cm⁻¹. HRMS (ESI): *m/z* Calculated for C₁₉H₁₉NO₂Si[M]⁺: 321.1183, found 321.1185.

(9S,13S,14S,17R)-17-((E)-2-(dimethyl(phenyl)silyl)vinyl)-13-methyl-7,8,9,11,12,13,14,15,16,17-decahydro-6H-cyclopenta[a]phenanthrene-3,17-diol

CAS registry No [2676952-64-8], colorless oil; ¹H NMR (400 MHz, CDCl₃): δ 7.55–7.50 (s, 2H),

7.43–7.31 (s, 3H), 7.11 (d, $J = 8.4$ Hz, 1H), 6.65–6.53 (m, 2H), 6.34 (d, $J = 19.2$ Hz, 1H), 5.93 (d, $J = 18.8$ Hz, 1H), 5.64 (br, 1H), 2.79 (s, 2H), 2.32–2.20 (m, 1H), 2.13–1.99 (m, 2H), 1.97–1.80 (m, 3H), 1.71 (br, 1H), 1.59 (d, $J = 7.6$ Hz, 1H), 1.52–1.24 (m, 7H), 0.96 (s, 3H), 0.37 (s, 6H). ^{13}C NMR (100 MHz, CDCl_3): δ 153.6, 152.4, 138.9, 138.3, 134.0, 132.5, 129.1, 127.9, 126.6, 124.6, 115.4, 112.9, 85.5, 49.3, 47.1, 43.9, 39.5, 36.1, 32.5, 29.7, 27.5, 26.4, 23.6, 14.4, -2.2, -2.3.

butyl 3-(dimethyl(phenyl)silyl)propanoate

CAS registry No. [1335304-11-4], colorless oil; ^1H NMR (400 MHz, CDCl_3): δ 7.54–7.45 (m, 2H), 7.38–7.30 (m, 3H), 4.02 (t, $J = 6.8$ Hz, 2H), 2.27 (t, $J = 8.4$ Hz, 2H), 1.63–1.51 (m, 2H), 1.42–1.31 (m, 2H), 1.09 (t, $J = 8.4$ Hz, 2H), 0.92 (t, $J = 7.6$ Hz, 3H), 0.29 (s, 6H). ^{13}C NMR (100 MHz, CDCl_3): δ 175.1, 138.3, 133.7, 129.2, 128.0, 64.4, 30.8, 29.0, 19.2, 13.8, 11.0, -3.2.

3-(dimethyl(phenyl)silyl)propanenitrile

CAS registry No. [17983-79-8], colorless oil; ^1H NMR (400 MHz, CDCl_3): δ 7.50–7.46 (m, 2H), 7.41–7.36 (m, 3H), 2.29–2.22 (m, 2H), 1.18–1.11 (m, 2H), 0.34 (s, 6H). ^{13}C NMR (100 MHz, CDCl_3): δ 136.7, 133.6, 129.7, 128.2, 121.3, 12.3, 12.1, -3.4.

diethyl (2-(dimethyl(phenyl)silyl)ethyl)phosphonate

Colorless oil; ^1H NMR (400 MHz, CDCl_3): δ 7.51–7.46 (m, 2H), 7.39–7.32 (m, 3H), 2.29–2.22 (m, 2H), 4.15–4.01 (m, 4H), 1.68–1.57 (m, 2H), 1.30 (t, $J = 7.2$ Hz, 2H), 1.05–0.93 (m, 2H), 0.29 (s, 6H); ^{13}C NMR (100 MHz, CDCl_3): δ 137.8, 133.6, 129.3, 128.0, 61.6 (d, $J = 7.0$ Hz), 20.5, 19.1, 16.5 (d, $J = 6.0$ Hz), 7.5 (d, $J = 9.0$ Hz), -3.5. IR (ATR): 2977, 1414, 1236, 1019, 952, 806, 725, 702, 466. HRMS (ESI): m/z Calculated for $\text{C}_{14}\text{H}_{15}\text{O}_3\text{PSi}[\text{M}]^+$: 300.1296, found 300.1311.

dimethyl(phenyl)(2-(phenylsulfonyl)ethyl)silane

CAS registry No. [196937-97-0], colorless oil; ¹H NMR (400 MHz, CDCl₃): δ 7.89–7.82 (m, 2H), 7.68–7.61 (m, 1H), 7.57–7.51 (m, 2H), 7.43–7.31 (m, 5H), 3.01–2.92 (m, 2H), 1.20–1.12 (m, 2H), 0.28 (s, 6H). ¹³C NMR (100 MHz, CDCl₃): δ 138.7, 136.6, 133.7, 133.5, 129.6, 129.3, 128.3, 128.3, 52.6, 8.6, -3.3.

3-(dimethyl(phenyl)silyl)cyclohexanone

CAS registry No. [67262-98-0], colorless oil; ¹H NMR (400 MHz, CDCl₃): δ 7.49–7.42 (m, 2H), 7.38–7.33 (m, 3H), 2.40–2.07 (m, 5H), 1.83–1.61 (2H, m), 1.48–1.22 (m, 2H), 0.3 (s, 3H). ¹³C NMR (100 MHz, CDCl₃): δ 212.7, 136.7, 134.0, 129.4, 128.0, 42.5, 42.0, 29.9, 27.7, 26.1, -5.2, -5.3.

4-(Dimethylphenylsilyl)tetrahydro-2H-pyran-2-one

CAS registry No. [156033-13-5], colorless oil; ¹H NMR (400 MHz, CDCl₃): δ 7.50–7.46 (m, 2H), 7.40–7.35 (m, 3H), 4.36–4.21(m, 2H), 2.61–2.52 (m, 1H), 2.32–2.22 (m, 1H), 1.90–1.80 (m, 1H), 1.70–1.58 (m, 1H), 1.44–1.34 (m, 1H), 0.33 (s, 6H). ¹³C NMR (CDCl₃, 100 MHz): δ 171.6, 135.6, 133.9, 129.7, 128.2, 70.4, 30.9, 23.7, 18.5, -5.6, -5.6

ethyl 3-(dimethyl(phenyl)silyl)but-3-enoate

CAS registry No. [13950-56-6], colorless oil; ¹H NMR (400 MHz, CDCl₃): δ 7.55–7.48 (m, 2H), 7.36–7.32 (m, 3H), 5.86–5.83 (m, 1H), 5.59–5.56 (m, 1H), 3.99 (q, *J* = 7.2 Hz, 2H), 3.09 (s, 2H), 1.17 (t, *J* = 7.2 Hz, 3H), 0.40 (s, 6H). ¹³C NMR (100 MHz, CDCl₃): δ 172.0, 143.0, 137.5, 134.1, 130.5, 129.2, 127.9, 60.6, 41.9, 14.2, -2.92.

3-(dimethylphenylsilyl)-1,3-diphenyl-1-propanone

CAS registry No. [118356-60-8], colorless oil; ¹H NMR (400 MHz, CDCl₃): δ 7.79–7.77 (m, 2H), 7.50–.27 (m, 8H), 7.25–7.13 (m, 2H), 7.09–6.97 (m, 3H), 3.56–3.41 (m, 1H), 3.25–3.06 (m, 2H), 0.29 (s, 3H), 0.23 (s, 3H). ¹³C NMR (100 MHz, CDCl₃): δ 199.2, 142.5, 137.2, 136.9, 134.3, 132.8, 129.4, 128.5, 128.2, 128.0, 127.9, 127.8, 124.9, 39.0, 31.2, -3.7, -5.0.

***N*-((dimethyl(phenyl)silyl)(phenyl)methyl)aniline**

CAS registry No. [1283154-25-5], yellow oil; ¹H NMR (400 MHz, CDCl₃): δ 7.49–7.31 (m, 5H), 7.23–7.18 (m, 3H), 7.16–6.90 (m, 5H), 6.67–6.41 (m, 3H), 4.17–4.05 (m, 2H), 0.34 (s, 3H), 0.26 (s, 3H); ¹³C NMR (100 MHz, CDCl₃): δ 148.7, 142.2, 135.3, 134.5, 130.0, 129.1, 128.4, 128.2, 116.2, 125.6, 117.4, 113.6, 55.3, -4.2, -5.3.

***N*-((dimethyl(phenyl)silyl)(4-methoxyphenyl)methyl)aniline**

CAS registry No. [1677677-54-1], colorless oil; ¹H NMR (400 MHz, CDCl₃): δ 7.50–7.35 (m, 5H), 7.07–6.97 (m, 4H), 6.8–6.74 (m, 2H), 6.67–6.41 (m, 3H), 4.17–4.05 (m, 2H), 3.74 (s, 3H), 0.32 (s, 3H), 0.26 (s, 3H). ¹³C NMR (100 MHz, CDCl₃): δ 157.7, 148.7, 135.4, 129.9, 129.1, 128.1, 127.1, 117.3, 113.8, 113.6, 55.3, 49.4, -4.3, -5.3.

***N*-((dimethyl(phenyl)silyl)(4-fluorophenyl)methyl)-4-fluoroaniline**

Colorless oil; ¹H NMR (400 MHz, CDCl₃): δ 7.48–7.30 (m, 5H), 7.12–6.97 (m, 2H), 6.90–6.80 (m, 2H), 6.75–6.68 (m, 3H), 4.07 (d, *J* = 5.6 Hz, 1H), 3.96 (d, *J* = 5.6 Hz, 1H), 0.34 (s, 3H), 0.26 (s, 3H); ¹³C NMR (100 MHz, CDCl₃): δ 161.2 (d, *J* = 242.0 Hz), 155.9 (d, *J* = 234.0 Hz), 144.7, 137.5 (d, *J* = 3.3 Hz), 134.9, 134.4, 130.1, 128.3, 127.3 (d, *J* = 8.0 Hz), 115.7, 115.5 (d, *J* = 23.0 Hz), 115.3 (d, *J* =

21.0 Hz), 114.3 (d, $J = 8.0$ Hz), 50.3, -4.5, - 5.4. IR (ATR): 2964, 1601, 1506, 1228, 1122, 827, 738, 700, 532, 465 cm^{-1} . HRMS (ESI): m/z Calculated for $\text{C}_{21}\text{H}_{21}\text{FO}_2\text{NSi}[\text{M}]^+$: 353.1411, found 353.1404.

1,2-diphenylhydrazine

CAS registry No. [122-66-7], yellow solid; ^1H NMR (400 MHz, CDCl_3): δ 7.26–7.17 (m, 4H), 6.89–6.80 (m, 6H), 5.56 (s, 2H). ^{13}C NMR (100 MHz, CDCl_3): 149.0, 131.1, 129.5, 129.2, 123.0, 120.0, 122.5.

1,2-di-*m*-tolylhydrazine

CAS registry No. [621-26-1], yellow solid; ^1H NMR (400 MHz, CDCl_3): δ 7.09 (t, $J = 8.0$ Hz, 2H), 6.68–6.65 (m, 6H), 5.52 (s, 2H), 2.28 (s, 6H); ^{13}C NMR (100 MHz, CDCl_3): δ 152.9, 139.0, 131.7, 128.9, 122.9, 120.5, 21.4.

1-(4-methoxyphenyl)-2-phenylhydrazine

CAS registry No. [953-12-8], yellow solid; ^1H NMR (400 MHz, CDCl_3): δ 7.24–7.18 (m, 2H), 6.88–6.81 (m, 3H), 6.80 (s, 4H), 5.58 (s, 1H), 5.43 (s, 1H), 3.74 (s, 3H); ^{13}C NMR (100 MHz, CDCl_3): δ 142.9, 129.5, 120.0, 115.0, 113.9, 112.5, 55.9.

4,4-bis(dimethyl(phenyl)silyl)butan-2-one

Colorless oil, ^1H NMR (400 MHz, CDCl_3): δ 7.47–7.43 (m, 4H), 7.32–7.28 (m, 6H), 2.46 (d, $J = 6.0$ Hz, 6H), 1.73 (s, 3H), 1.26 (t, $J = 6.0$ Hz, 1H), 0.22 (s, 6H), 0.19 (s, 6H). ^{13}C NMR (100 MHz, CDCl_3): δ 207.8, 139.3, 134.0, 129.0, 127.8, 40.6, 29.4, 6.2, -1.3, -2.2. IR (ATR): 2952, 1712, 1434, 1250,

1117, 840, 788, 733, 640 cm^{-1} . HRMS (ESI): m/z Calculated for $\text{C}_{20}\text{H}_{28}\text{OSi}_2[\text{M}]^+$: 340.1679, found 340.1674.

methyl 3,3-bis(dimethylphenylsilyl)propanoate

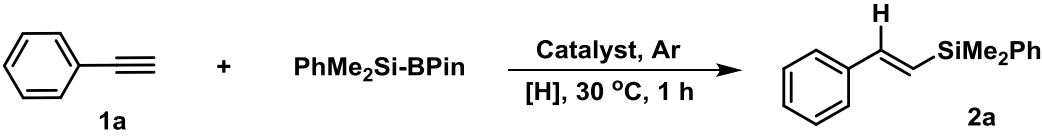
CAS registry No. [1256931-34-6], colorless oil; ^1H NMR (400 MHz, CDCl_3): δ 7.48–7.43 (m, 4H), 7.34–7.28 (m, 6H), 3.38 (s, 3H), 2.38 (d, $J = 6.4$ Hz, 6H), 1.06 (t, $J = 6.4$ Hz, 1H), 0.22 (s, 6H), 0.19 (s, 6H). ^{13}C NMR (100 MHz, CDCl_3): δ 174.8, 139.1, 134.0, 129.0, 127.8, 51.6, 31.0, 8.5, -1.4, -2.4.

3. Results and discussion

3.1. Cu₃N NC catalyzed-hydrosilylation of alkynes

The Cu catalyzed-hydrosilylation of alkynes is a useful method for synthesizing various valuable vinylsilanes [11–17]. Hence, the author selected the hydrosilylation of phenylacetylene (**1a**) as a model reaction to investigation for the optimized reaction conditions, and the data are summarized in **Table 5-1**. In the preliminary experiment, the reaction of **1a** (0.25 mmol) with PhMe₂Si-BPin (1.2 eq. of **1a**) was carried out in ethanol with Cu₃N NC under Ar atmosphere at 30 °C for 1 h, and (*E*)-dimethyl(phenyl)(styryl)silane (**2a**) was obtained in 73% yield (entry 1). Cuprous oxide nanocube (Cu₂O NC) with the same morphology and size as Cu₃N NC exhibited much worse activity, providing **2a** in only 4% yield (entry 2). Other Cu catalysts, such as CuI, CuO, and Cu₃P, were inactive

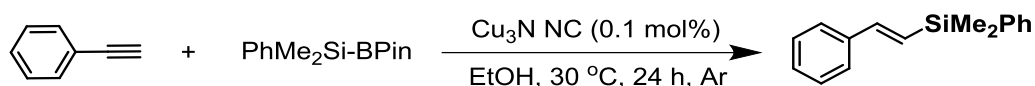
Table 5-1. Hydrosilylation of **1a** using various Cu catalysts.



Reaction scheme: Phenylacetylene (**1a**) + PhMe₂Si-BPin $\xrightarrow{[H], 30\text{ }^\circ\text{C}, 1\text{ h}}$ (*E*)-dimethyl(phenyl)(styryl)silane (**2a**)

Entry	Catalyst	[H] sources	Yield of 2a ^b (%)
1	Cu ₃ N NC	EtOH	73
2	Cu ₂ O NC	EtOH	4
3	CuI	EtOH	0
4	CuO	EtOH	0
5	Cu ₃ P	EtOH	0
6 ^c	Cu ₃ N NC	EtOH	90
7 ^c	Cu ₃ N NC	H ₂ O	64
8 ^{c,d}	Cu ₃ N NC	EtOH	92
9 ^c	Cu ₃ N NC (3rd run)	EtOH	90

^a Reaction conditions: **1a** (0.25 mmol), PhMe₂Si-BPin (1.2 eq., 0.3 mmol), catalyst (Cu: 5 mol%), [H] sources (1.0 mL), 30 °C, under Ar. ^b Yield was calculated through ¹H NMR analysis using 1,4-dinitrobenzene as an internal standard. ^c PhMe₂Si-BPin (1.5 eq., 0.375 mmol). ^d EtOH (7.0 eq., 0.1 mL).



1a, 1.02 g, 10 mmol

2a, 2.13 g, 89% isolated yield

TON = 894

Scheme 5-2. Gram-scale experiment of hydrosilylation of **1a** using $\text{Cu}_3\text{N NC}$.

Table 5-2. Comparison of $\text{Cu}_3\text{N NC}$ catalytic system and reported catalytic systems for hydrosilylation of alkynes with $\text{PhMe}_2\text{Si-BPin}$

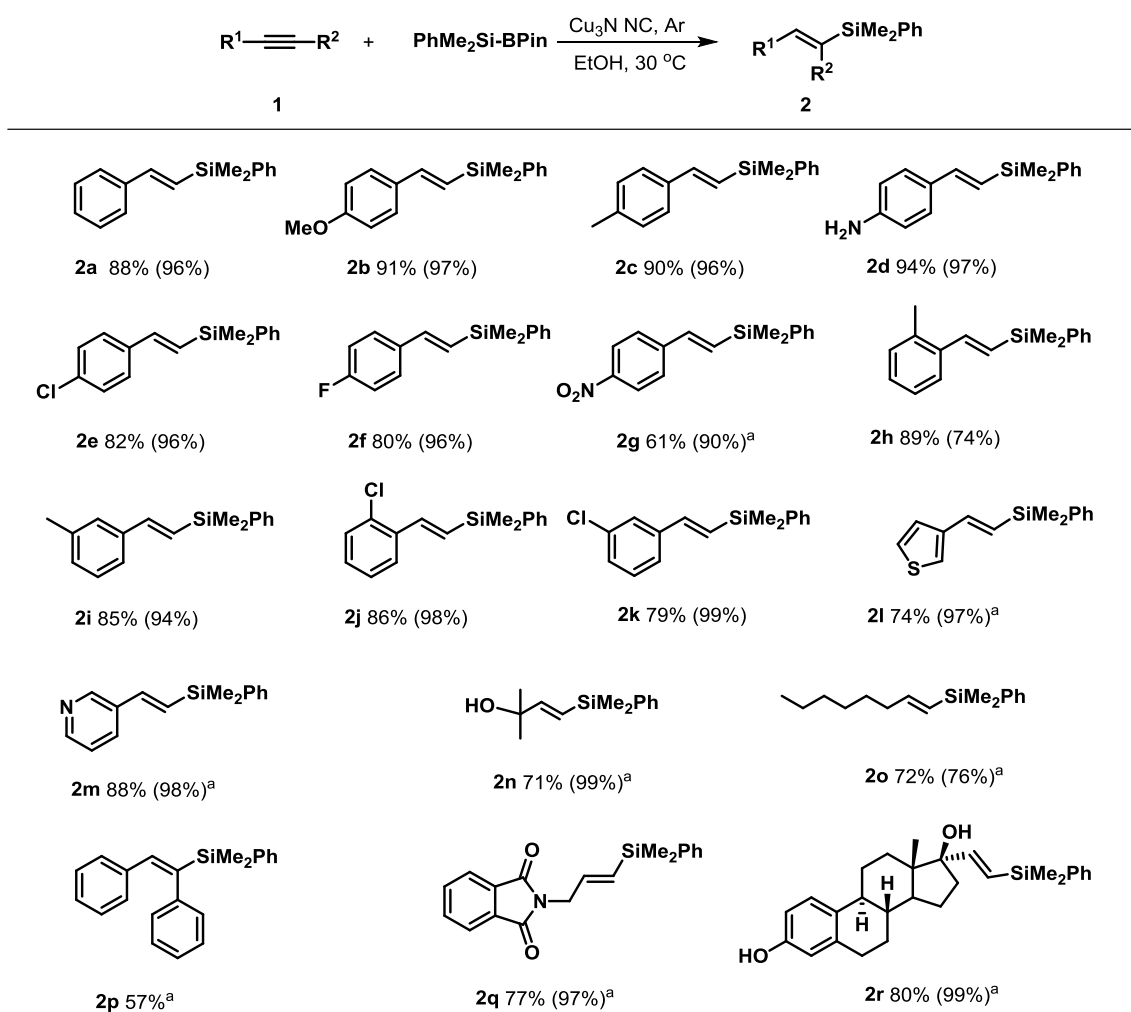
Entry	Catalyst	Additive	Solvent	Temp. (°C)	TON	Ref.
1	$\text{Cu}_3\text{N NC}$	-	EtOH	30	894	<i>This work</i>
2	CuCl	L1 / <i>t</i> -BuONa	MeOH/THF	-20	10	11
3	[Cu(dmp)(Xantphos TEPD)]PF ₆	K ₂ CO ₃	CH ₃ CN/ H ₂ O	30	490	17
4	FeO/MgO	PPh ₃	Toluene	160	24	19
5	Me ₂ Zn (1.1 eq.)	Bu ₃ P	THF	50	-	20

Note: **L1** = Johnphos.

(entries 3–5). Increasing the amount of $\text{PhMe}_2\text{Si-BPin}$ to 1.5 equivalent improved the conversion of **1a** and afforded a 90% yield of **2a** (entry 6). The use of H₂O as a hydrogen source decreased yield of **2a** compared with that of EtOH (entry 7 vs 1) [18]. Notably, introducing EtOH (7 eq. of **1a**) as an additive resulted in 92% yield of **2a** (entry 8). This is the first time that the hydrosilylation of **1a** was achieved over a heterogeneous Cu catalyst (**Table 5-2**). The reuse experiments were conducted to check the durability of $\text{Cu}_3\text{N NC}$. After the reaction, $\text{Cu}_3\text{N NC}$ was separated from the reaction mixture and reused for several times without any significant loss of activity (entry 9). Moreover, the $\text{Cu}_3\text{N NC}$ catalyst system was applicable to gram-scale synthesis, affording **2a** in 89% isolated yield with a TON exceeding 894 based on the total number of Cu atoms used in the reaction (**Scheme 5-2**). This TON

value is greater than that in previously reported Cu catalytic systems.

Then, the applicability of this Cu₃N NC catalytic system was investigated through the hydrosilylation of a series of alkyne substrates (**Scheme 5-3**). Aromatic alkynes with electron-donating (e.g., -OMe, -Me, and -NH₂) or -withdrawing groups (e.g., -Cl, -F, and -NO₂) located at *para*-position worked well under optimized conditions (**2a-2g**). *meta*-Substituted aromatic alkynes were also tolerated and converted to desired products in high yields (**2h-2k**). In addition, the reaction conditions were compatible with the heterocyclic substrates for example 3-ethynylpyridine and 3-ethynylthiophene (**2l** and **2m**). Remarkably, the scope of this method can be applied to aliphatic alkynes (**2n** and **2o**). The reaction of internal alkyne (diphenylacetylene) also proceeded smoothly to afford **2p** in 57% yield. Moreover, bioactive compounds, **2q** and **2r**, were obtained in satisfied yields through the hydrosilylation of corresponding alkynes. These results demonstrated that the high catalytic performance of Cu₃N NC in the hydrosilylation of alkynes.

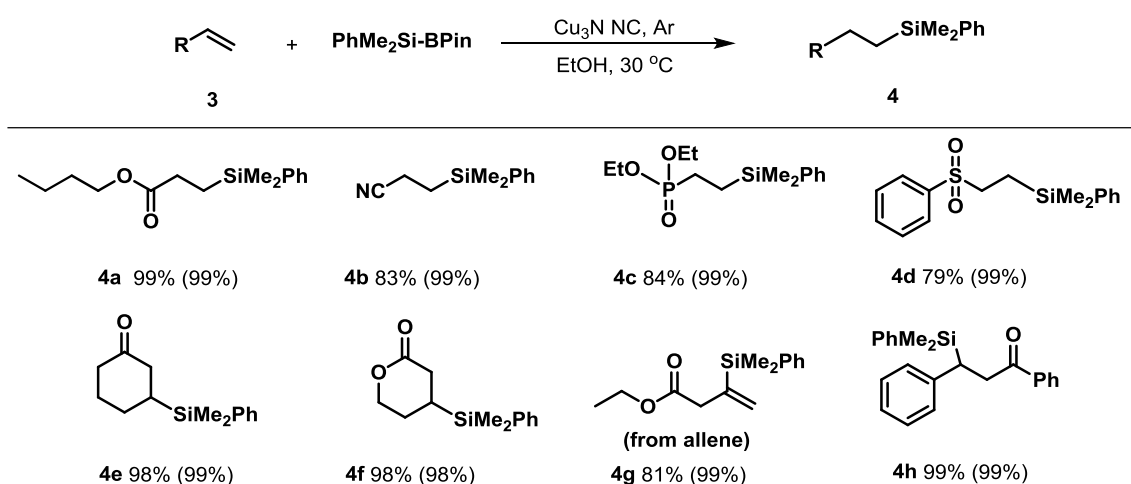


Scheme 5-3. Cu₃N NC catalyzed-hydrosilylation of alkynes. Reaction conditions: **1** (0.25 mmol), PhMe₂Si-BPin (0.375 mmol), Cu₃N NC (2.5 mg, 5 mol% of Cu), EtOH (0.1 mL), Ar, 30 °C, 1 h. Isolated yields. Regioselectivity in parentheses was determined by GC-MS or ¹H NMR analysis. ^a 12 h.

3.2. Cu₃N NC catalyzed-hydrosilylation of alkenes and allenes

Hydrosilylation of alkenes is an important and efficient method for preparation of silanes [21–27]. Then, to expand the scope of this method, the hydrosilylation of alkenes was evaluated, and the results were summarized in **Scheme 5-4**. Butyl acrylate underwent β-silylation reaction to provide

the **4a** in 99% yield. Acrylonitrile was also effectively silylated, and **4b** was obtained in 83% yield. Moreover, the reaction of diethylvinylphosphonate proceeded smoothly to afford the **4c** in 84% yield, while the reported Cu catalytic system is inactive for this substrate [21]. The β -silylsulfone was also tolerated and provided **4d** in 79% yield. From cyclic ketones, the corresponding silanes (**4e** and **4f**) were also obtained in excellent yields. Furthermore, allene (**3g**) was readily converted to the desired product **4g**. The bioactive compound, chalcone, was active, affording **4h** in 99% yield. This is the first example that the hydrosilylation of alkenes and allenes with PhMe₂Si-BPin achieved over a heterogeneous catalyst.

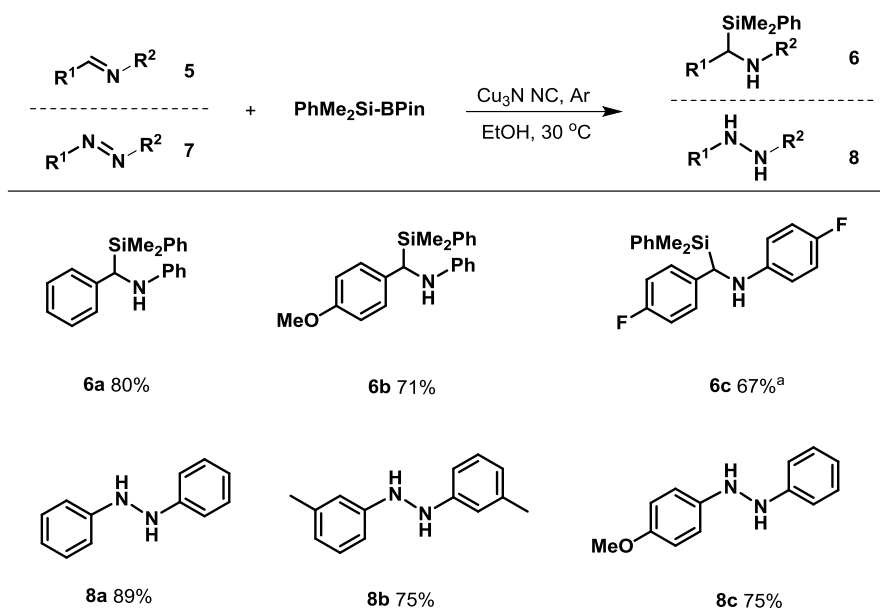


Scheme 5-4. Cu₃N NC catalyzed-hydrosilylation of alkenes and allene to silanes. Reaction conditions: **3** (0.25 mmol), PhMe₂Si-BPin (0.375 mmol), Cu₃N NC (2.5 mg, 5 mol% of Cu), EtOH (0.1 mL), Ar, 30 °C, 12 h. Isolated yields. Regioselectivity in parentheses was determined by GC-MS or ¹H NMR analysis.

3.3. Cu₃N NC catalyzed-hydrosilylation of imines and azobenzenes

Imines, a class of commercially available and useful unsaturated compounds [28], were also treated in this hydrosilylation reaction. Notably, the reaction of several imine derivatives proceeded smoothly under base- and ligand-free conditions (**Scheme 5-5**). The *N*-benzylidenaniline underwent the reaction to afford the desired silane (**6a**) in 80% isolated yield. Substituted benzylidenaniline derivatives were also tolerated, generating the desired silanes in high yields (**6b** and **6c**). This is the first time that the hydrosilylation of imines was achieved over a heterogeneous metal catalyst.

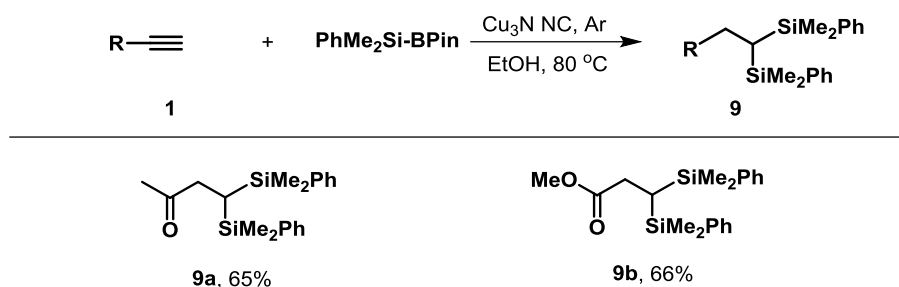
Aromatic azo compounds are essential fine chemicals and have broad applications in organic synthesis [29]. In an attempt to further expand the scope of this methodology, the author turned the attention to the hydrosilylation of azobenzenes (**7**). The reaction of azobenzene (**7a**) with PhMe₂Si-BPin yielded the 1,2-diphenylhydrazine (**8a**) instead of corresponding silane (1-(dimethyl(phenyl)silyl)-1,2-diphenylhydrazine). The author speculated that the 1-(dimethyl(phenyl)silyl)-1,2-diphenylhydrazine may be formed during the reaction and protonated in a proton solvent to afford the **8a** [30, 31]. To confirm this speculation, control experiments of the hydrosilylation of **7a** were performed. No conversion of **7a** was observed in the absence of PhMe₂Si-BPin, suggesting that the generation and protonation of 1-(dimethyl(phenyl)silyl)-1,2-diphenylhydrazine was involved during the hydrosilylation reaction. Next, several azobenzene derivatives were treated in the reaction, and the hydrazines were obtained in good yields (**8b** and **8c**). This study provided a new synthetic protocol for the preparation of hydrazines.



Scheme 5-5. $\text{Cu}_3\text{N NC}$ catalyzed-hydrosilylation of imines and azobenzenes. Reaction conditions: **5** or **7** (0.25 mmol), $\text{PhMe}_2\text{Si-BPin}$ (0.375 mmol), $\text{Cu}_3\text{N NC}$ (2.5 mg, 5 mol% of Cu), EtOH (0.1 mL), Ar, 30 °C, 12 h. Isolated yields. ^a EtOH (1.0 mL), 80 °C, 1 h.

3.4. $\text{Cu}_3\text{N NC}$ catalyzed-dihydrosilylation of alkynes

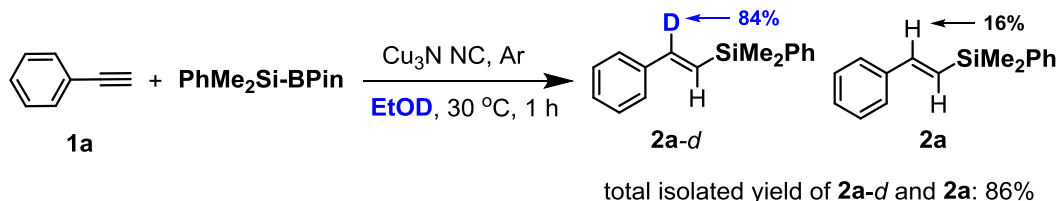
Geminal bis(silanes), a crucial class of organic compounds, have been widely used in organic chemistry since they have high stability and propensity to undergo a variety of transformations [32]. Catalytic dihydrosilylation of alkynes is a useful and straight-forward method for synthesis of geminal bis(silanes). Recently, several research groups have reported dihydrosilylation reaction of alkynes with hydrosilanes (e.g., HSiEt_2 , PhSiH_3) through transition-metal catalysis [33–35]. To date, the dihydrosilylation reaction of alkynes with silyl boronate for *gem*-bis(silanes) synthesis by heterogeneous metal catalysts has never been reported yet. Therefore, the author reported a new method of synthesizing geminal bis(silanes) by means of $\text{Cu}_3\text{N NC}$ -catalyzed dihydrosilylation of alkynes. As shown in **Scheme 5-6**, the dihydrosilylation of terminal alkynes proceeded smoothly, affording the *gem*-bis(silanes) in acceptable yields (**9a** and **9b**).



Scheme 5-6. $\text{Cu}_3\text{N NC}$ catalyzed-dihydrosilylation of alkynes. Reaction conditions: **1** (0.25 mmol), $\text{PhMe}_2\text{Si-BPin}$ (0.75 mmol), $\text{Cu}_3\text{N NC}$ (2.5 mg, 5 mol% of Cu), EtOH (2 mL), Ar, 80 °C, 1 h. Isolated yields.

3.5. Proposed mechanism

To investigate the proposed mechanism, the deuterium-labeling experiment was performed. The hydrosilylation of **1a** was carried out in EtOD, and the **2a-d** was obtained (**Scheme 5-7**), demonstrating the participation of EtOH in the reaction.



Scheme 5-7. The deuterium-labeling experiment of the hydrosilylation of **1a**.

Based on this observation and the previous works, the author provided a proposed mechanism of hydrosilylation of unsaturated compounds. Initially, the EtOH molecule was activated by the Lewis acid-base sites on $\text{Cu}_3\text{N NC}$. Next, the $\text{PhMe}_2\text{Si-BPin}$ was absorbed on $\text{Cu}_3\text{N NC}$ and reacted with activated EtOH to afford the EtO-BPin. Followed by the absorption of unsaturated compounds on Cu sites and the reaction of Cu-Si species, the addition intermediate was formed. Finally, the desired products were produced through the hydrogen transfer to the Cu intermediate, and

the $\text{Cu}_3\text{N NC}$ catalyst was regenerated. Thus, the cooperative catalysis of $\text{Cu}_3\text{N NC}$ combining its Lewis acid-base property is key to the efficient hydrosilylation of unsaturated compounds.

3.6. Outlook

Sequential continuous-flow reactions using heterogeneous catalyst-packed columns have been considered as a next-generation technology for chemical processes since catalyst separation is not required [36]. Therefore, the author speculates that the $\text{Cu}_3\text{N NC}$ catalytic system may be applied in the continuous-flow synthesis of silanes through catalytic hydrosilylation reactions, and this research is undergoing.

4. Conclusion

This chapter described a green and efficient method for synthesizing silanes via the Cu₃N NC catalyzed-hydrosilylation of unsaturated compounds. In this method, a wide range of substrates, including alkynes, alkenes, imines, and azobenzenes, were tolerated and generated the desired products in good to excellent yields. Moreover, the dihydrosilylation of alkynes was achieved over Cu₃N NC catalyst, providing a novel method for *gem*-(bis)silanes synthesis. The synthetic utility of this protocol had also been demonstrated by the gram-scale synthesis of vinylsilane with low catalyst loading (0.01 mol % of Cu, TON = 894). This is the first example that a heterogeneous Cu catalyst achieved the hydrosilylation of various unsaturated compounds. These findings will significantly contribute to the development of green sustainable technology for producing valuable silanes.

References

- 1 C. Cheng, J. F. Hartwig, *Chem. Rev.*, **2015**, *115*, 8946–8975.
- 2 Y. Nakao, T. Hiyama, *Chem. Soc. Rev.*, **2011**, *40*, 4893–4901.
- 3 Y. Tsuji, T. Fujihara, *Chem. Rec.*, **2016**, *16*, 2294–2313.
- 4 T. Fujihara, Y. Tsuji, *Synthesis*, **2018**, *50*, 1737–1749.
- 5 B. S. Takale, R. R. Thakore, E. Etemadi-Davan, B. H. Lipshutz, *Beilstein J. Org. Chem.*, **2020**, *16*, 691–737.
- 6 J. Chen, J. Guo, Z. Lu, *Chin. J. Chem.*, **2018**, *36*, 1075–1109.
- 7 X. D. J. Vyas, M. Oestreich, *Angew. Chem. Int. Ed.*, **2010**, *49*, 8513–8515.
- 8 O. Riant, N. Mostefai, J. Courmarcel, *Synthesis*, **2004**, *18*, 2943–2958.
- 9 J. R. Wilkinson, C. E. Nuyen, T. S. Carpenter, S. R. Harruff, R. Van Hoveln, *ACS Catal.*, **2019**, *10*, 8961–8979.
- 10 J.-J. Feng, W. Mao, L. Zhang, M. Oestreich, *Chem. Soc. Rev.*, **2021**, *50*, 2010–2073.
- 11 P. Wang, X.-L. Yeo, T.-P. Loh, *J. Am. Chem. Soc.*, **2011**, *133*, 1254–1256.
- 12 C.K. Hazra, C. Fopp, M. Oestreich, *Chem. Asian J.*, **2014**, *9*, 3005–3010.
- 13 H. Zhou, Y.-B. Wang, *ChemCatChem*, **2014**, *6*, 2512–2516.
- 14 Q.-Q. Xuan, C.-L. Ren, L. Liu, D. Wang, C.-J. Li, *Org. Biomol. Chem.*, **2015**, *13*, 5871–5874.
- 15 M. Wang, Z.-L. Liu, X. Zhang, P.-P. Tian, Y.-H. Xu, T.-P. Loh, *J. Am. Chem. Soc.*, **2015**, *137*, 14830–14833.
- 16 M. Zhong, X. Pannecoucke, P. Jubault, T. Poisson, *Chem. Eur. J.*, **2021**, *27*, 11818–11822.
- 17 Y. Gao, S. Yazdani, A. Kendrick IV, G. P. Junor, T. Kang, D. B. Grotjahn, G. Bertrand, R. Jazzar, K. M. Engle, *Angew. Chem. Int. Ed.*, **2021**, *60*, 19871–19878.
- 18 L. He, L.-C. Wang, H. Sun, J. Ni, Y. Cao, H.-Y. He, K.-N. Fan, *Angew. Chem. Int. Ed.*, **2009**, *48*, 9538–9541.

- 19 A. Khan, A. M. Asiri, S. A. Kosa, H. Garcia, A. Grirrane, *J. Catal.*, **2015**, *329*, 401–412.
- 20 Y. Nagashima, D. Yukimori, C. Wang, M. Uchiyama, *Angew. Chem.*, **2018**, *130*, 8185–8189.
- 21 J. A. Calderone, W. L. Santos, *Org. Lett.*, **2012**, *14*, 2090–2093.
- 22 Q.-Q. Xuan, N.-J. Zhong, C.-L. Ren, L. Liu, D. Wang, Y.-J. Chen, C.-J. Li, *J. Org. Chem.*, **2013**, *78*, 11076–11081.
- 23 F. Meng, H. Jang, A. H. Hoveyda, *Chem. Eur. J.*, **2013**, *19*, 3204–3214.
- 24 T. Kitanosono, L. Zhu, C. Liu, P. Xu, S. Kobayashi, *J. Am. Chem. Soc.*, **2015**, *137*, 15422–15425.
- 25 J. Plotzitzka, C. Kleeberg, *Inorg. Chem.*, **2016**, *55*, 4813–4823.
- 26 S. Pashikanti, J. A. Calderone, M. K. Nguyen, C. D. Sibley, W. L. Santos, *Org. Lett.*, **2016**, *18*, 2443–2446.
- 27 R. Arai, Y. Nagashima, T. Koshikawa, K. Tanaka, *J. Org. Chem.*, **2022**, DOI: 10.1021/acs.joc.2c01885.
- 28 D. J. Vyas, R. Fröhlich, M. Oestreich, *Org. Lett.*, **2011**, *13*, 2094–2097.
- 29 A. Grirrane, A. Corma, H. Carcía, *Science*, **2008**, *322*, 1661–1664.
- 30 M. B. Ansell, G. E. Kostakis, H. Braunschweig, O. Navarro, J. Spencer, *Adv. Synth. Catal.*, **2016**, *358*, 3765–3769.
- 31 W. Wu, F. Zhang, N. Liu, Z. Wei, J. Xu, Z. He, Y. Guo, Baomin Fan, *Asian J. Org. Chem.*, **2022**, *11*, e202200336.
- 32 L. Gao, Y. Zhang, Z. Song, *Synlett*, **2013**, *24*, 139–144.
- 33 W. Chen, H. Song, J. Li, C. Cui, *Angew. Chem. Int. Ed.*, **2020**, *59*, 2365–2369.
- 34 M.-Y. Hu, J. Lian, W. Sun, T.-Z. Qiao, S.-F. Zhu, *J. Am. Chem. Soc.*, **2019**, *141*, 4579–4583.
- 35 G. Wang, X. Su, L. Gao, X. Liu, G. Li, S. Li, *Chem. Sci.*, **2021**, *12*, 10883–10892.
- 36 W.-J. Yoo, H. Ishitani, Y. Saito, B. Laroche, S. Kobayashi, *J. Org. Chem.*, **2020**, *85*, 5132–5145.

General Conclusions

This thesis deals with the studies on the development of copper nitride (Cu_3N) as highly efficient catalysts for various environmentally benign organic reactions, for example (i) hydroxylation of aryl halides to phenols, (ii) oxidation of indoles to indolin-3-ones and 2-ketoanilide derivatives, (iii) hydroboration of alkynes to boronates, and (iv) hydrosilylation of unsaturated compounds to silanes.

Firstly, the author reviewed the fundamental background of metal nitrides, especially Cu_3N , and focused on the preparation and characterization of Cu_3N materials. In addition, the activity of Cu_3N catalysts in the photocatalysis, electrocatalysis, and organic reactions was systematically summarized, and the limitation of the applicability of Cu_3N catalysts was also described.

In Chapter II, the author mentioned that nanocubic Cu_3N (nano- Cu_3N) prepared by calcination method efficiently promoted the hydroxylation of aryl halides to phenols under ligand-free conditions. This method showed good functional group tolerance to afford a wide range of phenols in good yields. nano- Cu_3N is the first heterogeneous Cu catalyst for the hydroxylation of aryl chlorides under additive-free conditions. The N atoms in nano- Cu_3N may serve as functional N ligands to promote this reaction.

Chapter III described the unique catalysis of a Cu_3N nanocube ($\text{Cu}_3\text{N NC}$) for oxidation of indoles. This catalytic system can be operated under additive-free conditions in an aqueous solvent with O_2 as sole oxidant and exhibited good functional group tolerance to produce the desired indolin-3-ones and 2-ketoanilide derivatives in moderate to good yields. This is the first application of the Cu_3N in oxidative reactions. Moreover, $\text{Cu}_3\text{N NC}$ catalyst could be recovered and reused without

significant loss in its catalytic activity, providing a green and sustainable method for preparation of nitrogen atom containing organic compounds. The high catalytic activity of Cu_3N NC is benefited from the N–Cu–N structure on surface that promotes the conversion of O_2 to superoxide species.

The next chapter revealed an efficient heterogeneous catalysis of Cu_3N NC for the hydroboration of alkynes to vinyl boronates. The Cu_3N NC showed outstanding activity, promoting the hydroboration of various alkynes to afford the desired vinyl boronates in good yields. It is worthy to note that the hydroboration of alkynes under additive-free and mild reaction conditions is achieved for the first time over a heterogeneous Cu catalyst. Moreover, Cu_3N NC was applicable to the hydroboration of alkynes with tetrahydroxydiboron to synthesize vinyl boronic acids. Control experiments and spectroscopic analyses disclosed that the Lewis acid-base property of Cu_3N NC may be the key factor for its high activity.

In Chapter V, the author mentioned an efficient method for synthesizing silanes through the hydrosilylation of unsaturated compounds with Cu_3N NC catalyst. A wide range of substrates, including alkynes, alkenes, imines, and azobenzenes, were efficiently converted to the desired products in excellent yields. Moreover, the Cu_3N NC catalytic system was applicable to the gram scale experiment. This is the first example that a heterogeneous Cu catalyst for the hydrosilylation of unsaturated compounds to silanes.

The author believes that this study will not only make a significant contribution to the development of green and efficient methods for organic synthesis but also bring a deep understanding of metal nitride materials. The developed Cu_3N catalysts and their superior catalytic activity in organic reactions discussed here demonstrate that the metal nitrides are the next-generation catalysts for

achieving various valuable chemical processes.

Finally, the author envisages further developments for the Cu_3N catalysis as follows.

1. Development of efficient supported metal nanoparticle catalysts for organic transformation is attractive since the supported metal nanoparticle catalysts may offer drastic changes in catalytic activity and selectivity compared with the pure metal nanoparticles due to the interaction of metal nanoparticles with the functional supports. It is expected that the novel supported- Cu_3N catalysts can be designed and prepared through the impregnation method or precipitation-deposition method. Therefore, the author hopes that the interaction between supports and Cu_3N would change the electronic structure of Cu species, which might increase its activity in organic synthesis.
2. In the last decades, molecular photocatalytic organic synthesis has developed into a vast field of research. As mentioned in this thesis, Cu_3N is a semiconductor with an indirect band gap energy ~ 1.4 eV and its optical absorption coefficient value of $\sim 10^5 \text{ cm}^{-1}$. Benefiting from this essential property, the Cu_3N has good catalytic potential in photocatalytic organic synthesis. Hence, the author envisions that the Cu_3N nanoparticles may work as an efficient photocatalyst to achieve some previously unattainable organic reactions.

List of Publications

- [1] **Hang Xu**, Sho Yamaguchi, Takato Mitsudome, Tomoo Mizugaki.
“Copper nitride nanocube catalyst for highly efficient hydroboration of alkynes”
Organic & Biomolecular Chemistry, **2023**, DOI: 10.1039/D2OB02130G.
- [2] **Hang Xu**, Sho Yamaguchi, Takato Mitsudome, Tomoo Mizugaki.
“Green oxidation of indoles using molecular oxygen over a copper nitride nanocube catalyst.”
European Journal of Organic Chemistry, **2022**, e202200826.
- [3] **Hang Xu**, Sho Yamaguchi, Takato Mitsudome, Tomoo Mizugaki.
“A copper nitride catalyst for the efficient hydroxylation of aryl halides under ligand-free conditions.”
Organic & Biomolecular Chemistry, **2021**, 19, 6593–6597.

Related Works

- [1] **Hang Xu**, Liangying Wu, Jing Tian, Jun Wang, Pun Wang, Xiyu Niu, Xiaoquan Yao.
“Ordered mesoporous carbon nitride supported copper nanoparticles: a superior catalyst for homo- & cross-coupling of terminal alkynes under base-free conditions”
European Journal of Organic Chemistry, **2019**, 2019, 6690–6696.
- [2] **Hang Xu**, Keying Wu, Jing Tian, Li Zhu, Xiaoquan Yao.
“Recyclable Cu/C₃N₄ composite catalysed homo- and cross-coupling of terminal alkynes under mild conditions”
Green Chemistry, **2018**, 20, 793–797.
- [3] **Hang Xu**, Jun Wang, Pun Wang, Xiyu Niu, Yidan Luo, Li Zhu, Xiaoquan Yao.
“Recyclable Cu/C₃N₄ composite catalyzed AHA/A₃ coupling reactions for the synthesis of propargylamines”
RSC Advance, **2018**, 8, 32942–32947.

Acknowledgement

The author wishes to express his deepest gratitude to Professor Tomoo Mizugaki (Department of Materials Engineering Science, Graduate School of Engineering Science, Osaka University), for the instructive guidance and encouragement throughout the present work. Hearty thanks are made to Associate Professor Takato Mitsudome (Department of Materials Engineering Science, Graduate School of Engineering Science, Osaka University) for his helpful and useful suggestion. The author deeply thanks Assistant Professor Sho Yamaguchi (Department of Materials Engineering Science, Graduate School of Engineering Science, Osaka University) for numerous valuable comments. Their immense knowledge and plentiful experience have encouraged the author in all the time of his academic research and daily life.

The author wishes to thank for Prof. Takayuki Hirai (Department of Materials Engineering Science, Graduate School of Engineering Science, Osaka University) and Prof. Norikazu Nishiyama (Department of Materials Engineering Science, Graduate School of Engineering Science, Osaka University) for their valuable comments and helpful advises. The author would like to thank Dr. Yoshitaka Nakajima (Institute for Nano Science Design Center, Osaka University) for helpful advice and suggestion for TEM observation. He also expresses great gratitude to Associate Professor Yasutaka Kitagawa (Department of Materials Engineering Science, Graduate School of Engineering Science, Osaka University) and Dr. Yasukazu Hirao (Department of Chemistry, Graduate School of Science, Osaka University) for the helpful discussion on the reaction mechanism. The author deeply grateful to Professor Xiaoquan Yao (Department of Applied Chemistry, School of Material Science and Technology, Nanjing University of Aeronautics and Astronautics) for his kind help and encouragement.

Thanks must be made to Dr. Shu Fujita, Dr. Min Sheng, Mr. Hiroya Ishikawa, Mr. Tomohiro Tsuda, Mr. Katsumasa Sakoda, Mr. Daiki Kiyohira, Mr. Kazuto Ohashi, and Mr. Noboa Guerrón José Fernando. The author would like to extend sincere thanks to his friends, Ms. Fanjing Zhang and Mr. Jun Liu, for the cherished time spent together in social settings. The author also wishes to thank his parents Shitian Xu and Xianxiang Fang for their continuous supports. Finally, thanks are extended to all the members of Mizugaki laboratory for their helpful discussion and kind friendship.

This study was supported financially by the Japanese Government (Monbukagakusho: MEXT) Scholarship.

Hang XU